12-2010

Biochemical Characterization of Theromin, a Novel Leech Inhibitor, and the Interaction between the Fourth Metalbinding Domain of Wilson Disease Protein and Its Copper(I) Chaperone HAH1

Brian A. Zeider
Western Michigan University

BIOCHEMICAL CHARACTERIZATION OF THEROMIN, A NOVEL LEECH INHIBITOR, AND THE INTERACTION BETWEEN THE FOURTH METAL-BINDING DOMAIN OF WILSON DISEASE PROTEIN AND ITS COPPER(I) CHAPERONE HAH1

by

Brian A. Zeider

A Dissertation
Submitted to the
Faculty of The Graduate College
in partial fulfillment of the
requirements for the
Degree of Doctor of Philosophy
Department of Chemistry
Advisor: David Huffman Ph.D.

Western Michigan University
Kalamazoo, Michigan
December 2010

BIOCHEMICAL CHARACTERIZATION OF THEROMIN, A NOVEL LEECH INHIBITOR, AND THE INTERACTION BETWEEN THE FOURTH METAL-BINDING DOMAIN OF WILSON DISEASE PROTEIN AND ITS COPPER(I) CHAPERONE HAH1

Brian A. Zeider, Ph.D.

Western Michigan University, 2010

Theromin, a novel thrombin inhibitor from the leech *Theromyzon tessulatum*, has been shown to be the strongest inhibitor to date. There has been a lot of attention on direct thrombin inhibitors as a much more efficient drug for anticoagulation therapy. One main reason for the need of strong direct thrombin inhibitors is that the current therapy, heparin, causes alternative clotting events in some patients where antibodies are made to the heparin/thrombin complex and causes clots to occur by different methods. Recently there has been a strong inhibitor from a leech used, hirudin, that can inhibit with a K_i of 21 fM. This is the strongest inhibitor currently used as a therapy for patients suffering from clotting issues. This work investigated a leech inhibitor that has a K_i of 13 fM making it an even better candidate for therapies as it will inhibit more efficiently.

Copper is scrupulously regulated within the cell to maintain proper balance of redox activity and storage. One protein involved in this process is Wilson disease protein, which is responsible for moving copper into vesicles for either storage or removal from the cell. Previous work has shown copper is transferred to the Wilson disease protein via its metallochaperone, HAH1. The proposed mechanism for this transfer seems to involve a transient 3-coordinate copper(I) intermediate. Similar

work done on *Saccharomyces cerevisiae* has shown that a 3-coordinate intermediate could exist between Atx1 (analogue of HAH1) and its partner Ccc2. Trapping this intermediate involved selective mutation of individual cysteines involved in the copper(I) binding.

ACKNOWLEDGMENTS

I would like to graciously thank Dr. David Huffman for his support, guidance, and opportunities to not only work in his lab, but also other opportunities such as studying NMR at CERM in Florence, Italy and attending the International Conference for Biological Inorganic Chemistry (ICBIC14) in Nagoya, Japan. I would also like to thank my other committee members: Dr. Ekkhard Sinn, Dr. Susan Stapleton, and Dr. Thomas Thamman for their support and suggestions throughout my time at Western Michigan University. Finally, I'd like to thank Dr. Ivano Bertini for allowing me the opportunity to visit CERM, and Dr. Simone Ciofi and Dr. Francesca Cantini for their help in teaching me some of the techniques involved in protein NMR and providing housing and a fellowship while I was there, and the Huffman group for their help and suggestions throughout my time at WMU. Overall, I'd like to thank the Chemistry Department at Western Michigan University and Western Michigan University itself for giving me the opportunity to attend and receive my Ph.D.

Brian A. Zeider

TABLE OF CONTENTS

Table of Contents—continued

CHAPTER

CHAPTER

CHAPTER

Table of Contents—continued

LIST OF TABLES

LIST OF FIGURES

LIST ABBREVIATIONS

Ag(I) ..... Silver(I)

Arg or R ..... Arginine

Asp or N ..... Asparagine

ATP7A ..... Menkes Gene

ATP7B ..... Wilson Disease Protein Gene

Atx1 ..... Yeast Homolog to HAH1

BASIL ..... Bauer's Axially Symmetric Independent Ligands Model

Ccc2 ..... Yeast Homolog ATPase to Wilson Disease Protein

Ccc2a ..... First Metal-Binding Domain of Ccc2

Cd(II) ..... Cadmium(II)

CSV ..... Chemical Shift Variation

Cu(I) or (II) ..... Copper(I) or (II)

CueR ..... Copper Efflux Repressor Protein

Cys or C ..... Cysteine

DTT ..... Dithioltheitol

ESI ..... Enzyme/Substrate/Inhibitor Complex

ESI ..... Electrospray Ionization

ES ..... Enzyme/Substrate Complex

EI ..... Enzyme/Inhibitor Complex

Eq ..... Equivalents

EXAFS ..... Extended X-ray Absorption Fine Structure

Gly or G ..... Glycine

GSH ..... Glutathione

GST ..... Glutathione S-Transferase

HAH1 ..... Human Copper(I) Metallochaperone

Hg(II) ..... Mercury(II)

His or H ..... Histidine

HR ..... High Resolution

HRGF ..... High Resolutin Gel Filtration

HSQC ..... Heterospin Quantum Coherence

IPTG ..... Isopropyl β-D-1-Thiogalactopyranoside

LB ..... Luria-Bertani

Lys or L ..... Lysine

MerR ..... Mercury Repressor Protein for mer operon

nm ..... Nanometers

NMR ..... Nuclear Magnetic Resonance

NOE ..... Nuclear Overhauser Effect

NQI ..... Nuclear Quadripole Interaction

PAC ..... Perturbed Angular Correlation

SDS-PAGE ..... Sodium Dodecyl Sulfate Polyacrylamide Gel Electrophoresis

Ser or S ..... Serine

SOC ..... Super Optimal Culture

TCEP ..... Tris(2-carboxyethyl)phosphine

TRI ..... Synthetic Triple Helix Peptides

Trx .....Thioredoxin

Tyr or Y..... Tyrosine

UV-Vis.....Ultraviolet Visible

WLN# .....Wilson Metal-Binding Domain #

WLNP ..... Wilson Disease Protein

XANES .....X-ray Absorption Near Edge Structure

CHAPTER 1

BLOOD CLOTTING MECHANISMS AND INHIBITION

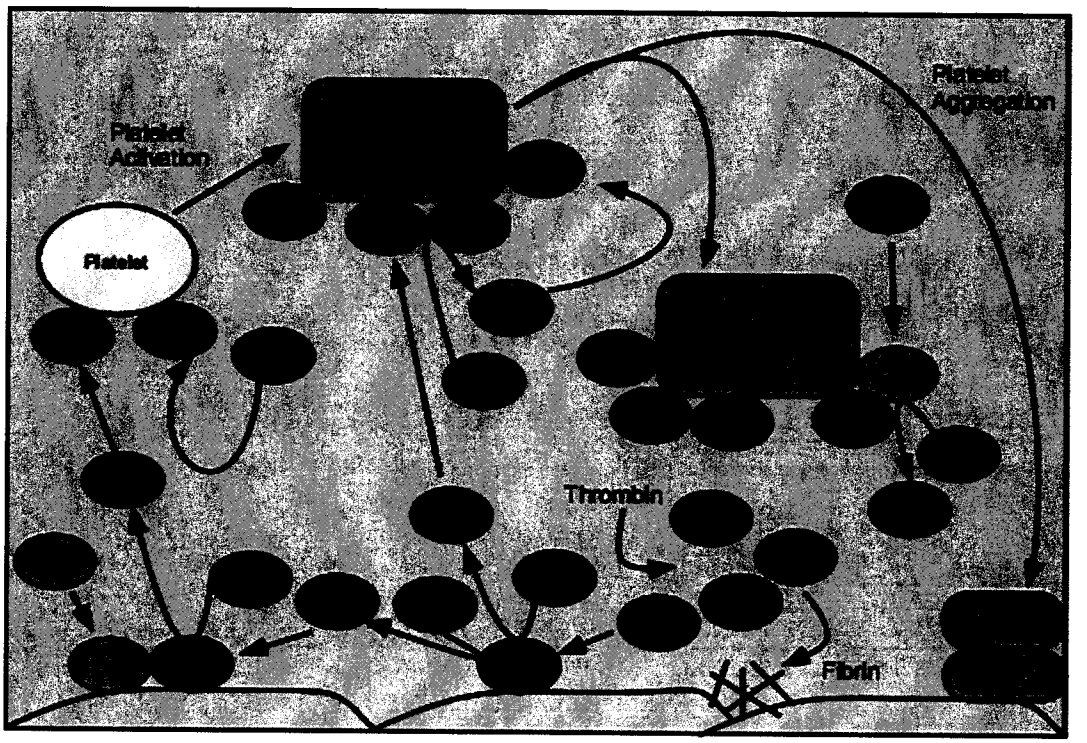

Figure 1.1: Illustration of the blood clotting cascade (*1-4*).

Blood clotting problems are very prevalent in the United States. The American Heart Association reported that more people die of a thrombosis (blood clot) than of AIDS and cancer combined. Most of these deaths occur from what is called a pulmonary embolism (PE) (*5, 6*). More commonly blood clots exhibit themselves as deep vein thrombosis (DVT) (*5, 9*). There are several drugs available

that can significantly reduce the possibility of getting, or even help dissolving, a clot. The most commonly prescribed drug on the market today is Coumadin® (warfarin); it works by inhibiting vitamin K from activating proconvertin (FVII). FVIIa activates Christmas factor (FIXa) that activates Stuart Factor (FXa) which in turn cleaves prothrombin (inactive) to produce α-thrombin (active) (*13, 14*) (**Figure 1.1**). α-Thrombin is the penultimate step in the blood clotting cascade, and is essential for both procoagulation and anticoagulation.

More recently, drugs are being developed that inhibit α-thrombin directly. Direct α-thrombin inhibition would be a stronger and faster anticoagulant. One such drug contained hirudin, a small peptide, that directly binds to α-thrombin to inhibit its ability to cleave fibrinogen. This inhibition is unique in that it binds to α-thrombin stronger than any other direct inhibitor to date. It also exhibits the ability to bind to α-thrombin in both its anticoagulant and procoagulant state. Drug discovery is moving toward small peptides rather than organic based molecules. This may lead to fewer side effects in the long run, as the peptides can be recycled by the body's natural proteases, resulting in less metabolites to combat.

1.1 Blood Clotting Cascade

The blood clotting cascade involves a very complicated, yet scrupulously regulated, set of proteases that work in concert to create and destroy clots to facilitate repair of blood vessels. **Figure 1.1** illustrates the complexity of this process as well as how tightly controlled it is. The blood clotting process involves two different pathways, the extrinsic and intrinsic. The distinction between the two pathways is

reflected by their names, the extrinsic requires factors not typically found in the blood, whereas the intrinsic pathway involves only factors inside the blood (*15*).

1.1.1 Extrinsic Pathway

The extrinsic pathway is the first pathway activated when damage is done to the cells of the vessel wall (*3, 16-18*). There has been evidence that it plays a role in the intrinsic pathway as well (See **Section 1.2**). It has been shown that tissue factor (TF) is constitutively expressed in many cell lines, especially those near blood vessels, i.e. skin surface, brain, lungs, and even the placenta (*19, 20*). Tissue factor is a membrane bound glycoprotein that has a high affinity for Factor VII in the blood (*3*). A cut in the blood vessel exposes the TF to the Factor VII and forms a complex with it in the presence of Ca(II) (*21*). This complex is essential to the initiation of the extrinsic cascade because it activates FVII, which can then go on to activate FX and FIX. From this point, the scheme gets highly complicated and much more regulated to propagate clots. This is also the point where the two clotting mechanisms converge.

1.1.2 Intrinsic Pathway

In the intrinsic pathway clotting occurs with factors inside the blood (*22*). This clotting mechanism is more complicated than the extrinsic and involves a more sophisticated mechanism. In this cascade FXII is activated to FXIIa when it comes in contact with a negatively charged surface such as glass or in disease states (*22-25*). The function of FXII is still unclear because individuals with deficiencies don't

exhibit hemological problems. The intrinsic coagulation cascade can be used as a measure for clotting times in the blood. This indicates the amount of clotting factor in the blood, and it is a measure to how "thin" the blood is; thin refers to the fluidity of blood. FXII was discovered in 1980 when a person with no other hemological issues exhibited prolonged clotting times (*25, 26*). A study discovered her blood didn't contain the clotting Factor XII which is the initiation step of the clotting cascade by interaction with the glass surface. In vivo, however, the intrinsic pathway can be activated by articular cartilage (a subset of cartilage between joints), endotoxin, L-homocysteine, skin, chondroitin sulfate, calcium pyrophosphate and a clot already in progress (which seems to be an accepted common process for this coagulation cascade) (*22, 27, 28*).

The activation of FXII leads to conversion of prekallikrein (also known as Fletcher factor) to kallikrein, which further activates FXI (*22*). Ultimately the newly activated FXIa goes on to activate FIX which then associates with FVIIIa and Ca(II) to make the tenase complex that activates FXa (*29-31*). This is essentially where the two processes converge.

The intrinsic pathway has been described as having two functions, response as inflammation from disease and as a way to maintain a clot. Clots have the proper charge on them to elicit the intrinsic response until the wound is repaired and activated α-thrombin has been brought to physiological levels.

1.1.3 Clot Formation

The remaining clotting mechanisms occur regardless of the initiation of the clotting event. Once FX has been activated the clot formation moves along quite quickly toward clot formation. FXa is the clotting factor that cleaves prothrombin (FII) to α-thrombin (FIIa). α-thrombin is the penultimate step in clot formation. Once active, which will be more clearly defined later in this discussion, it has two major jobs for creating clots. First it cleaves fibrinogen into fibrin monomers which is the clotting material itself and second it works in conjunction with Ca(II) and fibrin to activate FXIII. FXIII plays an essential role as it crosslinks the fibrin molecules to make the clot hard and impenetrable.

1.2 α-Thrombin

α-Thrombin (**Figure 1.2**) is the next to last step of the blood clotting cascade. It cleaves fibrinogen into fibrin monomers and activates FIII so the clot can harden

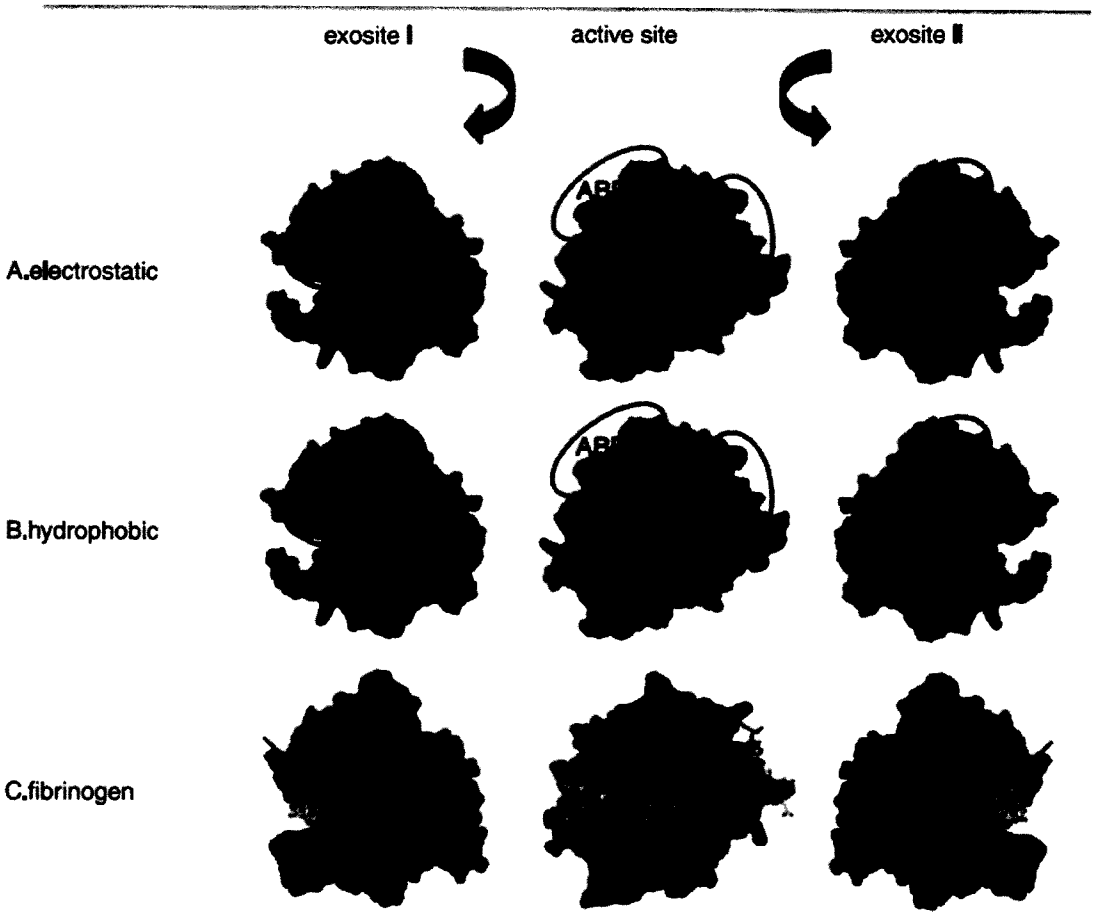

Figure 1.2: Thrombin surfaces describing the electrostatic and hydrophobic regions, as well as where fibrinogen fits into the structure. For Further information about the importance of these features of the exosites, refer to Section 2.1(*11*).ABEII is exosite II, ABEI is exosite I and the active site is where the catalytic triad is located.

(**Figure 1.1**). α-Thrombin has been the target for many drugs to date, such as heparin and Leprudin® (rHirudin). These sorts of drugs act much more effectively than, for

instance, warfarin, which works by inhibiting vitamin K dependent synthesis of FII, VII, IX, X, and regulatory factors: proteins C, S, and Z (*32, 33*). The drawback with warfarin is the need for it to slowly build up in the bloodstream. Warfarin is not a fast acting molecule and it takes time to properly regulate the dosage. Because of this, it is typically taken in conjunction with heparin for the first two weeks. This is both expensive and time consuming; whereas direct α-thrombin inhibitors would be more beneficial. Heparin is a direct α-thrombin inhibitor, but there are problems with long term use of heparin, i.e. the heparin-α-thrombin complex may induce creation of antibodies to the extent that it would actually cause other clotting elsewhere. Some emphasis has been placed on finding a direct α-thrombin inhibitor that would work more effectively and alleviate the issues associated with heparin. There has been a plethora of research associated with α-thrombin in its various forms to try and understand its activity and regulate it. α-Thrombin is a very diverse enzyme that can carry out a clotting event and also initiate destruction of the clot once it is not needed. This section will discuss the nuances of α-thrombin that allow it to do its job and how it is regulated and inhibited.

1.2.1 Proteolytically Cleaved Forms of α-Thrombin

α-Thrombin has four distinct forms, each differing by the cleavage of small peptide fragments. For example, α-thrombin exists in the blood as prothrombin (concentration in the blood 1.2μM (*34*)), which is then cleaved by FXa to create α-thrombin (in this discussion it will be noted as "thrombin") (concentration in blood – independent of clotting event – 0.06 μM - 0.09 μM (*34*)) which is the most common

form. The cleavage of α-thrombin by Factor Xa occurs after an extrinsic event has occurred (i.e. a laceration of the blood vessel). It is the most specific protease form, and can perform all the activities of the α-thrombin protease. Once in the active form, α-thrombin can be further degraded by autolytic cleavage, or by FXa to make two distinct forms, β and γ-thrombin (*35*). These two, less active forms are created by cleavage of the B-chain of α-thrombin. The β-thrombin is created by cleaving the B-chain between Arg-106 and Tyr-107. γ-thrombin is created by further cutting of the β-thrombin B-chain between Lys-190 and Gly-191.

1.2.1.1 α-Thrombin

α-Thrombin is a serine protease whose main function is cleavage of soluble fibrinogen into insoluble fibrin molecules. α-Thrombin is made of two chains connected by one disulfide bond; the A-chain is composed of 36 amino acids (*36, 37*) and the B-chain contains 264 amino acid residues (*38*). The structural features of α-thrombin are 2 exosites (*39-42*), a sodium binding site (*12, 43-45*), fibrinogen recognition site (*46-48*), an active site containing the catalytic triad, and various other sequences that recognize other inhibitors and small molecules (**Figure 1.2**). Each of these features will be discussed in detail to understand how all these sites work in concert to allow α-thrombin to function.

1.2.1.1.1 α-Thrombin Exosites

Thrombin has two exosites that are highly positive and recognize certain binding partners (**Figure 1.2** and **1.3**). The site labeled as exosite I binds a whole

host of different molecules such as: fibrinogen (*49-51*), fibrin (*49, 50, 52*), residues 54-65 of hirudin (*7, 50, 53, 54*), thrombomodulin (*55-58*), α-thrombin receptor (*59*), and an acidic portion of the heparin co-Factor II (*60*). Exosite 2 binds heparin and other similar molecules (*61-64*), the chondroitin sulfate moiety of thrombomodulin (*65, 66*), and the inhibitor hemadin (*11, 39*). Other molecules target both exosites, such as FV and FVa (*40, 41, 67*), FVIII (*39, 68*), and bothrojaracin (*69, 70*). Nearly every event involving α-thrombin utilizes the exosites in one way or another. Huntington (2005) described ratios of negative charge: hydrophobicity was important in discriminating the use of one exosite from another (*11*). **Table 1.1** shows different negative charge/hydrophobicity ratios for various exosite targets. Exosite I favors targets with a negative charge/hydrophobicity ratio of approximately 1, whereas exosite II favors targets with a negative charge/hydrophobicity ratio nearly 2.5 times larger. This suggests that the exosites can accommodate differing levels of hydrophobicity. An interesting experiment would be to cleave off the negatively charged residues and determine whether the inhibitors become more promiscuous; there are no current studies reported in the literature that have looked at this.

Exosite I has some hydrophobic residues on the surface, whereas exosite II has none (*71*). This accounts for the negative charge/hydrophobicity ratio described. Another interesting feature of these exosites is they are exactly opposite each other in location on α-thrombin and have allosteric control of the nonbinding exosite (i.e. hirudin binding to exosite I causes an allosteric shift in exosite II to make it inoperable as well). This is an important control mechanism for α-thrombin, wherein

one binding partner controls the activity of the enzyme rather than multiple binding partners which would disrupt all activity.

1.2.1.1.2 Sodium Binding

Second in importance only to the exosites is the sodium (Na) binding site. This site regulates what function thrombin is going to perform. For example, when sodium is bound, α-thrombin is in the coagulant form because it cleaves fibrinogen with high specificity. When sodium is not bound it becomes an anticoagulant, by binding to thrombomodulin – increasing its affinity for protein C activation (*44*). The nomenclature for these two states is "fast" and "slow", related to the procoagulant activity.

Table 1.1: Relative ratios of anionic character vs. hydrophobic character to describe the selectivity characteristics between the two (*11*).

	Binding Sequence	Fraction Negative Charge	Fraction Hydrophobic	Ratio
Exosite I:				
	DSDWPFCSDEDWNY	0.36	0.36	1
Fibrinogen Aα	DFEEIPEEY*LQ	0.55	0.45	1.2
Hirudin	EGEEDDDY*LDLEKIFSEDDDY	0.58	0.35	1.7
HCII	*IDIVD	0.33	0.33	1
PAR1	DKYEPFWEDEEK			
Average		0.45 ± 0.11	0.37 ± 0.05	1.2 ± 0.3
Exosite II:				
Hemadin	EFEEFEIDEEE	0.72	0.27	2.7
GpIbα	DEGDTDLY*DY*PEEDTEGD	0.68	0.26	2.6
Fibrinogen γ'	ETEY*DSLY*PEDD	0.75	0.33	2.3
Average		0.72 ± 0.03	0.29 ± 0.03	2.5 ± 0.2

Sodium binding has an allosteric effect on the α-thrombin molecule; this has been noted in the crystal structures in the literature of both the fast and slow forms (**Figure 1.3**) (*43*). One way the allosteric control was observed was from the structures that indicate many changes that took place and even blockage of the active site in the absence of sodium (*71*). The sodium plays a major role in regulation of the enzymes activities. In the blood, the α-thrombin is available in nearly equivalent concentrations of both sodium bound and unbound (approximately 2:3 Na:Apo). This is due to the concentration of salt in the blood (140mM) being insufficient to completely saturate the enzyme. A corollary to these findings is that α-thrombin molecules with a dysfunctional Na binding site lead to bleeding issues (*43, 71*). The proportions of fast and slow forms of α-thrombin allow for direct control by the substrates themselves. Since α-thrombin has such a diverse list of duties it needs to be very tightly regulated to keep the blood fluid yet allow localized repair of vessels.

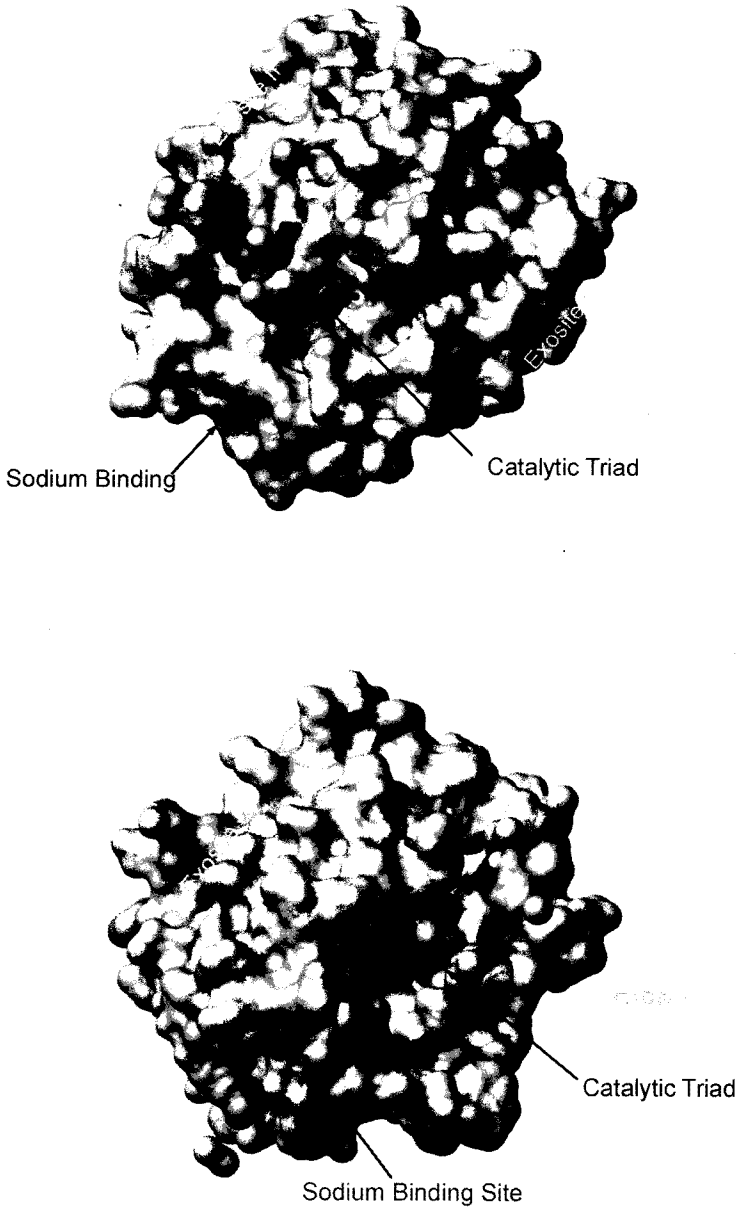

Figure 1.3: Thrombin makes some extensive allosteric changes upon binding of sodium. Top, sodium bound, shows the open active site of thrombin, whereas; bottom, apo form, shows the active site blocked by an allosteric shift to close off the catalytic triad. Fast form, top PDB ID: 1SG8, and Slow form, bottom, PDB ID: 1SGI (*12*).

1.2.1.1.3 α-Thrombin Active Site

The active site is where the fibrinogen cleavage occurs. α-Thrombin is a serine protease, which consists of a catalytic triad used in cleaving fibrinogen into fibrin monomers. The active site is located in the B chain of the protease. This is where the catalytic triad resides, His57, Asp102, and Ser195 are located (*61*). The catalytic triad works by aspartate removing the proton of histidine which in turns weakens the O-H bond of the serine, in essence lowering its pK_a to allow it to attack the carbonyl carbon of the peptide and proteolytically cleaving the amide bond (*72, 73*). The specificity for fibrinogen stems from its attraction and orientation on exosite I.

1.2.1.1.4 α-Thrombin Functionality

α-Thrombin is the penultimate step in the blood clotting cascade, and it also has the reverse activity of anticoagulation by activating protein C. Some of α-thrombin's activity as a procoagulant enzyme has been discussed in Section 1, however, the anticoagulation features need some discussion here. α-Thrombin's anticoagulant abilities are somewhat indirect in that thrombomodulin binds to thrombin (slow form), which allows for activation of protein C (an anticoagulant protein). Protein C, in conjunction with protein S, then cleaves and inactivates FVa and FVIIIa preventing prothrombin cleavage and ultimately stopping creation of active protease (*74, 75*). Thrombomodulin is a membrane protein expressed on the surface of endothelial cells (*76, 77*). The thrombomodulin-α-thrombin complex

increases the activation of protein C a thousand-fold, and prevents any fibrinogen lysis by competing for its binding site (*75, 77*). Once protein C is activated, it complexes with protein S, which exists in the blood either on platelets or endothelium (*78-81*). This complex, as stated before inactivates FVa and FVIIIa (**Figure 1.4**).

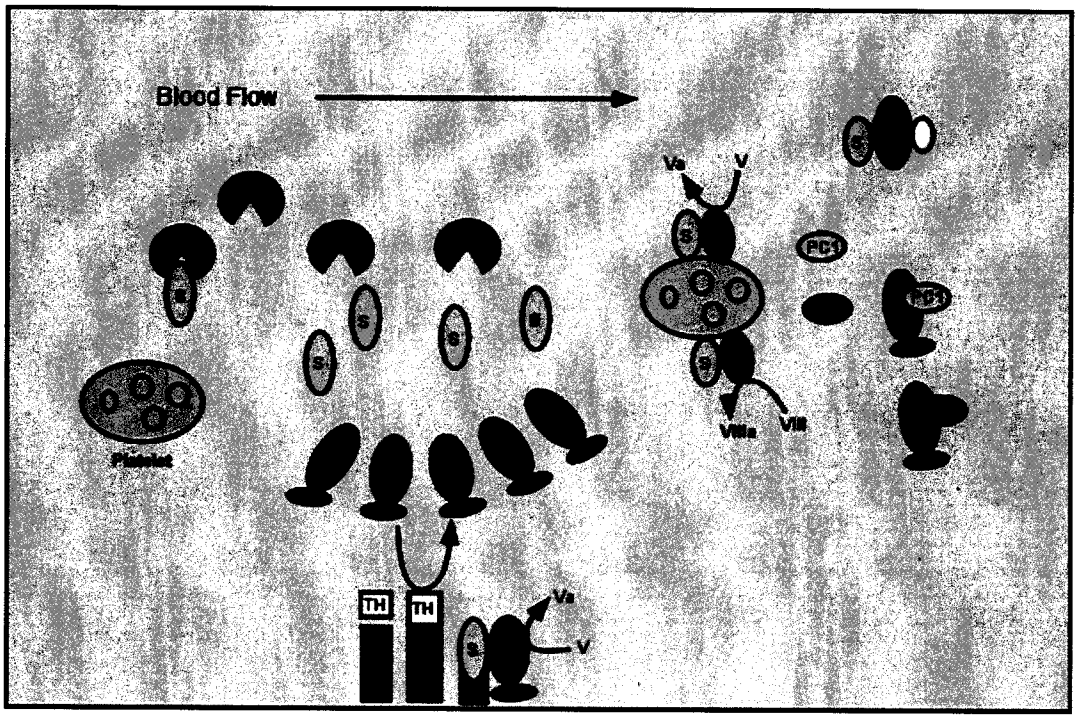

Figure 1.4: A cartoon describing the anticoagulant abilities of α-thrombin as it binds to thrombomodulin, and activates protein C (*75*).

Blood coagulation in the body requires a lot of maintenance and tight regulation in order to keep our blood in a fluid state during normal function and then quickly make a clot where necessary to prevent blood loss and sepsis. The

coagulation cascade is ultimately set up to highly favor the anticoagulant mechanisms. However, when there is intrusion to the system, whether that be a cut or infection, only a very small amount of initiator is needed due to the very large turnover rate for these proteases, hence the cascade. It is very much like a waterfall, it starts off slow then all of a sudden, and it picks up speed very quickly to protect the circulatory system.

1.3 α-Thrombin Inhibitors

The coagulation cascade does its job with accuracy and speed, but there are times when there is a breakdown in the system. In these cases therapies are needed to regulate the system until physiological conditions return. Overclotting of the blood can occur for many different reasons, from too much clotting factor present in the blood, to problems with protein C or protein S (previously discussed as anticoagulant proteins), or trauma (i.e. either intrusion such as a blow to a vessel or surgery).

Typically clotting in the legs would not be an issue, however, the blood clots sometimes aren't completely hardened like a normal clot and can break off and travel closer to the lungs, which ultimately prevents oxygen from being taken into the blood (when a clot is in the lungs it is called a pulmonary embolism). Even though there are many different ways to end up with overactive clotting, the therapies are the same. Most often when a clot is noticed there are two therapies that are administered simultaneously, warfarin and heparin. Heparin binds directly to α-thrombin and inhibits it very effectively, while warfarin blocks vitamin K dependent synthesis of FII, VII, IX, X, and regulatory factors: proteins C, S, and Z (*32, 33*). The issue with

warfarin, is that it is a dose response inhibitor, and therefore needs to build up in the system and be constantly monitored for proper "thinness" of the blood.

While these therapies are very useful and effective, they aren't without problems. Warfarin, has been approved for use since the 1950s and was originally (and still is today) used as a potent killer of rodents (by causing deadly bleeding events), however the issues with this drug are its interactions with a lot of commonly used medicines (i.e. aspirin and other NSAIDs – Non-Steroid Anti-Inflammatory Drugs) and interactions with foods. Heparin, however, is used quite often as a quick and direct inhibitor of α-thrombin, but it too has its problems, such as heparin-induced thrombocytopenia. Thrombocytopenia is the development of low platelet count due to heparin-dependent IgG antibodies that are formed and activate the platelets (*82*). Briefly the mechanism involves IgG induction toward the heparin bound to platelet Factor 4. The tail of the IgG then binds to a protein receptor on the platelets that activates them to create microparticles. These microparticles induce the formation of clots, and diminish the level of platelets in the blood (*82-85*).

These drugs and issues are only the most common among a whole host of issues that are related to different anticoagulation therapies. For this reason, there has been a lot of interest in direct α-thrombin inhibitors that could effectively inhibit its activity. One such molecule is the leech inhibitor hirudin, having the trade name Leprudin (which is a recombinant form of hirudin).

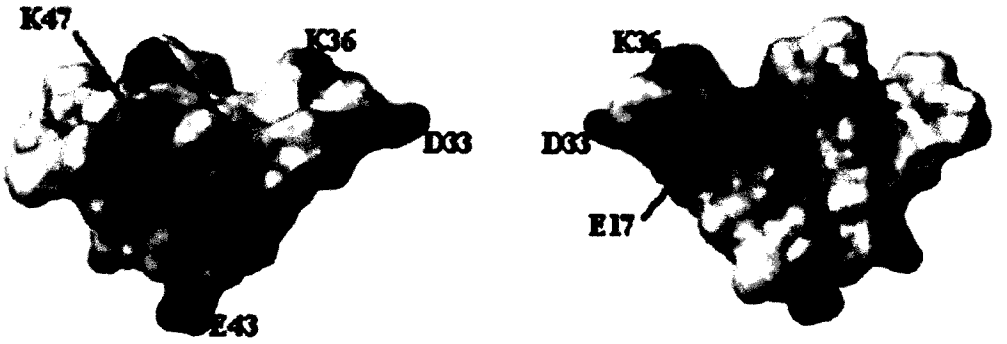

Figure 1.5: Charged Surface map of rHirudin (desulfonated tyrosine 63). This is a stereo view each being 180° from each other (*10*).

1.4 Hirudin

Hirudin (**Figure 1.5**) is a small, 65 amino acid residue, peptide inhibitor from the leech *Hirudo medicinalis* (*7, 54, 86*). Its structure has a hydrophobic core made of the N-terminal portion of the peptide containing three disulfide bonds holding it rigid and a very hydrophilic (acidic) C-terminal end (*87*). There is a posttranslational modification of a sulfated tyrosine at residue 63, which is not present in the recombinant form (*87, 88*). This difference between the two structures accounts for a 10 fold decrease in activity for the recombinant form. It has been found to bind to α-thrombin very strongly (K_i=21 fM (*89*) for recombinant, some previously have reported K_i=100 fM (*54*)), with high specificity. The difference in the inhibition constants is due to the differences in the amino acid sequences.

There are a few NMR structures that have been developed of the hirudin structure itself (*88, 90*). The main goal of these structures was to understand whether the modified tyrosine could be the reason for the difference in inhibition constant. To date, it is still unclear exactly what role if any the sulfonated tyrosine is playing, even though there has been speculation it helps in exosite I binding. Many groups have tried different expression systems to see if the inhibition is affected and what the

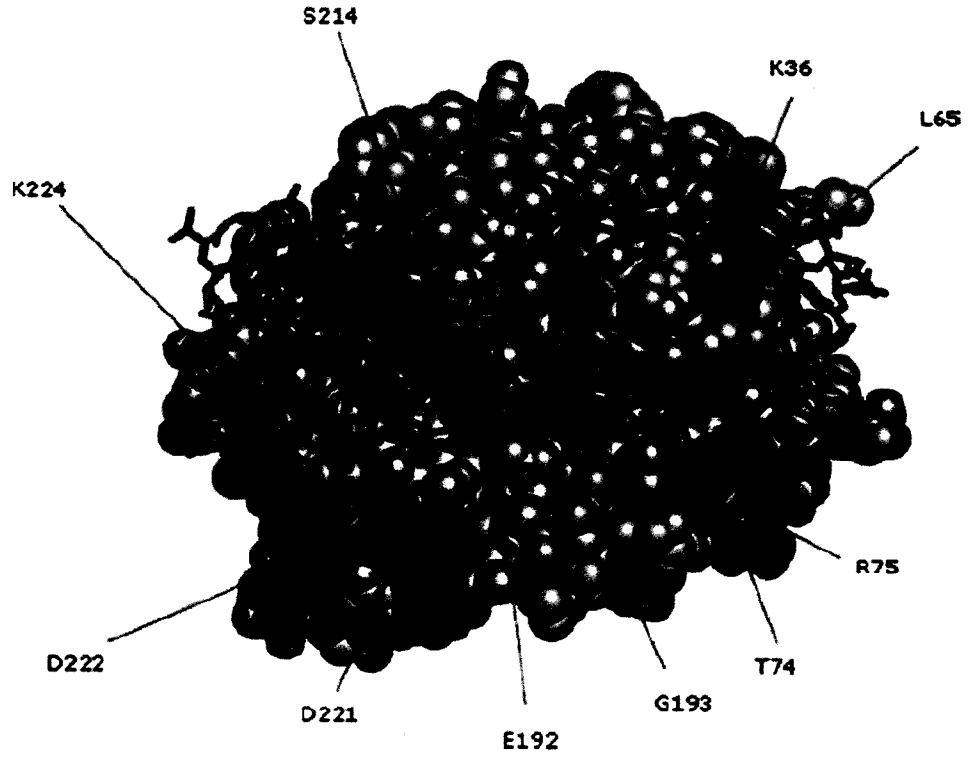

Figure 1.6: Hirudin, the blue sticks, is shown bound to thrombin. The red space-filled residues are implicated in the fast form of thrombin, and the green are implicated in the slow form. The yellow space-filled residue is lys-244 which plays an important role in hirudin binding. It is important to note that hirudin binding is independent of sodium binding (*7, 8*).

phenotypes of the protein were (**Table 1.2**).

As previously stated hirudin binds to exosite I, which is the same place fibrinogen binds. This feature makes this peptide a very advantageous therapy for patients that are prone to some of the adverse side effects of the other medications. Many crystal structures exist of hirudin, and many homologues, binding to α-thrombin at exosite I (*54*). **Figure 1.6** shows hirudin bound to α-thrombin, and interestingly not only does it bind to the exosite , but also to the active site as well. These finding are novel because only recently has the hirudin/α-thrombin structure been deconvoluted. The technology wasn't available to get a clear idea where and how hirudin binding was occurring. Earlier studies used a combination of crystallography and structures of hirudin binding to determine with low resolution the structure of hirudin bound to α-thrombin.

Hirudin binding to α-thrombin has a big impact on the blood environment because not only does it prevent fibrinogen binding and ultimately cleaving, it also prevents Factor V, VIII, XIII from binding as well (*87, 91*). One exciting feature of hirudin binding is that it can bind and inhibit fibrin bound α-thrombin. This is a major benefit as the fibrin-α-thrombin structure has a large impact on the increase in thrombus size.

Table 1.2: A list of different expression systems tried as hosts for over expression of rHirudin (*87*).

Expression System	Protein Yield	Comments	References
Bacteria *Escherichia Coli* *Streptomyceslivid ans*	~1mg/L (intracellular) 200-300mg/L (Intermembrane Space) 0.25–0.5 mg/L(secreted)	Reduced activity of the N-terminal methionine modified hirudin; expression of authentic N-terminal hirudin into periplasmic space; no	(*92-94*)
Yeast *Saccharomycesce revisiae* *Hansenula polymorpha* *Pichia pastoris*	40–500 mg/L (Secreted 1,500 mg/L (Secreted) 1,500 mg/L (Secreted)	Efficient secretion into culture supernatant; no sulfation at Tyr; *S. cerevisiae*-derived hirudin gained market approval from FDA; *H. polymorpha*-derived hirudin is being evaluated in phase III clinical trials	(*95-98*)
Fungi *Acremonium chrysogenum*	7 mg/L (S)	No detectable hirudin under intracellular expression	(*99*)
Insect cells	0.4 mg/L (S)	HV-1 showed higher expression than HV-2	(*100*)
Mammals BHK cells	0.05 mg/L(S)	Sulfation at Tyr	(*101*)
Plants Oilseed rape Tobacco	0.55 anti-α-thrombin units/mg oil body protein	Oleosin–hirudin fusion expression; Oleosin–hirudin fusion expression;	(*102-104*)

The hirudin homolog Lepirudin® was approved in 1998 by the FDA as a therapy to combat heparin-induced thrombocytopenia (*105*). Lepirudin® is made recombinantly by yeast and is the recombinant form of hirudin with several modifications: tyrosine 63 is not sulfonated and an isoleucine replaced a leucine at the N-terminus.

Since the success of hirudin, there have been other direct α-thrombin inhibitors discovered. One in particular that shows much promise is theromin. It is a small 67 amino acid peptide capable of binding very tightly to α-thrombin, and completely shutting it down.

1.5 Theromin

Theromin is a 67 residue peptide capable of wrapping itself around α-thrombin as it inhibits (*89*). This peptide contains 16 cysteines capable of making 8 disulfide bonds which seem to be essential to elicit a strong inhibition α-thrombin inhibition. These observations were from mass spec studies in conjunction with inhibition studies that found the monomer had a much decreased inhibition constant than did the dimer form (dimer K_i=12 fM, while monomer was much lower) (*89*). Theromin's inhibition constant makes it the strongest inhibitor to date. To date there is little known about this peptide and therefore is the crux of this study. It is very important to understand whether there is a difference in inhibition properties between native and recombinant hirudin (which preliminary results indicate not, based on comparison of Salzet's (*89*) wildtype theromin studies and this project's recombinant studies). It would also be important to more fully understand how the structure

behaves and get structural data for binding to α-thrombin. A combination of this data and possibly even analogs would lead to an even stronger direct α-thrombin inhibitor.

1.6 Physiological Significance of Theromin

Little biophysical data has been collected for theromin. However, it is important to understand the physiological impact of theromin in the host blood. For example how fast does it degrade in the blood, and further does it maintain the blood in a fluid state much longer than necessary for the leech to eat? These "big picture" ideas haven't been explored for this inhibitor nor has it been for a similar inhibitor, hirudin. One could expect these inhibitors are very specific to their targets, so no alternative binding would occur. Many studies still need to be done on these types of inhibitors as to what the concentration of the inhibitor is in the saliva of the leech and whether the leech can use the inhibitor in other ways to regulate its own homeostatic mechanisms.

1.7 Objectives of This Study

Theromin, as alluded to previously, seems to be a promising new small molecule for anticoagulation therapy. Wildtype theromin has a K_i of 12 fM, making it the strongest inhibitor to date. Currently though, the yield from a leech is insufficient to economically mass produce it, so recombinant technology would be the alternative. The objective of this study was to express the protein at high levels using a pET system, and then use the protein made to determine the K_i of the recombinant form. Posttranslational modifications of the peptide in the leech have not been

observed, so the K_i should be similar to that measured by Salzet (*89*). A second objective of this project is to use theromin's homology to metallothioneins and determine if it too can bind Cu(I). This could serve useful, as therapies are needed that control copper regulation in people who have Wilson's disease, but many modifications would be needed to convert theromin from an inhibitor to a chelator, as it can't serve both functions simultaneously. A combination of these data would move theromin closer to becoming a new, stronger direct α-thrombin inhibitor.

1.8 References

1. Macfarlane, R. G. (1964) An Enzyme Cascade in the Blood Clotting Mechanism, and Its Function as a Biochemical Amplifier, *Nature 202*, 498-499.

2. Mann, K. G., Jenny, R. J., and Krishnaswamy, S. (1988) Cofactor proteins in the assembly and expression of blood clotting enzyme complexes, *Annu Rev Biochem 57*, 915-956.

3. Davie, E. W., Fujikawa, K., and Kisiel, W. (1991) The coagulation cascade: initiation, maintenance, and regulation, *Biochemistry 30*, 10363-10370.

4. Davie, E. W. (2003) A brief historical review of the waterfall/cascade of blood coagulation, *J Biol Chem 278*, 50819-50832.

5. Tapson, V. F. (2008) Acute pulmonary embolism, *N Engl J Med 358*, 1037-1052.

6. Dalen, J. E., and Alpert, J. S. (1975) Natural history of pulmonary embolism, *Prog Cardiovasc Dis 17*, 259-270.

7. Rydel, T. J., Tulinsky, A., Bode, W., and Huber, R. (1991) Refined structure of the hirudin-thrombin complex, *J Mol Biol 221*, 583-601.

8. Mengwasser, K. E., Bush, L. A., Shih, P., Cantwell, A. M., and Di Cera, E. (2005) Hirudin binding reveals key determinants of thrombin allostery, *J Biol Chem 280*, 26997-27003.

9. Kyrle, P. A., and Eichinger, S. (2005) Deep vein thrombosis, *Lancet 365*, 1163-1174.

10. Song, X., Mo, W., Liu, X., Zhu, L., Yan, X., Song, H., and Dai, L. (2007) The NMR solution structure of recombinant RGD-hirudin, *Biochem Biophys Res Commun 360*, 103-108.

11. Huntington, J. A. (2005) Molecular recognition mechanisms of thrombin, *J Thromb Haemost 3*, 1861-1872.

12. Pineda, A. O., Carrell, C. J., Bush, L. A., Prasad, S., Caccia, S., Chen, Z. W., Mathews, F. S., and Di Cera, E. (2004) Molecular dissection of Na+ binding to thrombin, *J Biol Chem 279*, 31842-31853.

13. Becker, R. C. (2002) *Antithrombic Therapy. 2nd ed.* , Professional Communications Inc. .

14. Bowen, D. J. (2002) Haemophilia A and haemophilia B: molecular insights, *Mol Pathol 55*, 1-18.

15. Camerer, E., Kolsto, A. B., and Prydz, H. (1996) Cell biology of tissue factor, the principal initiator of blood coagulation, *Thromb Res 81*, 1-41.

16. Mackman, N., Tilley, R. E., and Key, N. S. (2007) Role of the extrinsic pathway of blood coagulation in hemostasis and thrombosis, *Arterioscler Thromb Vasc Biol 27*, 1687-1693.

17. Maynard, J. R., Dreyer, B. E., Stemerman, M. B., and Pitlick, F. A. (1977) Tissue-factor coagulant activity of cultured human endothelial and smooth muscle cells and fibroblasts, *Blood 50*, 387-396.

18. Weiss, H. J., Turitto, V. T., Baumgartner, H. R., Nemerson, Y., and Hoffmann, T. (1989) Evidence for the presence of tissue factor activity on subendothelium, *Blood 73*, 968-975.

19. Mackman, N. (1995) Regulation of the tissue factor gene, *Faseb J 9*, 883-889.

20. Fleck, R. A., Rao, L. V., Rapaport, S. I., and Varki, N. (1990) Localization of human tissue factor antigen by immunostaining with monospecific, polyclonal anti-human tissue factor antibody, *Thromb Res 59*, 421-437.

21. Vijaya, L., Rao, M., and Rapaport, S. I. (1988) Activation of factor VII bound to tissue factor: A key early step in the tissue factor pathway of blood coagulation, *Proc Natl Acad Sci U S A 85*, 6687-6691.

22. Gailani, D., and Renne, T. (2007) Intrinsic pathway of coagulation and arterial thrombosis, *Arterioscler Thromb Vasc Biol 27*, 2507-2513.

23. Gailani, D., and Renne, T. (2007) The intrinsic pathway of coagulation: a target for treating thromboembolic disease?, *J Thromb Haemost 5*, 1106-1112.

24. Vroman, L., Adams, A. L., Fischer, G. C., and Munoz, P. C. (1980) Interaction of high molecular weight kininogen, factor XII, and fibrinogen in plasma at interfaces, *Blood 55*, 156-159.

25. Schmaier, A. H. (2008) The elusive physiologic role of Factor XII, *J Clin Invest 118*, 3006-3009.

26. Ratnoff, O. D., and Colopy, J. E. (1954) A familial hemorrhagic trait associated with a deficiency of a clot-promoting fraction of plasma, *J Clin Invest 34*, 602-613.

27. Kottke-Marchant, K. (2010) *The role of coagulation in arterial and venous thrombosis*, Humana Press.

28. Schmaier, A. H., and McCrae, K. R. (2007) The plasma kallikrein-kinin system: its evolution from contact activation, *J Thromb Haemost 5*, 2323-2329.

29. Kalafatis, M., Egan, J. O., van 't Veer, C., Cawthern, K. M., and Mann, K. G. (1997) The regulation of clotting factors, *Crit Rev Eukaryot Gene Expr 7*, 241-280.

30. Brummel, K. E., Paradis, S. G., Branda, R. F., and Mann, K. G. (2001) Oral anticoagulation thresholds, *Circulation 104*, 2311-2317.

31. Sheehan, J. P., and Lan, H. C. (1998) Phosphorothioate oligonucleotides inhibit the intrinsic tenase complex, *Blood 92*, 1617-1625.

32. Ansell, J., Hirsh, J., Poller, L., Bussey, H., Jacobson, A., and Hylek, E. (2004) The pharmacology and management of the vitamin K antagonists: the Seventh ACCP Conference on Antithrombotic and Thrombolytic Therapy, *Chest 126*, 204S-233S.

33. Freedman, M. D. (1992) Oral anticoagulants: pharmacodynamics, clinical indications and adverse effects, *J Clin Pharmacol 32*, 196-209.

34. Croy, C. H., Koeppe, J. R., Bergqvist, S., and Komives, E. A. (2004) Allosteric changes in solvent accessibility observed in thrombin upon active site occupation, *Biochemistry 43*, 5246-5255.

35. Boissel, J. P., Le Bonniec, B., Rabiet, M. J., Labie, D., and Elion, J. (1984) Covalent structures of beta and gamma autolytic derivatives of human alpha-thrombin, *J Biol Chem 259*, 5691-5697.

36. Walz, D. A., and Seegers, W. H. (1974) Amino acid sequence of human thrombin A chain, *Biochem Biophys Res Commun 60*, 717-722.

37. Butkowski, R. J., Elion, J., Downing, M. R., and Mann, K. G. (1977) Primary structure of human prethrombin 2 and alpha-thrombin, *J Biol Chem 252*, 4942-4957.

38. Thompson, A. R., Enfield, D. L., Ericsson, L. H., Legaz, M. E., and Fenton, J. W., II. (1977) Human thrombin: partial primary structure, *Arch Biochem Biophys 178*, 356-367.

39. Verhamme, I. M., Olson, S. T., Tollefsen, D. M., and Bock, P. E. (2002) Binding of exosite ligands to human thrombin. Re-evaluation of allosteric linkage between thrombin exosites I and II, *J Biol Chem 277*, 6788-6798.

40. Esmon, C. T., and Lollar, P. (1996) Involvement of thrombin anion-binding exosites 1 and 2 in the activation of factor V and factor VIII, *J Biol Chem 271*, 13882-13887.

41. Dharmawardana, K. R., Olson, S. T., and Bock, P. E. (1999) Role of regulatory exosite I in binding of thrombin to human factor V, factor Va, factor Va subunits, and activation fragments, *J Biol Chem 274*, 18635-18643.

42. Colwell, N. S., Blinder, M. A., Tsiang, M., Gibbs, C. S., Bock, P. E., and Tollefsen, D. M. (1998) Allosteric effects of a monoclonal antibody against thrombin exosite II, *Biochemistry 37*, 15057-15065.

43. De Filippis, V., De Dea, E., Lucatello, F., and Frasson, R. (2005) Effect of Na+ binding on the conformation, stability and molecular recognition properties of thrombin, *Biochem J 390*, 485-492.

44. Di Cera, E., Guinto, E. R., Vindigni, A., Dang, Q. D., Ayala, Y. M., Wuyi, M., and Tulinsky, A. (1995) The Na+ binding site of thrombin, *J Biol Chem 270*, 22089-22092.

45. Wells, C. M., and Di Cera, E. (1992) Thrombin is a Na(+)-activated enzyme, *Biochemistry 31*, 11721-11730.

46. De Cristofaro, R., and Di Cera, E. (1992) Modulation of thrombin-fibrinogen interaction by specific ion effects, *Biochemistry 31*, 257-265.

47. Higgins, D. L., Lewis, S. D., and Shafer, J. A. (1983) Steady state kinetic parameters for the thrombin-catalyzed conversion of human fibrinogen to fibrin, *J Biol Chem 258*, 9276-9282.

48. Cheng, Y., Slon-Usakiewicz, J. J., Wang, J., Purisima, E. O., and Konishi, Y. (1996) Nonpolar interactions of thrombin and its inhibitors at the fibrinogen recognition exosite: thermodynamic analysis, *Biochemistry 35*, 13021-13029.

49. Naski, M. C., and Shafer, J. A. (1990) Alpha-thrombin-catalyzed hydrolysis of fibrin I. Alternative binding modes and the accessibility of the active site in fibrin I-bound alpha-thrombin, *J Biol Chem 265*, 1401-1407.

50. Chang, J. Y. (1991) Deciphering the structural elements of hirudin C-terminal peptide that bind to the fibrinogen recognition site of alpha-thrombin, *Biochemistry 30*, 6656-6661.

51. Stubbs, M. T., Oschkinat, H., Mayr, I., Huber, R., Angliker, H., Stone, S. R., and Bode, W. (1992) The interaction of thrombin with fibrinogen. A structural basis for its specificity, *Eur J Biochem 206*, 187-195.

52. Naski, M. C., and Shafer, J. A. (1991) A kinetic model for the alpha-thrombin-catalyzed conversion of plasma levels of fibrinogen to fibrin in the presence of antithrombin III, *J Biol Chem 266*, 13003-13010.

53. Anderson, P. J., Nesset, A., Dharmawardana, K. R., and Bock, P. E. (2000) Characterization of proexosite I on prothrombin, *J Biol Chem 275*, 16428-16434.

54. Grutter, M. G., Priestle, J. P., Rahuel, J., Grossenbacher, H., Bode, W., Hofsteenge, J., and Stone, S. R. (1990) Crystal structure of the thrombin-hirudin complex: a novel mode of serine protease inhibition, *Embo J 9*, 2361-2365.

55. Hofsteenge, J., Taguchi, H., and Stone, S. R. (1986) Effect of thrombomodulin on the kinetics of the interaction of thrombin with substrates and inhibitors, *Biochem J 237*, 243-251.

56. Bezeaud, A., Denninger, M. H., and Guillin, M. C. (1985) Interaction of human alpha-thrombin and gamma-thrombin with antithrombin III, protein C and thrombomodulin, *Eur J Biochem 153*, 491-496.

57. Ye, J., Liu, L. W., Esmon, C. T., and Johnson, A. E. (1992) The fifth and sixth growth factor-like domains of thrombomodulin bind to the anion-binding exosite of thrombin and alter its specificity, *J Biol Chem 267*, 11023-11028.

58. Fuentes-Prior, P., Iwanaga, Y., Huber, R., Pagila, R., Rumennik, G., Seto, M., Morser, J., Light, D. R., and Bode, W. (2000) Structural basis for the anticoagulant activity of the thrombin-thrombomodulin complex, *Nature 404*, 518-525.

59. Vu, T. K., Wheaton, V. I., Hung, D. T., Charo, I., and Coughlin, S. R. (1991) Domains specifying thrombin-receptor interaction, *Nature 353*, 674-677.

60. Becker, D. L., Fredenburgh, J. C., Stafford, A. R., and Weitz, J. I. (1999) Exosites 1 and 2 are essential for protection of fibrin-bound thrombin from heparin-catalyzed inhibition by antithrombin and heparin cofactor II, *J Biol Chem 274*, 6226-6233.

61. Bode, W., Turk, D., and Karshikov, A. (1992) The refined 1.9-A X-ray crystal structure of D-Phe-Pro-Arg chloromethylketone-inhibited human alpha-thrombin: structure analysis, overall structure, electrostatic properties, detailed

active-site geometry, and structure-function relationships, *Protein Sci 1*, 426-471.

62. Gan, Z. R., Li, Y., Chen, Z., Lewis, S. D., and Shafer, J. A. (1994) Identification of basic amino acid residues in thrombin essential for heparin-catalyzed inactivation by antithrombin III, *J Biol Chem 269*, 1301-1305.

63. Ciaccia, A. V., Willemze, A. J., and Church, F. C. (1997) Heparin promotes proteolytic inactivation by thrombin of a reactive site mutant (L444R) of recombinant heparin cofactor II, *J Biol Chem 272*, 888-893.

64. Carter, W. J., Cama, E., and Huntington, J. A. (2005) Crystal structure of thrombin bound to heparin, *J Biol Chem 280*, 2745-2749.

65. Ye, J., Esmon, C. T., and Johnson, A. E. (1993) The chondroitin sulfate moiety of thrombomodulin binds a second molecule of thrombin, *J Biol Chem 268*, 2373-2379.

66. Liu, L. W., Rezaie, A. R., Carson, C. W., Esmon, N. L., and Esmon, C. T. (1994) Occupancy of anion binding exosite 2 on thrombin determines Ca2+ dependence of protein C activation, *J Biol Chem 269*, 11807-11812.

67. Myles, T., Yun, T. H., Hall, S. W., and Leung, L. L. (2001) An extensive interaction interface between thrombin and factor V is required for factor V activation, *J Biol Chem 276*, 25143-25149.

68. Myles, T., Yun, T. H., and Leung, L. L. (2002) Structural requirements for the activation of human factor VIII by thrombin, *Blood 100*, 2820-2826.

69. Zingali, R. B., Jandrot-Perrus, M., Guillin, M. C., and Bon, C. (1993) Bothrojaracin, a new thrombin inhibitor isolated from Bothrops jararaca venom: characterization and mechanism of thrombin inhibition, *Biochemistry 32*, 10794-10802.

70. Monteiro, R. Q., Raposo, J. G., Wisner, A., Guimaraes, J. A., Bon, C., and Zingali, R. B. (1999) Allosteric changes of thrombin catalytic site induced by interaction of bothrojaracin with anion-binding exosites I and II, *Biochem Biophys Res Commun 262*, 819-822.

71. Di Cera, E. (2003) Thrombin interactions, *Chest 124*, 11S-17S.

72. Hedstrom, L. (2002) Serine protease mechanism and specificity, *Chem Rev 102*, 4501-4524.

73. Carter, P., and Wells, J. A. (1988) Dissecting the catalytic triad of a serine protease, *Nature 332*, 564-568.

74. Di Cera, E., Dang, Q. D., and Ayala, Y. M. (1997) Molecular mechanisms of thrombin function, *Cell Mol Life Sci 53*, 701-730.

75. Esmon, C. T. (1989) The roles of protein C and thrombomodulin in the regulation of blood coagulation, *J Biol Chem 264*, 4743-4746.

76. Wen, D. Z., Dittman, W. A., Ye, R. D., Deaven, L. L., Majerus, P. W., and Sadler, J. E. (1987) Human thrombomodulin: complete cDNA sequence and chromosome localization of the gene, *Biochemistry 26*, 4350-4357.

77. Vindigni, A., White, C. E., Komives, E. A., and Di Cera, E. (1997) Energetics of thrombin-thrombomodulin interaction, *Biochemistry 36*, 6674-6681.

78. Walker, F. J. (1980) Regulation of activated protein C by a new protein. A possible function for bovine protein S, *J Biol Chem 255*, 5521-5524.

79. Walker, F. J. (1981) Regulation of activated protein C by protein S. The role of phospholipid in factor Va inactivation, *J Biol Chem 256*, 11128-11131.

80. Harris, K. W., and Esmon, C. T. (1985) Protein S is required for bovine platelets to support activated protein C binding and activity, *J Biol Chem 260*, 2007-2010.

81. Stern, D. M., Nawroth, P. P., Harris, K., and Esmon, C. T. (1986) Cultured bovine aortic endothelial cells promote activated protein C-protein S-mediated inactivation of factor Va, *J Biol Chem 261*, 713-718.

82. Kelton, J. G., Sheridan, D., Santos, A., Smith, J., Steeves, K., Smith, C., Brown, C., and Murphy, W. G. (1988) Heparin-induced thrombocytopenia: laboratory studies, *Blood 72*, 925-930.

83. Amiral, J., Bridey, F., Dreyfus, M., Vissoc, A. M., Fressinaud, E., Wolf, M., and Meyer, D. (1992) Platelet factor 4 complexed to heparin is the target for antibodies generated in heparin-induced thrombocytopenia, *Thromb Haemost 68*, 95-96.

84. Rauova, L., Zhai, L., Kowalska, M. A., Arepally, G. M., Cines, D. B., and Poncz, M. (2006) Role of platelet surface PF4 antigenic complexes in heparin-induced thrombocytopenia pathogenesis: diagnostic and therapeutic implications, *Blood 107*, 2346-2353.

85. Greinacher, A. (2009) Heparin-induced thrombocytopenia, *J Thromb Haemost 7 Suppl 1*, 9-12.

86. Walsmann, P., and Markwardt, F. (1981) [Biochemical and pharmacological aspects of the thrombin inhibitor hirudin], *Pharmazie 36*, 653-660.

87. Sohn, J. H., Kang, H. A., Rao, K. J., Kim, C. H., Choi, E. S., Chung, B. H., and Rhee, S. K. (2001) Current status of the anticoagulant hirudin: its biotechnological production and clinical practice, *Appl Microbiol Biotechnol 57*, 606-613.

88. Haruyama, H., and Wuthrich, K. (1989) Conformation of recombinant desulfatohirudin in aqueous solution determined by nuclear magnetic resonance, *Biochemistry 28*, 4301-4312.

89. Salzet, M., Chopin, V., Baert, J., Matias, I., and Malecha, J. (2000) Theromin, a novel leech thrombin inhibitor, *J Biol Chem 275*, 30774-30780.

90. Nicastro, G., Baumer, L., Bolis, G., and Tato, M. (1997) NMR solution structure of a novel hirudin variant HM2, N-terminal 1-47 and N64-->V + G mutant, *Biopolymers 41*, 731-749.

91. Hoffmann, A., and Markwardt, F. (1984) Inhibition of the thrombin-platelet reaction by hirudin, *Haemostasis 14*, 164-169.

92. Bergmann, C., Dodt, J., Kohler, S., Fink, E., and Gassen, H. G. (1986) Chemical synthesis and expression of a gene coding for hirudin, the thrombin-specific inhibitor from the leech Hirudo medicinalis, *Biol Chem Hoppe Seyler 367*, 731-740.

93. Dodt, J., Schmitz, T., Schafer, T., and Bergmann, C. (1986) Expression, secretion and processing of hirudin in E. coli using the alkaline phosphatase signal sequence, *FEBS Lett 202*, 373-377.

94. de Taxis du Poet, P., Scacheri, E., Benatti, L., Nitti, G., Valsasina, B., and Sarmientos, P. (1991) Production of the HV1 variant of hirudin by recombinant DNA methodology, *Blood Coagul Fibrinolysis 2*, 113-120.

95. Mendoza-Vega, O., Hebert, C., and Brown, S. W. (1994) Production of recombinant hirudin by high cell density fed-batch cultivations of a Saccharomyces cerevisiae strain: physiological considerations during the bioprocess design, *J Biotechnol 32*, 249-259.

96. Sohn, J. H., Choi, E. S., Chung, B. H., Youn, D. J., Seo, J. H., and Rhee, S. K. (1995) Process development for the production of recombinant hirudin in

Saccharomyces cerevisiae: from upstream to downstream., *Proc Biochem 30*, 653-660.

97. Weydemann, U., Keup, P., Piontek, M., Strasser, A. W., Schweden, J., Gellissen, G., and Janowicz, Z. A. (1995) High-level secretion of hirudin by Hansenula polymorpha--authentic processing of three different preprohirudins, *Appl Microbiol Biotechnol 44*, 377-385.

98. Rosenfeld, S. A., Nadeau, D., Tirado, J., Hollis, G. F., Knabb, R. M., and Jia, S. (1996) Production and purification of recombinant hirudin expressed in the methylotrophic yeast Pichia pastoris, *Protein Expr Purif 8*, 476-482.

99. Radzio, R., and Kuck, U. (1997) Efficient synthesis of the blood-coagulation inhibitor hirudin in the filamentous fungus Acremonium chrysogenum, *Appl Microbiol Biotechnol 48*, 58-65.

100. Benatti, L., Scacheri, E., Bishop, D. H., and Sarmientos, P. (1991) Secretion of biologically active leech hirudin from baculovirus-infected insect cells, *Gene 101*, 255-260.

101. Skern, T., Bischoff, R., Jallat, S., Dott, K., Ali-Hadji, D., Clesse, D., Kieny, M. P., and Courtney, M. (1990) Sulphation of hirudin in BHK cells, *FEBS Lett 275*, 36-38.

102. Parmenter, D. L., Boothe, J. G., van Rooijen, G. J., Yeung, E. C., and Moloney, M. M. (1995) Production of biologically active hirudin in plant seeds using oleosin partitioning, *Plant Mol Biol 29*, 1167-1180.

103. Chaudhary, S., Parmenter, D. L., and Moloney, M. M. (1998) Transgenic Brassica carinata as a vehicle for the production of recombinant proteins in seeds., *Plant Cell Rep 17*, 195-200.

104. Giddings, G., Allison, G., Brooks, D., and Carter, A. (2000) Transgenic plants as factories for biopharmaceuticals, *Nat Biotechnol 18*, 1151-1155.

105. Greinacher, A., and Warkentin, T. E. (2008) The direct thrombin inhibitor hirudin, *Thromb Haemost 99*, 819-829.

CHAPTER 2

COPPER TRAFFICKING PATHWAYS

Copper is scrupulously regulated in cells (*1, 2*). It is used for many different processes such as redox activites (i.e. superoxide dismutase) (*3*) and respiration (i.e. cytochrome c oxidase) (*5, 6*), and iron transport (i.e. Fet3) (*7*). However disruptions in copper homeostasis can lead to problems such as Wilson's or Menkes disease, where copper is not regulated properly in the cells (*9*).

$$2Cu(I) \rightarrow Cu(II) + Cu(0)$$

$$O_2^{-\bullet} + Cu(II) \rightarrow O_2 + Cu(I)$$

$$Cu(I) + H_2O_2 \rightarrow Cu(II) + OH^- + OH^\bullet$$

$$\text{Overall Fenton Reaction: } O_2^{-\bullet} + H_2O_2 \rightarrow O_2 + OH^- + OH^\bullet$$

Figure 2.1: Chemical equations illustrating how copper(I) can disproportionate into the highly oxidative copper(II) and further undergo the Fenton reaction to make a highly reactive hydroxide radical.

2.1 Importance of Copper in Cells

Copper is moved through the cells in a very precise, well defined manner, and is important for many processes. It is also very toxic to cells in its unbound form, as it can create reactive oxygen species (ROS), as well as hydroxyl radicals (*10*). ROS can cause damage to a lot of different components of the cell, such as DNA, lipids, and proteins (*11*). Copper creates ROS by disproportionating in the cells to form copper(II) and copper(0), which the copper(I) can then undergo the Fenton reaction to create what is called a hyperactive hydroxide radical (*12*) (**Figure 2.1**).

This is very harmful to the cells and has been shown to lead to cancer (*13, 14*). The reason this is harmful is because copper(I) can disproportionate in water to become copper(0) and copper(II). One such defense is the use of superoxide dismutase; this enzyme catalyzes dismutation of superoxide radicals($O_2^{\bullet -}$) to molecular oxygen and peroxide (*15*). Another way the cells protect themselves from copper-induced ROS is by making sure there is little to no free copper. In the cells most all of the copper is either bound in proteins, bound by the glutathione within the cytosol (*16*), and possibly a copper chelator found in the mitochondria (*17, 18*).

2.2 Copper Movement Through Cells

While there is a fine line between copper being a benefit or a detriment, the cells have worked out very intricate mechanisms and storage procedures for making

sure the cells can use the copper yet not be destroyed by it (**Figure 2.2**).

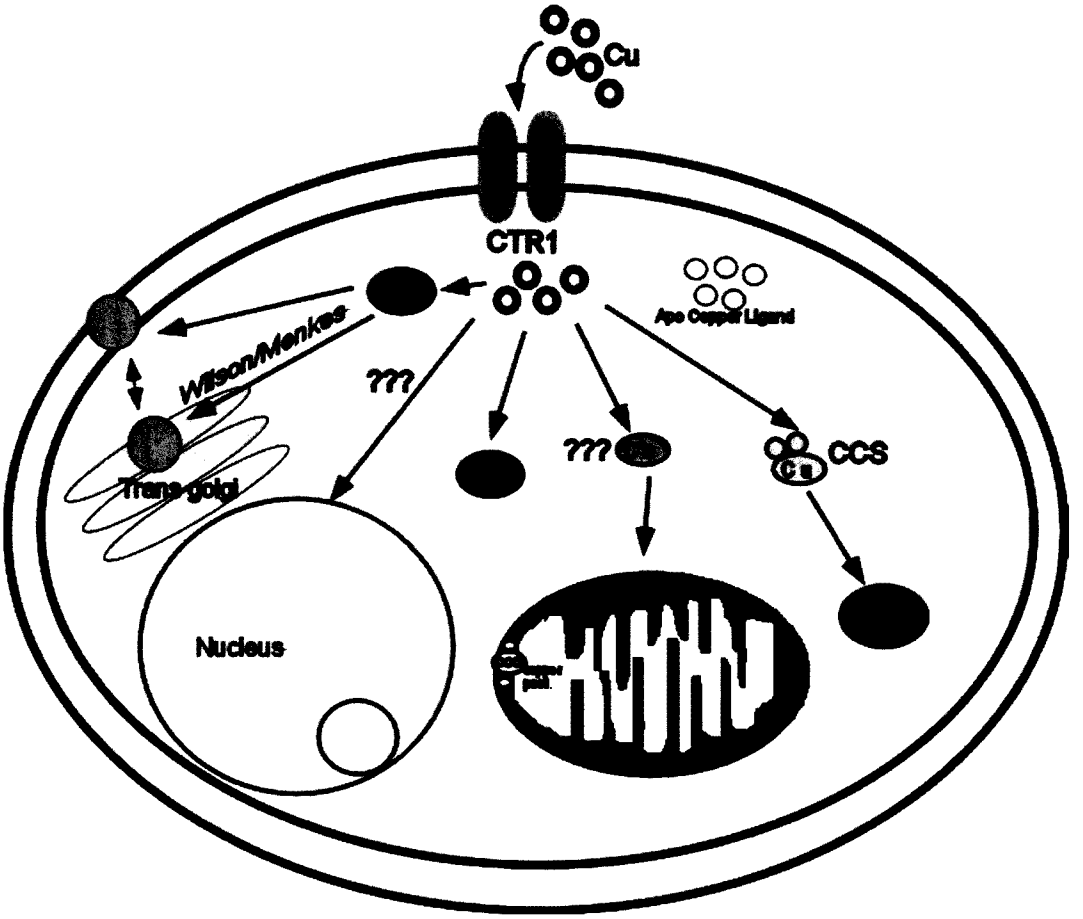

Figure 2.2: Illustration describing the different fates for copper (*1, 18-21*).

Copper is first reduced from copper(II) to copper(I) by a metalloreductase outside the cell either as the metal is transferred into the cell or just before by proteins encoded by *Fre1-7* genes (*22-24*). The copper is moved into the cell by a high affinity permease-like protein, Ctr1 (*25*). Ctr1 utilizes its methionine rich structure to move the copper through it into the cytosol (*25, 26*). Once in the cytosol, copper is picked up by several different molecues: CCS (*27, 28*), HAH1 (*29-31*), metallothioneins

(*19*), glutathione (*32*), and likely a few undiscovered transport proteins. CCS is a direct target for Cu/Zn superoxide dismutase, most often under copper limiting conditions (*27*). The HAH1 binds copper and delivers it to either Wilson disease protein (*33*) or Menkes protein (*34*). These two latter proteins are used by cells to either remove excess copper or move more copper into the cells respectively. There are some low molecular weight molecules found in the cytoplasm that bind up copper for storage and/or delivery to other proteins; for example the copper ligand found in the mitochondria is found in the apo state in the cytosol binding up copper to take back to the mitochondria for storage (*1, 35*). Finally, glutathione is found in cells at up to 5mM, and has an affinity for copper(I) in the millimolar range (*32*). This is very important, as described previously, because copper is toxic to the cells due to disproportionation and subsequent superoxide formation. Inside the cells, there is no free copper in solution (*36*).

There is one other compartment where copper is found, the mitochondria (*1, 35*). It has recently been shown that the mitochondria have its own pool of copper that it uses to create the various cofactors involved in cytochrome c oxidase assembly. The copper pool isn't just free copper, it is a pool of ligated copper by a small molecular weight molecule, similar to that of methanobactin (*1, 35*). It is believed this ligand could possibly act as the siderophores do for iron by leaving the mitochondria to find copper and bring it back.

2.2.1 Ctr1 Proteins

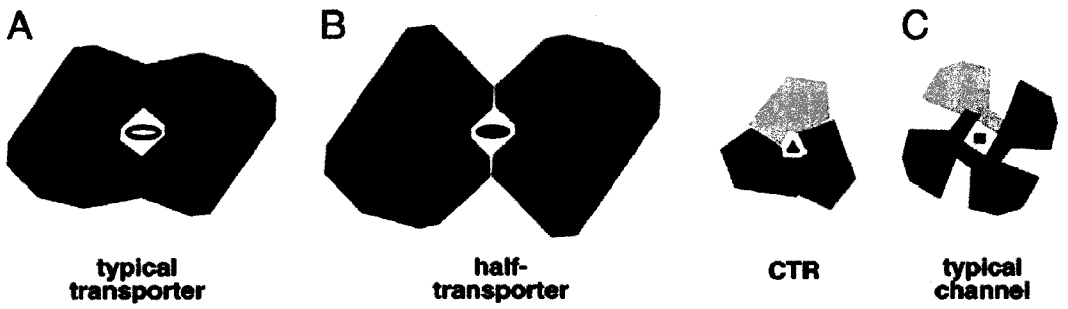

Figure 2.3: Predicted 2D representations of different types of proteins that move things across membranes. The Ctr protein family is a mix of a transporter and a channel.

Human Ctr1 is an integral transmembrane protein containing a trimer of 23 kDa monomers each containing three alpha helices (*37-39*). Data predicts this oligomerization is necessary for transport of copper into the cells, and that the interface between the tri-helices is important for copper transport (*37*). Ctr1 is very interesting in that it doesn't behave like a typical transporter or a channel. Unger *et. al.* (2006) showed structurally that this protein is novel in its structure, making it difficult to put it in a proper class of transporters. This work was done by cry-electron crystallography on 2D crystals in native phospholipid bilayers (**Figure 2.3**) (*37*).

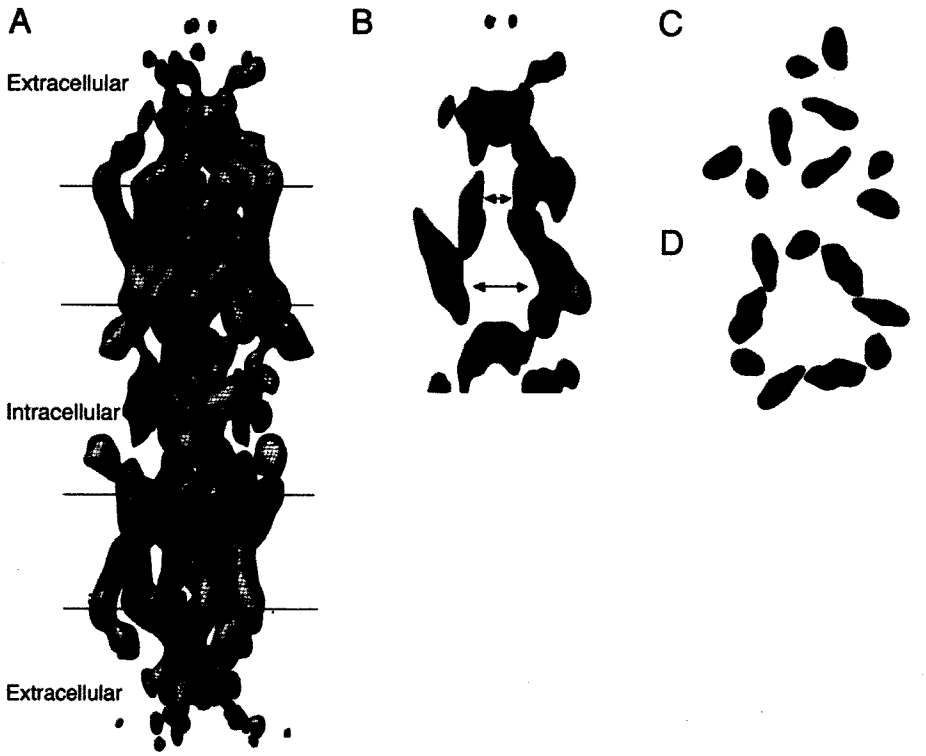

Figure 2.4: A.) A dimer of trimers showing the Ctr1 as it spans the membrane. B.) A slice through the structure in A. C.) and D.) is a longitudinal slice of the extracellular and intracellular portion respectively(*8*).

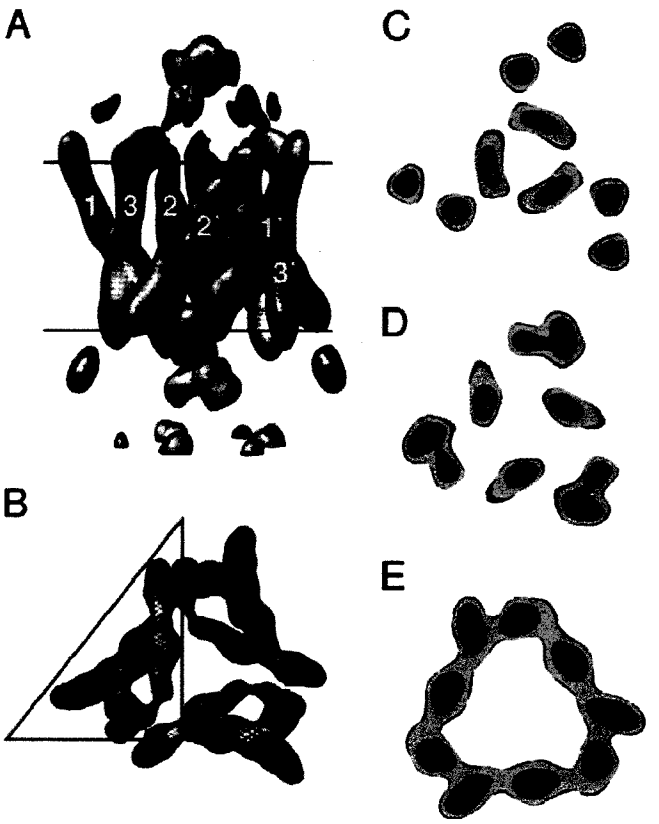

Figure 2.5: A and B show helix alignment of the helices that compose Ctr1. C-D is looking down the 3-fold axis from the extracellular, middle and intracellular portions, the pore forms a cone shape (*8*).

Unger described, as **Figure 2.3** depicts, that Ctr is a combination transporter and channel. Another interesting feature of this protein is that its transport is "passive", in that it doesn't require ATP to provide energy for the process. This could account for previous observations that transport is a slow process for this protein and there is a low turnover rate. More recently Unger *et. al.* determined a projected 3-dimensional structure of this protein (**Figure 2.4** and **2.5**). As determined previously, there are several residues residing in the second transmembrane domain that are important for copper transport. Structurally, however, there are three main

features of this protein: I. the extracellular N-terminal domain containing two regions rich in histidines and two met motifs containing many methionines arranged as either MXM or MXXM (*40, 41*), where the M2 region (MMMMPM) is imperative for copper uptake in limiting conditions (*26, 41-43*), II. Three monomeric triple helical structures (TM1-TM3) forming a "pore" in the lipid bilayer for transport and III. The C-terminal tail containing cysteines that have been shown, at least in yeast, to bind copper and be able to directly hand it to both Atx1 (copper chaperone) and Ccc2 (copper ATPase) (*4*) (**Figure 2.6**).

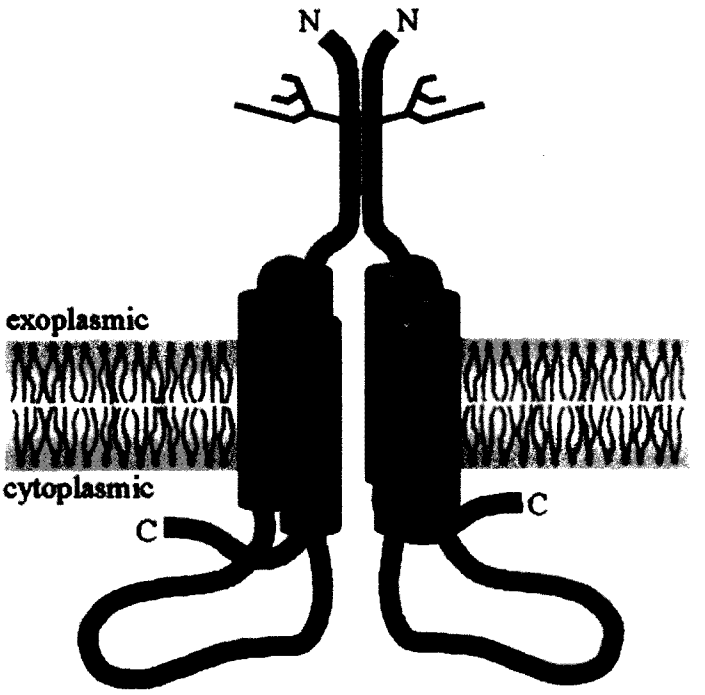

Figure 2.6: Cartoon representation of the Ctr1 (*4*).

The interactions of the C-terminus is very important to understand what the fate of copper is when it comes into the cells (*4*). As previously mentioned, copper can be transferred *in vitro* from the C-terminus to the Atx1 (*44*). This is a crucial relationship because there is no copper free in solution, so copper has to be transferred from one protein to another with an affinity gradient sufficient to keep it moving toward its target (*32*). It has been shown however the glutathione in the cell has a millimolar affinity for copper, but compared to chaperones like HAH1, having an affinity in the femtomolar range, it is not a competitor; however other reductants such as dithiothreitol (DTT) and tris(2-carboxyethyl)phosphine (TCEP) have very high affinities for copper(I) and must be removed from solution prior to experiments

(*45*). Glutathione may protect the copper by providing a third ligand to help protect the copper until it reaches its target (*16*). Data has shown that glutathione is able to transfer copper to many metalloproteins such as the copper metallothioneins (*16, 46, 47*). Data also has shown that glutathione can act as a ligand to Cu(I)HAH1 which in turn helps maintain it in a 2-coordinate state (*48*). HAH1 is the next step in the journey the copper takes to reach its final destination. HAH1 is one of a few metallochaperones that shuttle copper around the cells.

2.2.2 Copper Chaperone for Wilson Disease Protein (HAH1)

Once inside the cells, the targets for copper aren't sufficiently close spatially to the Ctr1 to directly receive the copper. For this reason chaperones are needed to move the copper to its final destination. Many of the copper chaperones have been shown to move more many different metals, and their structures have been elucidated. For instance, HAH1 has been shown to bind platinum (as cisplatin) (*49*), mercury(II) (*34, 50*), copper(I) (*34, 50*), silver(I) (*50*), and cadmium(II) (*34, 50*). This seems to be a crucial role for these chaperones to have as a few of these metals have detrimental effects on the cells.

2.2.2.1 Human Atox1: HAH1

HAH1 is a 68 amino acid protein that is responsible for delivering copper(I) to the domains of both the Wilson disease protein and the Menkes protein (*33, 34*). It has subfemtomolar affinity for copper(I) (*45, 51*). The very close similarity of these values indicates the handing off of copper is kinetically controlled rather than

thermodynamically controlled. HAH1 was discovered by screening cDNA libraries for a human homolog to the yeast Atx1 protein (*30*). What was discovered was a protein with approximately 47% homology. The structure of HAH1 contains a ferridoxin-like fold and a conserved metal binding motif, MXCXXC (*29*). Data also suggested this MXCXXC motif was used for binding copper(I) in cells. Interestingly it was also discovered that mutations in the metal-binding cysteines had a dramatic effect on Fet3 copper(I) incorporation. The C12G mutations had a dramatic effect on the amount of copper that could be incorporated into the Fet3, whereas the C15G mutations had little effect (*29*).

Earlier work using a yeast two hybrid study showed Atx1, the yeast homolog to HAH1, can deliver copper(I) to Ccc2p, the yeast homolog to both the Wilson disease protein and the Menkes protein (*33, 52*). Since these two proteins have a lot of homology to the respective human proteins, it serves to expect they interact in much the same way. There have been several studies that indicate HAH1 interacts with the domains of the two ATPases in a copper-dependent manner via the MXCXXC motif (*33, 53-56*).

To date there many structures, both by X-ray crystallography and NMR of various forms of HAH1. Hg(II)HAH1, Cd(II)HAH1, and Cu(I)HAH1 structures have

Figure 2.7: Model of CuHAH1 depicting the copper bound to the two cysteines of HAH1 (*57*).

all been solved by x-ray crystallography (*34*). However, Cu(I)HAH1 and apoHAH1 structures have been solved by NMR (*57*). In this dissertation the structures of the apo and copper-bound (**Figure 2.7**) solution structures and the mercury(II)-bound structures (**Figure 2.8**) are most important.

The solution structures of Cu(I)HAH1 indicate a copper bound monomer, which is markedly different from the structure determined by X-ray crystallography in that the Cu(I)HAH1 forms a copper-bridged dimer (*57*). This could just be due to a difference in technique for measuring the proteins. It was also noted that even when copper was bound the ferridoxin-like (βαββαβ) fold wasn't changed and there were very small rearrangements in the structure (*57*).

Previous work indicated that MerP, a mercury binding protein, contained the same metal binding motif as HAH1 does, and binds mercury(II) a 2-coordinate nature

Figure 2.8: Model of the Hg(II)HAH1 homodimer determined by X-ray crystallography (*34*).

(*58*). So it would be a natural assumption it could bind to HAH1. Data indicates that Hg(II)HAH1 is found in a dimerized state with a supposed distorted 4-coordinate Hg(II)-S species. The fourth coordinate was noted to be a longer distance than is required for a covalent bond to the metal (*34*).

2.2.3 Wilson Disease Protein and Interactions with Cu(I)HAH1

Wilson's disease is an autosomal recessive disorder that affects 1 in 30,000 people. The disease leads to accumulation of copper in the kidney, liver, brain and eyes (*59*). Due to the detriment to the body when copper is in excess, many

researchers have set out to understand how this protein functions so that more targeted therapies can be discovered.

2.2.3.1 Wilson Disease Protein (WLNP)

Wilson disease protein is a 1465 residue P_{1B}-type ATPase that utilizes ATP to move copper out of the cytoplasm of the cells (*60*). Wilson disease protein has a unique N-terminal tail made of six repeating units that can bind up to six equivalents of copper(I) (*56*). This tail can bind a host of different heavy metals, Hg(II), Zn(II), Cu(I), Cd(II), Fe(III), and Au(III) with different affinities (*55, 61-63*). The affinities were determined by using a radio labeled zinc (^{65}Zn) to do competition assays. The values of the affinities weren't described in this work, except for the fact that the trend in affinities was Cu(I)>>Cu(II)>>Zn(II)>>Ni(II)>>Co(II) and did not have any binding to either Fe(II) or Fe(III) (*55*).

There are four main domains on this protein: the 6 metal binding domains with the ability to accept one copper(I) each, 8 transmembrane helices that creates the pore for copper transport across the membrane, an actuator domain, and an ATP/phosphorylation domain containing a nucleotide binding domain and a phosphatase domain (*64*).

During copper homeostasis, the Wilson disease protein is localized in the trans-Golgi network where it can deliver copper to pertinent copper containing proteins such as ceruloplasmin. Then as the concentration of copper is increased to potentially toxic levels, it reversibly relocalizes to the plasma membrane or a storage vescicle (*65-67*).

Wilson disease protein's unique feature, as previously noted, is its approximately 650 residue N-terminal domain. This domain contains 6 homologous monomers that contain the metal-binding motif GMT(H)CXXC, the histidine residue replaces the threonine residue in domain 3, and each monomer can bind one equivalent of copper(I) (*51, 55, 56, 63, 68, 69*) . To date, constructs of WLN3-4 (*70*), WLN5-6 (*71*), WLN4 (*71, 72*), WLN2 (*73*), WLN1-6 (*74*) and most recently WLN4-6 (*75*) have been investigated. Of the constructs currently only the WLN3-4 and WLN5-6 have NMR structures.

WLN3-4 was unique in that the domain 3 and domain 4 acted independently of each other (*70, 71*), which was in contrast to the WLN5-6 that acts as a unit (*71*). Data also suggested that WLN3-4 aggregated in a concentration dependent manner, noted by a decrease in tumbling times with a decrease in WLN3-4 concentration. An interesting feature of the aggregation issue was that there were no detectable changes in NOEs with changes in concentration, so the authors suggested it was just due to random interactions with different patches on the construct. When copper(I) was added the aggregation was still present, illustrated by higher tumbling correlation times than would be expected for a single construct in solution (*57*). Consistent with the previous note that the domains act independently was the observation that copper loading prevented WLN4 from interacting with another WLN4 molecule, but didn't have any effect on the aggregation characteristics of WLN3.

Metal binding studies were also completed on the WLN3-4 construct. The data suggested that when copper was titrated in at substochiometric concentrations,

there were detectable changes in the ^{1}H-^{15}N HSQC for both domains. This was consistent with similar binding affinities for copper, which were determined to be: $(6.3\pm3.2)x10^{10}$ for WLN3 and $(2.5\pm1.3)x10^{10}$ for WLN4 (*69, 70*). The affinities were measured based on the bicinchoninic acid (BCA) assay. This assay takes into account the appearance of a distinctive red color that appears upon binding of copper(I) to it. Once measured, a program is used to determine the affinity constants. **Table 2.1** contains the measured affinities for copper by each of the WLNP domains and HAH1. Chemical shifts in the HSQC were also noted only for the metal binding region, indicating no changes in the folding of the domains upon metal binding.

Table 2.1: Tabulated values for copper affinities for the different metal-binding domains of Wilson disease protein and its copper chaperone, HAH1 (*69*).

Peptide:	Affinity constant, K_{Cu}, M^{-1}:
WLN1	$2.6\pm1.5 \times 10^{10}$
WLN2	$3.5\pm0.9 \times 10^{10}$
WLN3	$6.3\pm3.2 \times 10^{10}$
WLN4	$2.5\pm1.3 \times 10^{10}$
WLN5	$2.2\pm1.0 \times 10^{10}$
WLN6	$5.8\pm2.5 \times 10^{10}$
HAH1	$3.5\pm1.0 \times 10^{10}$

Finally interaction with Cu(I)HAH1 was investigated. NMR data showed chemical shifts in the metal binding region in both the domains even at substochiometric Cu(I)HAH1. Again this suggests Cu(I)HAH1 has similar affinities for both domains. However, one unique characteristic was the fact that in WLN4 there were peaks in the HSQC that appeared while others disappeared as Cu(I)HAH1 concentration was increased. This was in contrast to what happened to the WLN3 construct where no peaks seemed to disappear, but rather, a new peak appeared and increased with increasing Cu(I)HAH1 concentrations, this suggests there is slow exchange phenomenon in the case of WLN3, suggesting there is no complex formation. WLN4, however, could make a complex with Cu(I)HAH1 that increased as more Cu(I)HAH1 was added (a fast exchange phenomenon was observed), but

WLN3 seemed to accept the Cu(I) from HAH1, rather than form an NMR detectable complex, consistent with a new set of peaks that just increased in intensity. These data further strengthen the idea that WLN3 is unique and independent, at least compared to WLN4. The character of these domains is quite different from the WLN5-6 construct that acts as a tandem unit. This may be expected because they are spatially close together with somewhat of a longer linker region separating them from the WLN1-4.

WLN5-6 has been shown to exhibit the same ferridoxin folds as the WLN3-4 construct has, and was determined to be a rigid unit that tumbles together (*71*). With the rigidity of this structure comes the feature that there can be no metal transfer between WLN5 and WLN6. The tumbling correlation time for the WLN5-6 was measured to be 9.1±0.6 ns, which was consistent with twice the tumbling correlation time for a single WLN6 in solution, as well as what would be expected for a protein of approximately 16 kDa in size.

Further studies investigated the interaction of the WLN5-6 with both copper and with Cu(I)HAH1. WLN5-6 can bind two equivalents of copper, and consistent with the WLN3-4 construct, the folding of the domains were unaltered, described by chemical shifts in the HSQC spectrum localized to the metal binding regions. However, interestingly, when Cu(I)HAH1 was titrated in, there was no copper transfer to WLN5-6, indicated by lack of chemical shifts in the HSQC spectrum. Previous work by Larin *et. al.* using a yeast two hybrid technique showed that HAH1 interacted with many various combinations of domains, but not with WLN5 or WLN6

(*53*). So this work was further supported biophysically through the NMR experiments.

In light of this lack of interaction between Cu(I)HAH1 and WLN5-6, Cu(I)WLN4 was titrated into the WLN5-6. The data showed ~10% of the copper was transferred to WLN6 and almost nothing to WLN5. As the concentration of Cu(I)WLN4 was increased, more of the WLN6 was coordinated, and some of the WLN5. The data suggested copper(I) transfer, but did not indicate any detectable complex formation. These data suggest there are multiple roles of these domains, for example previous work has shown WLN2 and WLN4 are the primary targets for Cu(I)HAH1 (*53, 54, 73*), whereas this and other work suggest WLN5 and WLN6 must acquire copper from the other domains (*53, 71*). These data support the need for six metal binding domains, as it is a way to regulate and possibly detect the copper conditions in the cell.

There has also been work on a couple of the single domains, WLN2 and WLN4. These two domains seem to be the primary targets for Cu(I)HAH1 (*53, 54, 71, 76*). Previous work on WLN2 indicated it was the primary target for Cu(I)HAH1 and could possibly transfer copper to other domains. These observations are not congruent the work published to date. This indicates, at least in the whole WLN1-6 construct, all the domains can receive copper directly from Cu(I)HAH1 (*73*). Walker *et. al.* indicated that when the cysteines of the WLN2 was mutated, that destroyed the binding of copper to the rest of the protein. This observation is in stark contrast to the rest of the data for the WLNP. They suggested it was because of the folding of the

protein in solution which blocks access of Cu(I)HAH1 to the other domains. This also seems to contradict the latest data for Cu(I)HAH1 interaction with WLNP by NMR studies (*74*). Bertini's group showed that Cu(I)HAH1 could indeed interact with all of the 6 domains, which makes the story even more complicated because that is inconsistent with the WLN5-6 data. This raises the question as to how physiologically relavent is work on single or multiple domains that don't contain the whole construct. Achila *et. al.* showed that there is an interaction between WLN2 and Cu(I)HAH1 which supports previous data, as there were chemical shifts that increased as the Cu(I)HAH1 concentration was increased, as well as some broadening that occurred further indicating complex formation. It seems to be the consensus WLN2 is a target of Cu(I)HAH1, but what happens following that interaction is still to be fully elucidated.

Further work has been done on the single domain WLN4. This domain showed an increase in the amount of complex formation as compared to WLN2. This was indicated by the difference in tumbling correlation times; 5.5±0.4 ns for HAH1 bound to the WLN2 via copper and 7.2±0.7 ns for the same bound to WLN4. The higher tumbling correlation time indicates a higher amount of complex formation. A suggestion for this would be the electrostatic differences between WLN4 and WLN2 compared to and HAH1. WLN4 is highly negative and HAH1 is highly positive, suggesting at least a partial electrostatically strengthened interaction which would yield a higher amount of complex formation.

WLN4 seems very interesting in how it interacts with HAH1 as it forms a strong complex. The strength of the complex makes it a good candidate for elucidating a model for copper hand off. Rodriguez-Granillo *et. al.* used computer modeling to try and understand a potential mechanism for delivery of copper (*76*). Their data indicated that a 3-coordinate intermediate was energetically more stable than a 2-coordinate or 4-coordinate intermediate. They suggested also that there are two 3-coordinate species that exists during the hand off. Current work in this project investigates the likelihood of this being the case *in vitro.*

As mentioned previously, the Bertini groups data on the WLN1-6 was inconsistent with the WLN2 study and the WLN5-6 study. The WLN2 study indicated that WLN2 interaction was necessary for copper delivery to the different domains, at least when all six were intact, due to domains being blocked by the folding of the domains around each other. The WLN5-6 work showed there was no interaction between Cu(I)HAH1 and the WLN5-6; this too is in contrast to what the Bertini group has discovered. This again leaves the question as to consistency of construct formations because there is a lot of data that contradicts some of the ideas that have become dogmas in the Wilson protein field.

The NMR study of the WLN1-6 indicated a complex formation between Cu(I)HAH1 and WLN1, WLN2, and WLN4 (*74*). The other three domains, however, only exhibited copper transfer, and no complex formation could be observed. They also found there was no need for WLN1, WLN2, and WLN4 in order to transfer copper to the WLN3, WLN5, and WLN6 domains. This is important because some

previous data had suggested at least WLN2 was necessary for mediating copper addition to the other domains. In parallel to these findings, they didn't find any interaction of Cu(I)HAH1 with any of the domains where the cysteines were mutated to alanines, further showing that the interaction of Cu(I)HAH1 with the metal binding domains is metal-mediated, and not electrostatic for example.

Most recently, there was work done on the interaction of WLN4-6 involving interaction with Cu(I)HAH1 (*75*). This was an NMR study that seemed to show many things that are quite different from what has been published thus far. The first was that there was interaction of HAH1 with the domains in the absence of copper(I). This is contradictory to the work by Bertini's group where they mutated the cysteines to alanines and did not see any complex formation. This idea will be discussed further in the results section, as the NMR titrations performed in this project showed no interactions in the absence of copper. The data further suggested independent mobility of the 3 domains, which is counterintuitive to the idea that WLN56 acts as a unit. This data is very contrary to what has already been published and will need to be investigated further to understand what exactly is going on with these domains.

2.3 References

1. Leary, S. C., Winge, D. R., and Cobine, P. A. (2009) "Pulling the plug" on cellular copper: the role of mitochondria in copper export, *Biochim Biophys Acta 1793*, 146-153.

2. Pena, M. M., Koch, K. A., and Thiele, D. J. (1998) Dynamic regulation of copper uptake and detoxification genes in Saccharomyces cerevisiae, *Mol Cell Biol 18*, 2514-2523.

3. Galaleldeen, A., and Hart, P. J. (2007) Human Copper-Zinc Superoxide Dismutase and Familial Amyotrophic Lateral Sclerosis *Protein Reviews 6*, 327-344.

4. Xiao, Z., Loughlin, F., George, G. N., Howlett, G. J., and Wedd, A. G. (2003) C-Terminal Domain of the Membrane Copper Transporter Ctr1from Saccharomyces cerevisiae Binds Four Cu(I) Ions as a Cuprous-Thiolate Polynuclear Cluster: Sub-femtomolar Cu(I) Affinity of Three Proteins Involved in Copper Trafficking, *J Amer Chem Soc 126*, 3081-3090.

5. Yoshikawa, S. (2002) Cytochrome c oxidase, *Adv Protein Chem 60*, 341-395.

6. Ostermeier, C., Iwata, S., and Michel, H. (1996) Cytochrome c oxidase, *Curr Opin Struct Biol 6*, 460-466.

7. Askwith, C., Eide, D., Van Ho, A., Bernard, P. S., Li, L., Davis-Kaplan, S., Sipe, D. M., and Kaplan, J. (1994) The FET3 gene of S. cerevisiae encodes a multicopper oxidase required for ferrous iron uptake, *Cell 76*, 403-410.

8. De Feo, C. J., Aller, S. G., Siluvai, G. S., Blackburn, N. J., and Unger, V. M. (2009) Three-dimensional structure of the human copper transporter hCTR1, *Proc Natl Acad Sci U S A 106*, 4237-4242.

9. Sarkar, B. (1999) Treatment of Wilson and menkes diseases, *Chem Rev 99*, 2535-2544.

10. Halliwell, B., and Gutteridge, J. M. (1984) Oxygen toxicity, oxygen radicals, transition metals and disease, *Biochem J 219*, 1-14.

11. Apel, K., and Hirt, H. (2004) Reactive oxygen species: metabolism, oxidative stress, and signal transduction, *Annu Rev Plant Biol 55*, 373-399.

12. McCord, J. M., and Day Jr., E. D. (1977) Superoxide-dependent Production of Hydroxyl Radical Catalyzed by Iron-EDTA Complex, *FEBS Lett 86*, 139-142.

13. Toyokuni, S., Okamoto, K., Yodoi, J., and Hiai, H. (1995) Persistent oxidative stress in cancer, *FEBS Lett 358*, 1-3.

14. Waris, G., and Ahsan, H. (2006) Reactive oxygen species: role in the development of cancer and various chronic conditions, *J Carcinog 5*, 14.

15. McCord, J. M., and Fridovich, I. (1969) Superoxide dismutase. An enzymic function for erythrocuprein (hemocuprein), *J Biol Chem 244*, 6049-6055.

16. Freedman, J. H., Ciriolo, M. R., and Peisach, J. (1989) The role of glutathione in copper metabolism and toxicity, *J Biol Chem 264*, 5598-5605.

17. Cobine, P. A., Ojeda, L. D., Rigby, K. M., and Winge, D. R. (2004) Yeast contain a non-proteinaceous pool of copper in the mitochondrial matrix, *J Biol Chem 279*, 14447-14455.

18. Cobine, P. A., Pierrel, F., Bestwick, M. L., and Winge, D. R. (2006) Mitochondrial matrix copper complex used in metallation of cytochrome oxidase and superoxide dismutase, *J Biol Chem 281*, 36552-36559.

19. Pena, M. M., Lee, J., and Thiele, D. J. (1999) A delicate balance: homeostatic control of copper uptake and distribution, *J Nutr 129*, 1251-1260.

20. Robinson, N. J., and Winge, D. R. Copper metallochaperones, *Annu Rev Biochem 79*, 537-562.

21. Harrison, M. D., Jones, C. E., Solioz, M., and Dameron, C. T. (2000) Intracellular copper routing: the role of copper chaperones, *Trends Biochem Sci 25*, 29-32.

22. Georgatsou, E., and Alexandraki, D. (1999) Regulated expression of the Saccharomyces cerevisiae Fre1p/Fre2p Fe/Cu reductase related genes, *Yeast 15*, 573-584.

23. De Silva, D. M., Askwith, C. C., Eide, D., and Kaplan, J. (1995) The FET3 gene product required for high affinity iron transport in yeast is a cell surface ferroxidase, *J Biol Chem 270*, 1098-1101.

24. Shi, X., Stoj, C., Romeo, A., Kosman, D. J., and Zhu, Z. (2003) Fre1p Cu2+ reduction and Fet3p Cu1+ oxidation modulate copper toxicity in Saccharomyces cerevisiae, *J Biol Chem 278*, 50309-50315.

25. Lee, J., Pena, M. M., Nose, Y., and Thiele, D. J. (2002) Biochemical characterization of the human copper transporter Ctr1, *J Biol Chem 277*, 4380-4387.

26. Guo, Y., Smith, K., Lee, J., Thiele, D. J., and Petris, M. J. (2004) Identification of methionine-rich clusters that regulate copper-stimulated endocytosis of the human Ctr1 copper transporter, *J Biol Chem 279*, 17428-17433.

27. Jensen, L. T., and Culotta, V. C. (2005) Activation of CuZn superoxide dismutases from Caenorhabditis elegans does not require the copper chaperone CCS, *J Biol Chem 280*, 41373-41379.

28. Casareno, R. L., Waggoner, D., and Gitlin, J. D. (1998) The copper chaperone CCS directly interacts with copper/zinc superoxide dismutase, *J Biol Chem 273*, 23625-23628.

29. Hung, I. H., Casareno, R. L., Labesse, G., Mathews, F. S., and Gitlin, J. D. (1998) HAH1 is a copper-binding protein with distinct amino acid residues mediating copper homeostasis and antioxidant defense, *J Biol Chem 273*, 1749-1754.

30. Klomp, L. W., Lin, S. J., Yuan, D. S., Klausner, R. D., Culotta, V. C., and Gitlin, J. D. (1997) Identification and functional expression of HAH1, a novel human gene involved in copper homeostasis, *J Biol Chem 272*, 9221-9226.

31. Culotta, V. C., Klomp, L. W., Strain, J., Casareno, R. L., Krems, B., and Gitlin, J. D. (1997) The copper chaperone for superoxide dismutase, *J Biol Chem 272*, 23469-23472.

32. Banci, L., Bertini, I., Ciofi-Baffoni, S., Kozyreva, T., Zovo, K., and Palumaa, P. Affinity gradients drive copper to cellular destinations, *Nature 465*, 645-648.

33. Hamza, I., Schaefer, M., Klomp, L. W., and Gitlin, J. D. (1999) Interaction of the copper chaperone HAH1 with the Wilson disease protein is essential for copper homeostasis, *Proc Natl Acad Sci U S A 96*, 13363-13368.

34. Wernimont, A. K., Huffman, D. L., Lamb, A. L., O'Halloran, T. V., and Rosenzweig, A. C. (2000) Structural basis for copper transfer by the metallochaperone for the Menkes/Wilson disease proteins, *Nat Struct Biol 7*, 766-771.

35. Pierrel, F., Cobine, P. A., and Winge, D. R. (2007) Metal Ion availability in mitochondria, *Biometals 20*, 675-682.

36. Rae, T. D., Schmidt, P. J., Pufahl, R. A., Culotta, V. C., and O'Halloran, T. V. (1999) Undetectable intracellular free copper: the requirement of a copper chaperone for superoxide dismutase, *Science 284*, 805-808.

37. Aller, S. G., and Unger, V. M. (2006) Projection structure of the human copper transporter CTR1 at 6-A resolution reveals a compact trimer with a novel channel-like architecture, *Proc Natl Acad Sci U S A 103*, 3627-3632.

38. Nose, Y., Rees, E. M., and Thiele, D. J. (2006) Structure of the Ctr1 copper trans'PORE'ter reveals novel architecture, *Trends Biochem Sci 31*, 604-607.

39. Zhou, B., and Gitschier, J. (1997) hCTR1: a human gene for copper uptake identified by complementation in yeast, *Proc Natl Acad Sci U S A 94*, 7481-7486.

40. Klomp, A. E., Juijn, J. A., van der Gun, L. T., van den Berg, I. E., Berger, R., and Klomp, L. W. (2003) The N-terminus of the human copper transporter 1 (hCTR1) is localized extracellularly, and interacts with itself, *Biochem J 370*, 881-889.

41. Larson, C. A., Adams, P. L., Blair, B. G., Safaei, R., and Howell, S. B. The role of the methionines and histidines in the transmembrane domain of mammalian copper transporter 1 in the cellular accumulation of cisplatin, *Mol Pharmacol 78*, 333-339.

42. Liang, Z. D., Stockton, D., Savaraj, N., and Kuo, M. T. (2010) Mechanistic Comparison of Human High-Affinity CopperTransporter 1-Mediated Transport between Copper Ion and Cisplatin, *Molecular Pharmacology 76*, 843-853.

43. Eisses, J. F., and Kaplan, J. H. (2002) Molecular characterization of hCTR1, the human copper uptake protein, *J Biol Chem 277*, 29162-29171.

44. Xiao, Z., and Wedd, A. G. (2002) A C-terminal domain of the membrane copper pump Ctr1 exchanges copper(I) with the copper chaperone Atx1, *Chem Commun (Camb)*, 588-589.

45. Xiao, Z., and Wedd, A. G. The challenges of determining metal-protein affinities, *Nat Prod Rep 27*, 768-789.

46. Ferreira, A. M., Ciriolo, M. R., Marcocci, L., and Rotilio, G. (1993) Copper(I) transfer into metallothionein mediated by glutathione, *Biochem J 292 (Pt 3)*, 673-676.

47. Freedman, J. H., and Peisach, J. (1989) Intracellular copper transport in cultured hepatoma cells, *Biochem Biophys Res Commun 164*, 134-140.

48. Ralle, M., Lutsenko, S., and Blackburn, N. J. (2003) X-ray absorption spectroscopy of the copper chaperone HAH1 reveals a linear two-coordinate

Cu(I) center capable of adduct formation with exogenous thiols and phosphines, *J Biol Chem 278*, 23163-23170.

49. Boal, A. K., and Rosenzweig, A. C. (2009) Crystal structures of cisplatin bound to a human copper chaperone, *J Am Chem Soc 131*, 14196-14197.

50. Narindrasorasak, S., Zhang, X., Roberts, E. A., and Sarkar, B. (2004) Comparative analysis of metal binding characteristics of copper chaperone proteins, Atx1 and ATOX1, *Bioinorg Chem Appl*, 105-123.

51. Wernimont, A. K., Yatsunyk, L. A., and Rosenzweig, A. C. (2004) Binding of copper(I) by the Wilson disease protein and its copper chaperone, *J Biol Chem 279*, 12269-12276.

52. Pufahl, R. A., Singer, C. P., Peariso, K. L., Lin, S. J., Schmidt, P. J., Fahrni, C. J., Culotta, V. C., Penner-Hahn, J. E., and O'Halloran, T. V. (1997) Metal ion chaperone function of the soluble Cu(I) receptor Atx1, *Science 278*, 853-856.

53. Larin, D., Mekios, C., Das, K., Ross, B., Yang, A. S., and Gilliam, T. C. (1999) Characterization of the interaction between the Wilson and Menkes disease proteins and the cytoplasmic copper chaperone, HAH1p, *J Biol Chem 274*, 28497-28504.

54. van Dongen, E. M., Klomp, L. W., and Merkx, M. (2004) Copper-dependent protein-protein interactions studied by yeast two-hybrid analysis, *Biochem Biophys Res Commun 323*, 789-795.

55. DiDonato, M., Narindrasorasak, S., Forbes, J. R., Cox, D. W., and Sarkar, B. (1997) Expression, purification, and metal binding properties of the N-terminal domain from the wilson disease putative copper-transporting ATPase (ATP7B), *J Biol Chem 272*, 33279-33282.

56. Lutsenko, S., Petrukhin, K., Cooper, M. J., Gilliam, C. T., and Kaplan, J. H. (1997) N-terminal domains of human copper-transporting adenosine triphosphatases (the Wilson's and Menkes disease proteins) bind copper selectively in vivo and in vitro with stoichiometry of one copper per metal-binding repeat, *J Biol Chem 272*, 18939-18944.

57. Anastassopoulou, I., Banci, L., Bertini, I., Cantini, F., Katsari, E., and Rosato, A. (2004) Solution structure of the apo and copper(I)-loaded human metallochaperone HAH1, *Biochemistry 43*, 13046-13053.

58. Steele, R. A., and Opella, S. J. (1997) Structures of the reduced and mercury-bound forms of MerP, the periplasmic protein from the bacterial mercury detoxification system, *Biochemistry 36*, 6885-6895.

59. Roberts, E. A., and Schilsky, M. L. (2003) A practice guideline on Wilson disease, *Hepatology 37*, 1475-1492.

60. Lutsenko, S., and Kaplan, J. H. (1995) Organization of P-type ATPases: significance of structural diversity, *Biochemistry 34*, 15607-15613.

61. Vulpe, C., Levinson, B., Whitney, S., Packman, S., and Gitschier, J. (1993) Isolation of a candidate gene for Menkes disease and evidence that it encodes a copper-transporting ATPase, *Nat Genet 3*, 7-13.

62. Tanzi, R. E., Petrukhin, K., Chernov, I., Pellequer, J. L., Wasco, W., Ross, B., Romano, D. M., Parano, E., Pavone, L., Brzustowicz, L. M., and et al. (1993) The Wilson disease gene is a copper transporting ATPase with homology to the Menkes disease gene, *Nat Genet 5*, 344-350.

63. Bull, P. C., Thomas, G. R., Rommens, J. M., Forbes, J. R., and Cox, D. W. (1993) The Wilson disease gene is a putative copper transporting P-type ATPase similar to the Menkes gene, *Nat Genet 5*, 327-337.

64. Petrukhin, K., Lutsenko, S., Chernov, I., Ross, B. M., Kaplan, J. H., and Gilliam, T. C. (1994) Characterization of the Wilson disease gene encoding a P-type copper transporting ATPase: genomic organization, alternative splicing, and structure/function predictions, *Hum Mol Genet 3*, 1647-1656.

65. DiDonato, M., Hsu, H. F., Narindrasorasak, S., Que, L., Jr., and Sarkar, B. (2000) Copper-induced conformational changes in the N-terminal domain of the Wilson disease copper-transporting ATPase, *Biochemistry 39*, 1890-1896.

66. Hung, I. H., Suzuki, M., Yamaguchi, Y., Yuan, D. S., Klausner, R. D., and Gitlin, J. D. (1997) Biochemical characterization of the Wilson disease protein and functional expression in the yeast Saccharomyces cerevisiae, *J Biol Chem 272*, 21461-21466.

67. Schaefer, M., and Gitlin, J. D. (1999) Genetic disorders of membrane transport. IV. Wilson's disease and Menkes disease, *Am J Physiol 276*, G311-314.

68. Banci, L., and Rosato, A. (2003) Structural genomics of proteins involved in copper homeostasis, *Acc Chem Res 36*, 215-221.

69. Yatsunyk, L. A., and Rosenzweig, A. C. (2007) Cu(I) binding and transfer by the N terminus of the Wilson disease protein, *J Biol Chem 282*, 8622-8631.

70. Banci, L., Bertini, I., Cantini, F., Rosenzweig, A. C., and Yatsunyk, L. A. (2008) Metal binding domains 3 and 4 of the Wilson disease protein: solution structure and interaction with the copper(I) chaperone HAH1, *Biochemistry 47*, 7423-7429.

71. Achila, D., Banci, L., Bertini, I., Bunce, J., Ciofi-Baffoni, S., and Huffman, D. L. (2006) Structure of human Wilson protein domains 5 and 6 and their interplay with domain 4 and the copper chaperone HAH1 in copper uptake, *Proc Natl Acad Sci U S A 103*, 5729-5734.

72. Bunce, J., Achila, D., Hetrick, E., Lesley, L., and Huffman, D. L. (2006) Copper transfer studies between the N-terminal copper binding domains one and four of human Wilson protein, *Biochim Biophys Acta 1760*, 907-912.

73. Walker, J. M., Huster, D., Ralle, M., Morgan, C. T., Blackburn, N. J., and Lutsenko, S. (2004) The N-terminal metal-binding site 2 of the Wilson's Disease Protein plays a key role in the transfer of copper from Atox1, *J Biol Chem 279*, 15376-15384.

74. Banci, L., Bertini, I., Cantini, F., Massagni, C., Migliardi, M., and Rosato, A. (2009) An NMR study of the interaction of the N-terminal cytoplasmic tail of the Wilson disease protein with copper(I)-HAH1, *J Biol Chem 284*, 9354-9360.

75. Fatemi, N., Korzhnev, D. M., Velyvis, A., Sarkar, B., and Forman-Kay, J. D. NMR Characterization of Copper-Binding Domains 4-6 of ATP7B, *Biochemistry*.

76. Rodriguez-Granillo, A., Crespo, A., Estrin, D. A., and Wittung-Stafshede, P. Copper-transfer mechanism from the human chaperone Atox1 to a metal-binding domain of Wilson disease protein, *J Phys Chem B 114*, 3698-3706.

CHAPTER 3

MATERIALS AND EXPERIMENTAL METHODS

This chapter will tabulate and describe all the procedures used for the experiments as well as a listing of all chemicals, reagents, peptides, etc. This list will include purity and place of purchase. The methods in this section include: protein expression and purification, as well as theromin kinetics and metal binding studies. The methods also include NMR, UV-Vis spectroscopy studies to understand the various coordination environments around the Wilson disease protein and its copper chaperone, HAH1. A final discussion will involve probing the coordination environment of Hg(II)HAH1 in solution; comparing it to the published crystal structure.

3.1 Listing of Chemicals, Reagents, and Peptides

Table 3.1: List of proteins and their respective vectors, tags, and proteases.

Protein:	Vector:	Tag:	Protease:
Theromin	pET42a	Glutathione S-Transferase	Factor Xa
Wilson Domain 4 (WLN4)	pET32Xa/LIC	Thioredoxin	Factor Xa
HAH1	pET11d	None	NA
C15A WLN4	pET32aXa/LIC	Thioredoxin	Factor Xa
C18A WLN4	pET32aXa/LIC	Thioredoxin	Factor Xa
C15A HAH1	pET11d	None	NA
C12A HAH1	pET11d	None	NA

Table 3.2: Reagents, manufacturers, and purities (where available) used in the following experiments.

Reagent:	Part Number:	Manufacturer/Distributor:	Purity:
^{2}H Acetonitrile-d_3	423106	Sigma-Aldrich	
Acrylamide	164855000	Acros Organics	
Agarose	15510-019	Invitrogen	
L-Alanine	A7627-1G	Sigma Aldrich	
^{15}N-Ammonium Chloride		Cambridge Isotopes	
Ammonium Chloride	A661-500	Fisher Scientific	99.8%
Ammonium Persulfate	A3678-25G	Sigma–Aldrich	>98%
L-Arginine	A8094-25G	Sigma-Aldrich	
L-Aspartate	A9256-100G	Sigma-Aldrich	
Bathocuproine Difsulfonic Acid	100868	MP	
Bis-Acrylamide	BP171-25	Fisher Scientific	

Table 3.2 Continued

Boric Acid	BP168-1	Fisher Scientific	>99%
Carbenicillin	762024	Bio-World	
Coomasie Blue R-250	20278	Thermo Scientific	
Copper Standard for ICP-AES	SC194-100	Fisher Scientific	
^{13}C,^{15}N L-Cysteine	CNLM-3871-0	Cambridge Isotope Laboratories	^{13}C >97% ^{15}N >97%
L-Cysteine	3089	Fluka	
Dithionitrobenzene (DTNB)	D8130-106	Sigma-Aldrich	
Dithiothreitol (DTT)	1758-9030	Inalco Spa, Milano Italy	
EDTA	BP119-500	Fisher Scientific	>99.0%
Glacial Acetic Acid	64-19-7	Fisher Scientific	
^{13}C-D-Glucose		Cambridge Isotopes	
L-Glutamic Acid	G8540-25G	Sigma-Aldrich	
L-Glutamic Acid	G1251-100G	Sigma-Aldrich	
L-Glutathione (reduced)	G425-50G	Sigma–Aldrich	> 99 %
Guanidine Hydrochloride(GuCl)	BP178-500	Fisher Scientific	> 99%
Guanidine Hydrochloride	50933	Sigma-Aldrich	>99.5%
Glycine	G7126-100G	Sigma-Aldrich	
Hirudin	H7386	Sigma-Aldrich	
L-Histidine	H8000-5G	Sigma-Aldrich	
Concentrated Hydrochloric Acid	7647-01-0	Fisher Scientific	
Concentrated Nitric Acid	7697-37-2	Fisher Scientific	
Imidazole	56750	Sigma–Aldrich	>99.5%
Indium Standard for ICP-AES	IAA-049	Ultra Scientific	

Table 3.2 Continued

Iodoacetaminde			
IPTG	1758-1400	Inalco Spa, Milano Italy	
L-Isoleucine	I2752-1G	Sigma-Aldrich	
Kanamycin Sulfate	420311	Calibiochem	
L-Leucine	L8000-25G	Sigma Aldrich	
MEM Vitamins	25-020-CI	Mediatech Inc.	
Mercury(II) Choride		Fisher Scientific	
L-Methionine	M9625-5G	Sigma-Aldrich	
MES	BP300-100	Fisher Scientific	>98%
L-Phenylalanine	P5482-25G	Sigma-Aldrich	
L-Proline	P5607-25G	Sigma-Aldrich	
L-Serine	S4500-1G	Sigma-Aldrich	
Sodium Chloride	BP358-10	Acros Organics	>99.85%
Sodium Dithionite	SX0530-1	EM Science	
Sodium Dodecyl Sulfate (SDS)	15525-017	Gibcobrl	>99.5%
Sodium Hydroxide	S612-3	Fisher Scientific	
Sodium Phosphate, Dibasic Anhydrous	S393-3	Fisher Scientific	
Sodium phosphate, Monobasic, Monohydrate	BP330-1	Fisher Scientific	
S-2238 (Chromogenix)	820342-39	DiaPharma	
TEMED	BP150-100	Fisher Bioreagents	>97%
Tetrakis (Acetonitrile) Copper(I) Hexafluorophosphate	346276-5G	Sigma-Aldrich	>99%
Thiol Sulfide Quantification Kit	T6060	Invitrogen	
L-Threonine	T8625-1G	Sigma-Aldrich	

Table 3.2 Continued

α-Thrombin		Novagen	
Trichloroacetic Acid	BDH0310-500G	VWR	>99.0%
Tricine	807420	MP Biomedicals	
Tris	BP152-5	Fisher Scientific	
L-Tryptophan	T0254-1G	Sigma-Aldrich	
Tryptone	12111-1	Mo Bio Lab	
L-Tyrosine	93829	Fluka	
Urea	BP169-500	Fisher Scientific	>99%
L-Valine	V0500-1G	Sigma-Aldrich	
Yeast Extract	212720	Fisher Scientific	

Table 3.3: List of biological reagents used in the following experiments.

Biological Reagent:	**Part Number:**	**Manufacturer/Distributor:**
1Kb DNA Ladder	N3232S	NEB
BCA™ Protein Assay Kit	23225	Thermo Scientific
Benzonase	70746	Novagen
Bio-Rad Protein Assay Reagent	500-0006	Bio-Rad Laboratories, Inc.
BL21(DE3) Competent Cells	69450	Novagen
BugBuster® Reagent	70584-4	Novagen
Factor Xa (Bovine)	NA	Enzyme Research
Isoelectric Focusing Calibration Kit Broad pI(pH3-10)	17-0471-01	Amersham Biosciences
LMW Gel Filtration Calibration Kit	17-0442-01	Amersham Biosciences
Novablue Competent Cells	69825-4	Novagen
QIAprep® Spin Miniprep Kit(250)	27106	QIAGEN
Rainbow Protein Marker	RPN800E	GE Lifesciences
Rosetta(DE3) Competent Cells	70954-3	Novagen

Table 3.4: Listing of instrumentation used for experiments.

Instrument:	Details:	Applications:
GE Lifesciences (formerly Amersham) AKTA FPLC	Part Number: 18-1900-26	Protein Purification (See **Table 2.4**)
Olis Cary 14 UV Vis Spectrometer		Protein Quantification, UV-Vis Titrations, and Kinetics Experiments
Edinburgh Fluorimeter	FL900	Copper(I) Titrations
Isotemp Laboratory Refrigerator	Fisher Scientific	Housing AKTA FPLC and Amicon devices
UV/VIS Beckman Diode Array Spectrophotometer	Model Number: DU-7400	Protein Quantification
Sorvall Centrifuge	Model Number: RC 5B	Pelleting cell cultures, and concentrating proteins
Varian 500 MHz NMR (University of Michigan, Ann Arbor, MI)		^{1}H, ^{13}C, and ^{1}H-^{15}N HSQC Experiments
JEOL 400 MHz NMR (Western Michigan University, Kalamazoo, MI)		^{1}H, ^{13}C, and ^{1}H-^{15}N HSQC Experiments
Bruker 600-800 MHz NMR (Center for Magnetic Resonance, Florence, Italy)	With Cryoprobe	^{1}H-^{15}N HSQC, and mobility Experiments
Jasco CD Spectropolarimeter	Model Number: J815	Circular Dichroism experiments
Shimadzu HPLC		Light Scattering and Reverse phase chromatography
Electrospray Ionization Mass Spectometer		Protein mass measurements

Table 3.4 Continued

Minicycler Thermocycler	Model Number: PTC-150	PCR of genes
Bioflo310 Fermentor Bioreactor	New Brunswick Scientific	Large scale cultures
Microferm Fermentor	New Brunswick Scientific	Large scale cultures
Controlled Environment Shaker/Incubator	New Brunswick Scientific	Small scale cultures
Eppendorf Minispin Centrifuge	Model Number 5415	Small scale cell pellets and protein concentration

Table 3.5: GE Life Sciences AKTA FPLC columns.

Column:	**Function**	**Resin**	**Product code**
DEAE Sepharose	Anion Exchange	Diethylaminoethyl Sepharose	FF XK 26
CM Sepharose	Cation Exchange	Carboxymethyl Sepharose	FF XK 26
HisPrep FF16/10	His-tag Purification	Sepharose	28-9365-51
HiPrep 26/10 Desalting Column	Buffer Exchange	Superdex G-25 Superfine	17-5087-01
Hiload 26/60 Superdex 75 pg	Gel Filtration	Superdex 75 Prep Grade	17-1070-01
Hiload 16/60 Superdex 200 pg	Gel Filtration	Superdex 200 Prep Grade	17-1069-01
Superdex 75HR 10/300	Gel Filtration	Superdex 75, 13μm	17-1047-01
Superdex 75HR 10/300 Peptide Column	Gel Filtration	Crosslinked Agarose and Dextran, 13μm	17-5176-01

3.2 Protein Production and Biochemical Studies

These projects use proteins that are produced recombinantly. A list of these proteins and their expression vectors are found in **Table 3.1**. The transformation and expression of all proteins was the same with the exception of the antibiotic, whereas the purification was specific to the protein. Any mutants of the respective proteins were transformed, expressed, and purified exactly the same as their native proteins. Expression tags and proteases used to cleave them are also listed in **Table 3.1**.

3.2.1 Theromin Transformation, Expression, and Purification

The theromin gene constructed by Mr. Joel Lwande (**Figure 3.1**) was ligated into the pET42a vector, which contains resistance to the antibiotic kanamycin (*1*). The gene for theromin also had a fusion tag, glutathione S-transferase. A fusion was made for this protein to increase both the yield and solubility of the small peptide. The fusion also made it easier to selectively purify. A column specific to the glutathione S-transferase tag (GST tag) was used to select for the theromin fusion protein. The plasmid was transformed into Rosetta2(DE3) cells, exhibiting an inherent chloramphenicol resistance. Competent cells were removed from -80°C storage and put directly into ice to thaw.

^{1}E C E N T E C P R A C P G E Y E F D E D G C N
T C V C K G C D D A Q C R C S S D A N G C E S F
C T C N T R C S A A D E C N P R C T C K^{67}

Figure 3.1: Amino acid sequence of theromin, the orange residues constitute the negatively charged region of the peptide that is presumed to bind to the exosites. The blue residues are the 16 cysteines used to make the proposed functional dimer.

3 μL dimethylsulfoxide (DMSO) and 0.2 ng of plasmid (typically 1-2 μL of a 20 ng/mL solution) was introduced to the cells, then allowed to incubate on ice for 30 min. Following incubation the cells were heat shocked for 30-90 sec at 42°C (time depended on the volume of cells); this opens up the pores of the cells to allow the plasmid inside. The heat shocked cells were placed back on ice to revive them. The transformed cells were combined with 1 mL of SOC media (20 g/L bacterial tryptone, 5 g/L yeast extract, 10 mM NaCl, 2.5 mM KCl, 10 mM $MgCl_2$, 10 mM $MgSO_4$, 20 mM glucose, pH 7.0) and put in a shaker at 37°C and allowed to shake for 1 hr. The cells were then centrifuged at 10,000 rpm in the Minispin Eppendorf centrifuge for 15 sec to concentrate the cells for plating. The supernatant was removed from the pellet leaving about 100 μL for resuspension. The newly suspended cells were spread on an LB agar (10 g/L bacto-tryptone, 5 g/L yeast extract, 10 g/L NaCl, 15 g/L agar, pH 7.0) plate infused with 30 μg/mL kanamycin sulfate. The plate was grown in an incubator maintained at 37°C overnight.

The colonies on the plates were used to inoculate liquid LB media for growing cultures and expressing the protein. First, four 5 mL starter cultures were made containing 30 μg/mL kanamycin sulfate and incubated in a 37°C shaking incubator

until the media was warm (usually about 10 min). A single colony was chosen from the plate and inoculated into each of the four cultures; allowed to grow to an approximate optical density (OD_{600}) of 0.6-1.0 (about 1 hr), then inoculated into respective 1 L cultures containing the same concentration of kanamycin sulfate. From the 5 mL culture a 1 L culture was grown to an OD of 0.6-1.0 (usually 2-3 hr). The culture was then induced to overexpress the GST-Theromin fusion protein by adding IPTG to the media at a final concentration of 1 mM. The cells were then allowed to grow another 6-8 hr with 1 mL samples taken every hour to run on a gel as an induction test. Following expression, the cells were harvested by centrifugation at 3000xg for 20 min in a Sorvall centrifuge, equipped with an SLA3000 rotor spinning at about 4000 rpm. Once collected, the pellets were either stored at -20°C or immediately processed for protein removal and subsequent purification.

Removal of the protein, in this case a GST-Theromin fusion protein, involved using a Bugbuster® reagent to gently disrupt the cell membranes and benzonase nuclease was added to break up DNA into nucleotides. The cells were suspended in BugBuster® reagent/benzonase nuclease to 5 mL reagent and 1 μL reagent to 1 g pellet respectively, and shaken gently (usually 20-50 rpm) on a table top shaker for 1 hr. The cell debris was centrifuged with a Sorvall centrifuge equipped with an SS34 rotor spun at 15,000 rpm (12,000xg) for 20 min to leave the over-expressed protein suspended in the supernatant. The supernatant was decanted and stored at 4°C (no longer than 4 hr, otherwise precipitation occurred) to be loaded on a GST-tag FPLC column for initial purification (**Figure 3.2**).

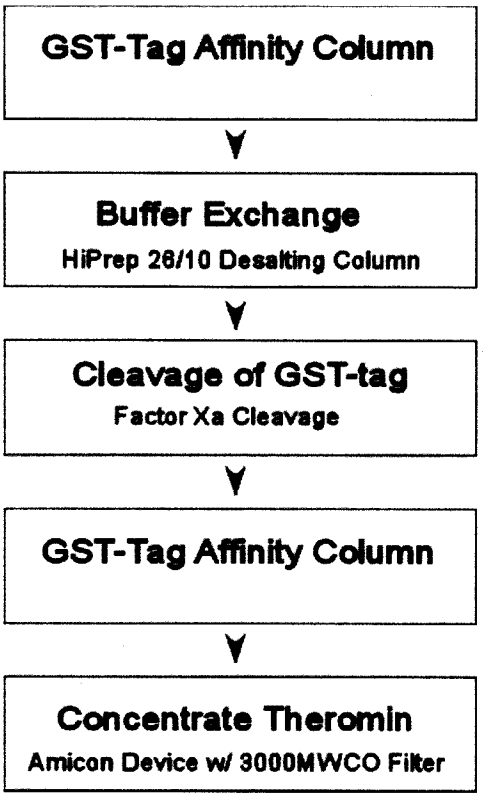

Figure 3.2: Purification and cleavage of GST-Theromin.

A GST-tag column containing glutathione S transferase was equilibrated with 10 column volumes (CV) (200 mL) of phosphate buffered saline at pH 7.3 (140 mM NaCl, 2.7 mM KCl, 10 mM Na_2HPO_4, 1.8 mM KH_2PO_4) for binding the GST-theromin and washing away the other proteins. After loading the protein, another 10 CV (200 mL) was used to wash out unbound sample. The protein was eluted with an isocratically with 50 mM Tris buffer pH 8.0 containing 10 mM L-glutathione. The flow rate for all FPLC processes was 1 mL/min.

Once the protein was eluted and run on an SDS-PAGE to determine purity, the protein was desalted using a desalting column equilibrated with Factor Xa buffer (100 mM NaCl, 50 mM Tris-HCl, 5 mM $CaCl_2$, pH 8.0). Up to 10 mL of protein solution could be added to the column using an injection loop on the FPLC and eluted at 6 mL/min. The newly exchanged protein was then concentrated to approximately 10 mL and 10 μg of Factor Xa was added per milligram protein (determined by a Bradford assay). Typically, cleavage was performed between 16-20 hr, monitored by a cleavage test. The cleavage test involved collecting 20 μL of the cleavage solution every 3-4 hr and loaded on an SDS-PAGE to determine the extent of cleavage.

Once cleavage was completed, the protein was loaded on the same GST-tag column as before, except the flow through was collected, as the GST-tag binds and theromin does not. The unbound theromin protein was washed from the column with two column volumes of phosphate buffered saline (8 g/L NaCl, 0.2 g/L KCl, 1.44 g/L Na_2HPO_4, 0.24 g/L NaH_2PO_4, pH 7.5). The theromin protein was then concentrated, in an Amicon device equipped with a 3000 Da molecular weight cut-off (MWCO) filter, to approximately 5-7 mL and stored at -20°C.

The concentration of theromin was measured by a thiol sulfide quantification kit from Invitrogen (T-6060). This kit uses modified papain to determine thiol concentration in proteins. Typical protein quantification methods (i.e. BCA or Bradford assays) aren't useful in determining theromin concentrations.

3.2.2 Inhibition Characterization

Theromin has a direct α-thrombin inhibition characteristic that is explored herein. The novelty of this peptide is its recombinant form, which could have different inhibition characteristics from those reported by Salzet (*2*). This section describes experiments ranging from kinetics to understanding the effect of salt on the effectiveness of inhibition.

3.2.2.1 Theromin Inhibition Kinetics

The kinetics experiments were carried out similar to Salzet *et. al.* experiments (*2*). They used a slow binding inhibition equation to describe α-thrombin's activity. Equation 3.1 describes a linear representation for slow tight binding noncompetitive inhibition kinetics, with equation 3.2 being a simplification made by Bieth (1980) (*3*).

$$I_t = E_t^i + K_t\left(\frac{i}{1-i}\right), \left(i = 1 - \frac{v_i}{v_0}\right) \tag{3.1}$$

$$\frac{[I]}{1-a} = \frac{1}{a}K_{i,app} + [P], \left(a = \frac{v_i}{v_0}\right) \tag{3.2}$$

The terms in Equation 3.1 are *i* which is a term to simplify the $1\text{-}v_i/v_0$ where v_i is the rate at any given enzyme concentration, v_0 is the maximum, initial rate, and E is the enzyme concentrations bound to inhibitor I, and K_t is the inhibition constant. Equation 3.2 is a simplified variation of Equation 3.1, where "a" is another variable to

describe the v_i/v_0 and these terms mean the same as previously. Equation 3.2 still accounts for the inhibitor concentration, I, and inhibition constant, $K_{i,app}$ ($K_{i,app}$ is the apparent inhibition constant), and the major difference is it is also affected by P, the concentration of product formed. Equation 3.2 is easily plotted as a linear equation in the form of y=mx+b. The kinetics experiments were carried out on an Olis Cary 14 UV-Vis spectrometer. The rates of α-thrombin cleavage were monitored by the cleavage of p-nitroaniline from a small modified peptide H-D-Phe-Pip-Arg. The change in absorbance was monitored at 405nm.

The α-thrombin was prepared to a final concentration of 34.3 pM in 25 mM Tris-HCl, pH 7.2 containing 136 mM NaOAc, 150 mM NaCl, 0.6% PEG2000, and 1% (w/w) BSA. The theromin was prepared in the same buffer and added to the α-thrombin solution to a final concentration of 98.4 pM. The S-2238 Chromozyme was added to the sample in different concentrations to get the specific variables for the equation previously mentioned. The S-2238 is a short modified peptide with a p-nitroanaline attached to it (H-D-Phenylalanyl-L-pipecolyl-L-arginine-p-nitroanaline hydrochloride) that when in the presence of α-thrombin gets cleaved between the arginine and the p-nitroanaline. The p-nitroanaline is yellow when removed from the modified peptide, so absorbance changes were monitored at 405 nm to determine kinetic changes in the activity of α-thrombin as theromin was added to the system. **Table 3.6** shows the experimental conditions of the kinetics experiments.

Table 3.6: Theromin inhibition kinetics set-up parameters, all components were made as stocks in the assay buffer.

Sample:	α-thrombin, pM:	Theromin, pM:	S-2238 Chromozyme, pM:
1	34.3	82.0	82.0
2	34.3	82.0	98.4
3	34.3	82.0	114.8
4	34.3	82.0	131.2
5	34.3	82.0	147.6
6	34.3	82.0	164.0
7	34.3	82.0	180.4

3.2.3 Wilson Disease Protein Domain 4 Transformation, Expression, and Purification

The Wilson disease protein domain 4 (WLN4) gene (**Figure 3.1**) was ligated into the pET32Xa/LIC vector containing an ampicillin resistance gene, as well as a Trx tag and a Factor Xa cleavage site. The transformation was done the same as discussed in **Section 2.2.1**, with the exception that the transformation of pET32Xa/LIC containing WLN4 was plated on LB agar plates containing 100 μg/mL ampicillin. The expression of WLN4 was also the same procedure as discussed for theromin; again with the exception of 100 μg/mL ampicillin was used instead of kanamycin.

The Trx-WLN4 protein, once overexpressed and harvested from the cells using a commercial reagent, and was then loaded on a HisPrep column equilibrated

with 50 mM Tris, 20 mM imidazole, and 500 mM NaCl at pH 8.0. The nickel(II) column was chelated by the poly-histidine tag (six histidines in a row), allowing all other proteins to pass through. The column was washed to remove unbound protein for 15 CV (300 mL) at a flow rate of 1.0 mL/min. The protein was then eluted with a linear gradient over 25 CV (500 mL) with 50 mM Tris, 500 mM imidazole, 500 mM NaCl at pH 8.0 and the same flow rate. The gradient typically produced a very nice sharp peak around 25% buffer B, which was Trx-WLN4 (based on SDS-PAGE). Tris buffer was chosen for this step because the thioredoxin needs to be cleaved off, and that is done in Factor Xa buffer which contains calcium. Typically, HisPrep columns run with a Tris binding buffer and a phosphate elution buffer, but when the cleavage buffer contains calcium it makes it more difficult to exchange the buffer. The calcium in the cleavage buffer precipitates out in phosphate buffer as calcium phosphate; this causes problems because protein will also precipitate with it.

After the Trx-WLN4 was collected, it was concentrated to approximately 10 mL in an Amicon device equipped with a 10 kDa MWCO filter. This concentrated solution was then injected on a desalting column equilibrated with Factor Xa buffer (See **Section 2.2.1**). The newly exchanged protein was concentrated a second time to approximately the same volume for cleavage of the thioredoxin tag. The Factor Xa was added at 10 μg per 1 mg of protein, determined by a Bradford assay, and takes between 16-20 hr to completely cleave thioredoxin.

SDS-PAGE verified complete cleavage, and the protein was passed through the same HisPrep column as the initial purification step to remove the tag. The

column was equilibrated with 50 mM Tris buffer containing 20 mM imidazole and 500 mM NaCl at pH 8.0, at a flow rate of 1.0 mL/min, flow through was collected for 3 CV (60 mL) of eluent. The WLN4 protein solution was collected and concentrated in an Amicon device equipped with a 3000 MWCO filter to 5-7 mL to be loaded on a Superdex 75 (26/60) gel filtration column. The column was equilibrated with 2 CV (640 mL) of 50 mM Tris containing 150 mM NaCl at pH 8.0, with a flow rate of 3 mL/min. Following equilibration the WLN4 solution was injected on the column and isocratically eluted with same buffer at a flow rate of 2.5 mL/min; 5 mL fractions were collected.

An SDS-PAGE was run to determine which peak contained WLN4 (elution volume of approximately 220 mL), and those fractions were collected and concentrated in the Amicon device equipped with a 3000 MWCO filter. The volume was reduced to 10 mL and the protein solution was exchanged into phosphate buffer. The exchange was done on a HiPrep desalting column equilibrated with 50 mM phosphate buffer at pH 7.5. Finally after the buffer exchange the protein was concentrated to 2-3 mL and quantified using a BCA assay.

3.2.4 $^{13}C,^{15}N$ Double Labeled Cysteine WLN4, Transformation Expression, and Purification

For a couple of the experiments it was necessary to make WLN4 with cysteines that were double labeled. To do this uniformly labeled $^{13}C,^{15}N$-L-cysteine was purchased from Cambridge Isotopes, and incorporated into the WLN4 protein. This procedure involved the use of specially modified BL21(DE3) CysE cells given as a gracious gift by Marie-Paule Strub at NIH. The CysE refers to these cells having a knock out of the serine acetyltransferase gene, which prevents these cells from making cysteine out of glucose. This is important because these cells need to take up and incorporate the $^{13}C,^{15}N$-L-cysteine provided in the media. These modified cells also have an inherent kanamycin resistance built in, which helps in to selection for these cells. The cells were received as a culture in a cold stab medium. The cells were then taken and plated on LB agar plates containing 50 μg/mL L-cysteine and 30 μg/mL kanamycin sulfate. The plates were stored in an incubator set at 37°C for overnight growth. The colonies were harvested from the plates and inoculated in six 5 mL cultures containing 50 μg/mL L-cysteine and 30 μg/mL kanamycin sulfate. The colonies were allowed to grow in a shaking incubator set at 37°C until the OD reached 0.6-1.0, then glycerol was added to a final concentration of 20% (v/v) and alliquoted into 2 mL cryogenic tubes which were first frozen on dry ice then moved to the -80°C freezer for storage.

Initially, the glycerol stock of BL21(DE3) CysE was used to inoculate an LB agar plate containing 50 μg/mL L-cysteine and 30 μg/mL kanamycin sulfate, and

grown overnight in an incubator set at 37°C. These colonies were harvested and inoculated into four 5 mL LB cultures containing 50 μg/mL L-cysteine and 30 μg/mL kanamycin sulfate and grown in a 37°C shaker until the OD_{600} was approximately 0.6. The cells were then inoculated into 200 mL LB media containing same components, and grown to an OD_{600} between 0.6-1.0 (approximately 2 hr). The cells were then gently pelleted in a Sorvall Centrifuge equipped with an SLA3000 rotor, centrifuged at 2,500 rpm for 10 min at 4°C. The supernatant was decanted and discarded and the pellet dried further by wicking up the small excess of media with a static free wipe. The pellet was then resuspended in an ice-cold solution of 80 mM $MgCl_2$ and 20 mM $CaCl_2$ and pelleted a second time under the conditions above. The cells were resuspended a second time in 500 μL solution of 100 mM $CaCl_2$. The now competent cells were immediately put on ice and transformed with the pET32aXaLIC vector containing the Trx-WLN4 gene.

To the competent cells was added 3 μL DMSO, and 1-2 μL (~20 ng/mL) plasmid and left on ice for 30 min. The partially transformed cells were then heat shocked at 42°C for 60-90 seconds and returned to the ice for 2 min. 1 mL of SOC media was added to the transformation and it was placed in a shaking incubator set at 37°C for 1 hr. Finally the cells were centrifuged in an Eppendorf centrifuge at 10,000 rpm for 2 min and approximately 1.3 mL of the supernatant was removed. The remainder was used to resuspend the cells and subsequently plate them on LB agar plates containing 50 μg/mL L-cysteine, 100 μg/mL ampicillin, and 30 μg/mL kanamycin sulfate, and grown in a 37°C incubator overnight.

The cells made in this way typically do not have high competence, so out of a 200 mL cell culture; the number of colonies is approximately 20-50. One colony from the plate was chosen to inoculate one of six 5 mL cultures containing the same components as the plates they came from. The 5 mL cultures were allowed to grow for approximately 2-3 hr (OD was ~0.6). Then the culture that had the highest OD was selected and used to inoculate a larger, 200 mL, culture identical in recipe to the 5 mL. The larger culture was allowed to grow to an OD of 0.6-1.0. Then it was gently pelleted in the Sorvall centrifuge at room temperature. The supernatant was decanted and discarded and 37°C water (autoclaved water was placed in the shaker to equilibrate to 37°C, so cells weren't shocked) was used to wash the surface of the pellet and then resuspend it. The water/cell suspension was used to inoculate the M9 minimal media equilibrated to 37°C. **Table 3.7** contains the recipe conditions of the M9 minimal media used for growing the BL21(DE3) CysE cells.

Table 3.7: Recipe for M9 minimal media used in growing cells capable of incorporating ^{13}C,^{15}N-L-cysteine into their proteins. *Note the 5X M9 media was made with the following recipe: 15g KH_2PO_4, 42.5g Na2HPO4•2H_2O, 2.5g NaCl in 1000 mL milliQ water (<18Ω). Also all components were filtered through a 0.22 μm syringe filter. HCl and NaOH amino acids refers to them being dissolved in those solutions at 0.100 N.

Component:	Concentration	Volume Added to 1L, mL	Notes:
M9 Media	5X*	200	
$MgSO_4$	1M	1	
$CaCl_2$	1M	0.3	Cloudy precipitate appears initially
Solution Q	Saturated	2	
MEM Vitamin Mix	Saturated	1	
HCl Amino Acids (A, N, R, G, S, Q, H, K, P, T, I, W, V, P, L, M)	100 mg/10 mL, 0.1N HCl	10	Suspend the amino acids after each addition, they tend to be low solubility
NaOH Amino Acids (E, D, Y)	100 mg/10 mL, 0.1N NaOH	10	High solubility
^{13}C,^{15}N-L-cysteine	25 mg/mL in 0.1N HCl	2	
Glucose	2 g/10 mL	10	
Kanamycin Sulfate	30 mg/mL	1	
Ampicillin	100 mg/mL	1	

The cells were grown in the M9 minimal media to an OD of 0.6-1.0, taking approximately six hours. The protein expression was induced with addition of IPTG to a final concentration of 1 mM. The cells were allowed to express of 8 hr, at which time they were harvested in a Sorvall centrifuge and stored at -20°C. Extraction of the protein and subsequent purification was done as described in **Section 2.2.2.**

WLN4 was concentrated to approximately 1 mM in 50 mM phosphate buffer pH 7.5 for NMR analysis.

3.2.5 ^{15}N WLN4 Transformation, Expression, and Purification

Transformation, expression and purification were performed the same for the ^{13}C,^{15}N-L-cysteine protein expression, except for one change. This expression used $^{15}NH_4Cl$, and didn't require the individual amino acids as these could be made from glucose, NH_4Cl, and sulfate. The cells used for the transformation were Rosetta(DE3) cells from stocks stored at -80°C.

3.2.6 ^{15}N and Native Isotope HAH1 Transformation, Expression, and Purification

HAH1 is expressed from the vector pET11d-HAH1 (ampicillin resistant). The transformation and expression is done in an identical fashion to the pET32aXa/LIC (Trx-WLN4). The differences are in the purification.

The cells are treated with a freeze-thaw technique that gently opens the membranes to let the protein out. The cells are frozen on liquid nitrogen (77 K) for 5 min, then they are thawed under cold water for 35 min, and the cycle is repeated 3 more times. Following the final freeze-thaw cycle, 240 mL extraction buffer (20 mM MES, 1 mM EDTA at pH 5.5), is added to the pellet. The pellet is suspended in the extraction buffer and gently shaken for 1 hr. The cell solution is then pelleted again in a Sorvall centrifuge equipped with an SS34 rotor, centrifuged at 15,000 rpm for 20 min. The supernatant, containing the protein was decanted into a Falcon 50 mL conical tube, and stored at 4°C.

The first step in the purification process used the pI of HAH1 (~7.5). This pI made this protein positive near physiological conditions (pH ~7.5), and it could bind to a cation exchange column. Most proteins in a cell are either hydrophobic or negative, very few are positively charged. HAH1 was loaded on a tandem set-up of a anion exchange column (DEAE) followed by a cation exchange column (CM) (refer to **Table 3.4** for column details), equilibrated with 20 CV (~1 L) binding buffer (20 mM MES, pH 6) at a flow rate of 2 mL/min. The DEAE column was used as a trap to bind most of the proteins in the supernatant solution, leaving a cleaner protein solution to allow binding to the CM column. There were also many proteins that flow through both columns and don't bind to either. After the HAH1 protein solution loaded on the columns, 20 CV (~1L) binding buffer was used to wash out unbound sample from the columns. The columns were then disconnected and the HAH1 was eluted from the CM column. Elution involved a linear gradient over 10 CV (~500 mL) of elution buffer (20 mM MES, 1 M NaCl, pH 6) at a flow rate of 2 mL/min. The HAH1 was detected with SDS-PAGE and pertinent fractions combined.

The HAH1 solution was then concentrated on an Amicon device equipped with a 3000 MWCO filter to approximately 20 mL (this protein expresses with very high efficiency so the volume isn't highly reduced at this point). The concentrated HAH1 solution was further purified by a Superdex75 (26/60) gel filtration column equilibrated with 50 mM phosphate buffer containing 150 mM NaCl at pH 7.5. Following this purification step the HAH1 was >95% pure, determined by SDS-PAGE, and reverse phase HPLC.

3.2.7 NMR Studies of the Intermediate Interaction Between WLN4 and HAH1

NMR studies were performed in collaboration with Ivano Bertini's group at the Center for Magnetic Resonance (CERM) in Florence, Italy. All measurements were conducted on Bruker Avance NMR Spectrometers at ^{1}H nominal frequencies of 500, 600, 700, and 800 MHz, and were equipped with cryogenically cooled probes. The experiments were double resonance techniques to detect chemical changes and mobility changes due to perturbations in the chemical environment, and ultimately in an interaction of the binding partners via copper(I).

After the proteins were expressed and purified, they were concentrated to nearly 1 mM, determined by Biorad or BCA assays. The labeling was of the mutant protein, this was to prevent any detection of homodimerization that could give a false positive as an interaction. The mutant protein was placed in an NMR tube in a Vac Atmospheres glove box equilibrated with nitrogen and maintained at <1 ppm O_2. The protein was reduced under a nitrogen atmosphere with 1 mM dithiothreitol (DTT). An initial ^{1}H-^{15}N HSQC spectrum was measured of the apo, unbound mutant. Then the binding partner was titrated in to a 1:1 ratio (determined via peak heights in the 1H NMR spectrum pertaining to well resolved isoleucines on both proteins). All NMR measurements were done at 300K (*4*). A ^{1}H-^{15}N HSQC spectrum was measured after each addition of respective native partner, this ensured there was no interaction in the absence of metal (*5*). Once a 1:1 ratio was measured of the two proteins, copper(I) was added [as tetrakis(acetonitrile) hexafluorophosphate

copper(I)] under the same nitrogen atmosphere. The copper(I) was titrated into the solution in approximately 10% increments until a 1:1 ratio was achieved between the proteins in solution and the copper(I). The ratio was determined comparing the copper(I) concentration to one of the proteins in solution. All ^{1}H-^{15}N HSQC spectra were collected on a Bruker Avance 700 MHz NMR equipped with a cryoprobe. Interactions were detected by chemical shifts in the 2D spectrum. However, shifts are not totally indicative of interaction, and mobility was used to be certain. Mobility gives information as to how fast a molecule, peptide in this case, is tumbling in solution. Ultimately, larger objects tumble slower than larger ones, so a monomer will tumble significantly faster than two proteins interacting with each other.

Once all spectra were collected the average chemical shifts of the peaks (each peak representing an amide pertaining to one amino acid) was determined to illustrate the extent of changes in the chemical environment around the binding site. To do this the chemical shifts are compared using Equation 3.3 (CSV is Chemical Shift Variation, where $\Delta\delta$ is change in chemical shift for the respective nucleus) (*6*).

$$CSV = \sqrt{\frac{[\Delta\delta(^{1}H)]^{2}+[\Delta\delta(^{15}N)/5]^{2}}{2}} \tag{3.3}$$

Mobility experiments were done on a Bruker Avance 600 MHz spectrometer equipped with a cryoprobe. Dynamics of the apo and titrated forms of the proteins were measured using techniques described by Ishima *et. al.* (*7*). Basically, relaxation

measurements are taken of R1 (longitudinal, Z^2-axis) and R2 (transverse, XY-plane), based on ^{15}N-mutant relaxation rates (*5, 8*). T1 and T2 are calculated using model free analysis software. The ratio of these rates can be correlated to the estimated tumbling time of a protein in solution. These rates are mass dependent, allowing for a distinctive difference between a monomeric protein and a complex in solution.

3.2.8 UV-Vis Titrations of WLN4-HAH1 Intermediate Interaction

The intermediates were also titrated together in the presence of copper(I) and other various similar, or at least tighter binding, metals [i.e. Ag(I) and Cd(II)]. The proteins were prepared as described in **Section 2.2.3**, and the buffer used in all titrations was 50 mM sodium phosphate buffer at pH 7.5. This buffer was used to be consistent with the NMR experiments.

The apo protein was prepared in the cuvette at a known concentration; typically two different concentrations were used, 5 mM and 20 mM. The lower concentration was used to detect metal to ligand charge transfer (MLCT) bands below 220 nm as the protein backbone absorbs in these regions and will overshadow any MLCT bands. The higher concentration of protein will give more distinct MLCT bands around 250-300 nm (253-261 nm should be a 2-coordinate) (*9, 10*) species and a bathochromic shift toward 270-300 (*10*) indicates a higher coordination species. Protein preparation was done in the Vac Atmospheres nitrogen glove box using degassed 50 mM phosphate buffer. The phosphate buffer was prepared and degassed with a Schlenk line equipped with a vacuum and argon. The phosphate solution was evacuated of oxygen for approximately 10 min with subsequent equilibration with

argon. This cycle was repeated for 1 hr with simultaneous sonication to remove dissolved oxygen. The buffer was then moved into the glove box for storage.

The native protein was then titrated with a 1 mM copper(I) solution that was prepared by addition of tetrakis(acetonitrile) hexafluorophosphate copper(I) to degassed milliQ water containing 10% acetonitrile. The stock copper(I) solution was prepared by degassing 500 mL milliQ water (<18 Ω) on a Schlenk line equipped with a vacuum and ultra high purity argon. The solution was then moved into the nitrogen atmosphere Vac Atmospheres glove box. A copper(I) complex was measured and diluted with the degassed water containing 10% (v/v) acetonitrile. This solution was capped with a septum and wrapped with parafilm to prevent oxygen contamination.

The cuvette was removed from the glove box and measured initially on the Olis Cary 14 UV-Vis spectrometer equipped with a split beam and a water jacketed cuvette holder. A second similar cuvette containing the same degassed phosphate buffer was put in the blank cuvette location to get simultaneous blank subtractions during each measurement. Once a blank measurement was determined (to remove the spectrum from the protein itself), the copper(I)-acetonitrile solution was titrated in (typically at 10%, substoichiometric, increments). The copper(I) solution was added to both the experimental cuvette and the blank cuvette, and measurements recorded. Once titrations reached a 1:1 ratio of native protein:copper(I), the mutant partner was titrated in. The mutant solution was prepared similar to the native protein except the concentration was five times higher as to not have a huge dilution effect. The dilution

effect was accounted for by dividing all spectra by the concentration of native protein, as it changed with changes in volume in the cuvette.

3.2.9 HAH1 ^{199}Hg(II) NMR

The HAH1 was prepared as described in **Section 2.2.6**. The $^{199}HgCl_2$ was added to half an equivalent to facilitate a dimerized mercury(II) species if one could exist, and spectra were collected at various pHs. The ^{199}Hg(II)HAH1 was prepared in phosphate buffer at 150 mM for pH values 7.5 and 8.5, and 200 mM CHES was used for pH values 9.4, 9.8, and 10.2.

The spectra were collected at room temperature on a Varian Inova 500 MHz spectrometer tuned to 89.48 MHz for ^{199}Hg and equipped with a 5 mm broadband probe (*10*). The reference used was a 0.1 mM $Hg(ClO_4)_2$ solution made in a 0.1 mM $HClO_4/D_2O$ solution, and measured at -2250 ppm (*11*). The samples were prepared under a flow of argon by adding 10-15 mg HAH1 to a 15% solution of D_2O, and the concentration of protein was determined by Ellman's test. The Hg(II) was then added as $^{199}Hg(NO_3)_2$ in appropriate amounts to equate to one-half equivalent based on protein concentration. A stock solution of 91% isotopically enriched ^{199}HgO was obtained from Cambridge Isotope Laboratories (*12*), where mercury(II) oxide was dissolved in hydrochloric acid and the pH was adjusted for NMR studies. The pH titrations were done with either HCl or KOH.

3.2.10 ^{199m}Hg(II) Perturbed Angular Correlation (PAC)

Perturbed angular correlation experiments were conducted to determine the coordination environment around the Hg(II). These experiments were done at the ISOLDE GLM beam line at CERN (Geneva, Switzerland). The protein was prepared by resuspending lyophilized HAH1 into either 150 mM phosphate buffer (pH 7.5 and 8.5) or 200 mM CHES buffer (pH 9.4, 9.8, and 10.2). The final concentration was approximately 20-50 μM.

150 μL water was added to a Teflon cup and frozen with liquid nitrogen, then mounted on the ISOLDE GLM beam line in a vacuum chamber. The frozen water was then infused with radioactive ^{199m}Hg(II) (has two gamma photons given off, $t_{½}$=43 min and second gamma photon given off 2.3 ns following 1st) over 1 hr. The ^{199m}Hg(II) was prepared by irradiating liquid lead with 1 GeV photons, then using a mass separator to select for the proper isotope.

The ice, mounted on the beam line, was thawed slowly (approximately 10 min) in a fume hood and under argon to prevent condensation of water vapor from the air. Mercury (II) chloride was added to the thawed water, followed by the appropriate buffer, and finally the protein. The pH was then adjusted since the temperature of the measurements was 1°C, the pH was adjusted for temperature dependence using the website: http://www.liv.ac.uk/buffers/buffercalc.html, left to equilibrate for 10 min, and finally sucrose was added to 55%. The sucrose was added to slow the tumbling of proteins due to Brownian motion.

The PAC instrument consisted of a 6-detector PAC camera set-up, and data collection and analysis was done with Prelude and Winfit software, developed by Butz *et. al.* and using a standard chi-square algorithm (*11*). An adjustment was made using a ^{199m}Hg(II) sample to make sure both γ-photons were given off to the same channel. Each nuclear quadripole interaction (NQI) was modeled using a different set of ν_Q, η, δ, τ_c. and A parameters. Equation 3.4 describes the parameter that describes the strength of the electronic environment and the mercury nucleus. *Q* represents the electronic dipole moment around the nucleus and V_{ZZ} represents the largest eigenvalue of the electric field gradient tensor.

$$\nu_Q = \frac{eQV_{ZZ}}{h} \tag{3.4}$$

The parameter η represents the asymmetry of the system (a value of 0 is used in any axially symmetric system, and values can range up to 1 in a highly asymmetrical system), δ is the relative frequency spread, τ_c is the rotational correlation time, and A is the amplitude of the signal (*11, 12*). Important to note, ν_Q doesn't directly account for the spectrum obtained from PAC so another parameter is introduced ω_1 representing the location of the 1st peak in the Fourier transform.

3.2.11 Hg(II)HAH1 Aggregation State by Gel Filtration

One final study of the Hg(II)HAH1 coordination studies was to determine the aggregation state at the various pH values; this may give information as to whether the different coordination states are monomeric or dimeric. Gel filtration can be used as an analytical method to determine apparent sizes of proteins due to differences in hydrodynamic radii. The radius of the protein is somewhat indicative of its molecular weight; the larger the protein the larger its hydrodynamic radius.

The Hg(II)HAH1 was prepared by purifying the HAH1 as described in **Section 2.2.6**. The HAH1 was then concentrated to approximately 500-1000 μM using ultrafiltration and 1 mM DTT added and allowed to reduce at room temperature for 30 min. The DTT was then removed using a PD10 buffer exchange column (into either the phosphate buffer or the CHES buffer). The protein was concentrated a second time, concentration determined using a BCA assay, and split into two samples (apo and metallated).

The apo sample was injected on an AKTA FPLC equipped with a HR10/30 gel filtration column, equilibrated with 3 CV (approximately 72 mL) of the proper buffer and pH (**Table 3.8**).

Table 3.8: Buffer composition for each pH of the Hg(II)HAH1 gel filtration studies. Note: all buffers were degassed/filtered prior to use, and the pH was adjusted for temperature dependent changes (studies done at 4°C).

Buffer (pH):	Composition:
Phosphate Buffer (7.5)	100 mM Pi buffer (Na_2PO_4, and NaH_2PO_4), 200 mM NaCl
Phosphate Buffer (8.5)	100 mM Pi buffer (Na_2PO_4, and NaH_2PO_4), 200 mM NaCl
CHES Buffer (9.4)	25 mM CHES, 100 mM NaCl
CHES Buffer (9.8)	25 mM CHES, 100 mM NaCl
CHES Buffer (10.2)	25 mM CHES, 100 mM NaCl

The flow rate for these studies was 0.5 mL/min, and samples were collected in 0.5 mL volumes. The apex of the peak was determined to be the elution volume of the protein, which was determined using the Unicorn software provided with the AKTA instrument.

A calibration curve was made at each of the pH values to get an appropriate mass independent of the buffer and pH used. Calibration of the column starts with an injection (25 µL) of a high molecular weight molecule, Blue Dextran. This polymer is large enough to not interact with any of the stationary phase and can be used as an indicator of the void volume (the volume which solutes that don't interact with the stationary phase elute). Next an injection of a 10% (v/v) acetone solution (50 µL) is run to determine the bed volume (total mobile phase volume of the column). The acetone is very small and will interact many times with the stationary phase. These two initial calibration injections give the usable volume of the column, or the volume where solutes would elute. The Blue Dextran elution volume (v_o) and the acetone

elution volume (v_t) are used for the calculation of the standard curve. The standard curve is made of a linear plot of the K_{av} (partition coefficient) vs. the log MW. A plot of elution volume vs. molecular weight would give a sigmoidal curve with asymptotes pertaining to solutes that are too large or too small for the resolution of the column. To account for the nonlinearity of the plot, a new term, K_{av}, is used. This term takes into account the void volume, the bed volume and the elution volume so this value becomes linear in comparison to the molecular weight. Equation 3.5 describes this relationship in order to determine the apparent molecular weight based on a set of standards.

$$K_{av} = \frac{v_e - v_0}{v_t - v_0} \tag{3.5}$$

The calibration curve was made by injecting 100 µL of a mixture of standards made by mixing 25 µL of each stock protein solution. **Table 3.9** shows the standards and their masses. The standards were injected as a mixture and eluted as a cluster of well-defined peaks. The Unicorn 5.0 software was again used to determine the apex of each of the peaks.

Table 3.9: List of calibration standards used on the HR10/30 gel filtration column to determine apparent molecular weights of the different aggregation states of apo and Hg(II)HAH1.

Calibration Standard:	Molecular Weight (Daltons):
Aprotinin	6,600
Cytochrome C	13,700
Carbonic Anydrase	29,000
Albumin	43,000
Blue Dextran	2,000,000

Figure 3.3 depicts a typical standard curve plot for calibrating the HR10/30 gel filtration column with the standards described in **Table 3.9**. After the calibration curve is calculated, the apoHAH1 and Hg(II)HAH1 protein was injected on the column with exactly the same conditions as the calibration curve (i.e. buffer and flow rate).

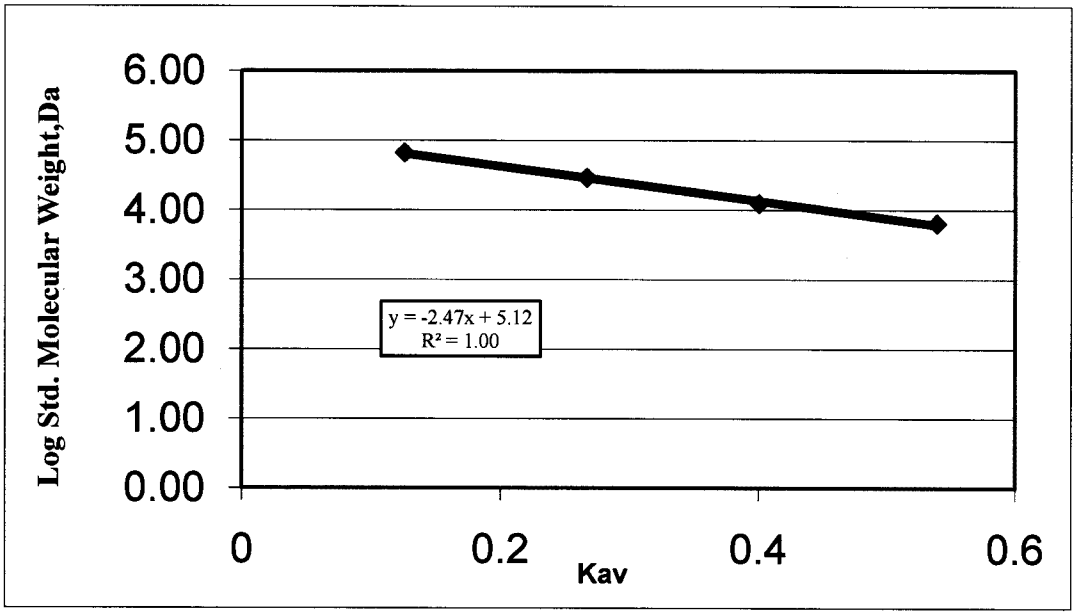

Figure 3.3: A typical plot used to determine a K_{av} value that corresponds to an apparent molecular weight.

Preparation of the Hg(II)HAH1 was done by adding one-half equivalent $HgCl_2$ to the protein solution. 100µl was injected on the column and ran at a flow rate of 0.5 ml/min. The apex of the peak was determined using the Unicorn 5.0 software, and calculated against the calibration curve to get the apparent mass. All apparent molecular weights were determined as described, changing only the buffer and pH of the mobile phase.

3.3 References

1. Lwande, J. (2004) SYNTHESIS AND CHARACTERIZATION OF A RECOMBINANT THROMBIN INHIBITOR, in *Chemistry Department*, Western Michigan University, Kalamazoo, MI, MS Thesis.

2. Salzet, M., Chopin, V., Baert, J., Matias, I., and Malecha, J. (2000) Theromin, a novel leech thrombin inhibitor, *J Biol Chem 275*, 30774-30780.

3. Bieth, J. G. (1980) Pathophysiological interpretation of kinetic constants of protease inhibitors, *Bull Eur Physiopathol Respir 16 Suppl*, 183-197.

4. Ottiger, M., Delaglio, F., and Bax, A. (1998) Measurement of J and dipolar couplings from simplified two-dimensional NMR spectra, *J Magn Reson 131*, 373-378.

5. Banci, L., Bertini, I., Cantini, F., Felli, I. C., Gonnelli, L., Hadjiliadis, N., Pierattelli, R., Rosato, A., and Voulgaris, P. (2006) The Atx1-Ccc2 complex is a metal-mediated protein-protein interaction, *Nat Chem Biol 2*, 367-368.

6. Avbelj, F., Kocjan, D., and Baldwin, R. L. (2004) Protein chemical shifts arising from alpha-helices and beta-sheets depend on solvent exposure, *Proc Natl Acad Sci U S A 101*, 17394-17397.

7. Ishima, R., and Torchia, D. A. (2000) Protein dynamics from NMR, *Nat Struct Biol 7*, 740-743.

8. Kay, L. E., Nicholson, L. K., Delaglio, F., Bax, A., and Torchia, D. A. (1992) Pulse sequences for removal of the effects of cross correlation between dipolar and chemical-shift anisotropy relaxation mechanisms on the measurement of heteronuclear T1 and T2 values in proteins *J Magn Reson 97*, 359-375.

9. Rousselot-Pailley, P., Seneque, O., Lebrun, C., Crouzy, S., Boturyn, D., Dumy, P., Ferrand, M., and Delangle, P. (2006) Model peptides based on the binding loop of the copper metallochaperone Atx1: selectivity of the consensus sequence MxCxxC for metal ions Hg(II), Cu(I), Cd(II), Pb(II), and Zn(II), *Inorg Chem 45*, 5510-5520.

10. Fujisawa, K., Imai, S., Kitajima, N., and Moro-oka, Y. (1998) Preparation, Spectroscopic Characterization, and Molecular Structure of Copper(I) Aliphatic Thiolate Complexes, *Inorg Chem 37*, 168-169.

11. Wrackmeyer, B., and Contreras, R. (1992) 199Hg NMR Parameters, *Annu. Rep. NMR Spectrosc. 24*, 267-329.

12. Iranzo, O., Thulstrup, P. W., Ryu, S. B., Hemmingsen, L., and Pecoraro, V. L. (2007) The application of (199)Hg NMR and (199m)Hg perturbed angular correlation (PAC) spectroscopy to define the biological chemistry of Hg(II): a case study with designed two- and three-stranded coiled coils, *Chemistry 13*, 9178-9190.

CHAPTER 4

BIOCHEMICAL PROPERTIES OF THEROMIN: A NOVEL THROMBIN INHIBITOR

4.1 Introduction

There has been a lot of attention placed on discovering better anticoagulation therapies for patients. Currently the most common anticoagulant drug is heparin. Heparin is a sulfated glycosaminoglycan, that the body naturally produces to help maintain the blood in a fluid state or help stop clotting when necessary (*1*). Heparin works by binding to the inhibitor antithrombin III, this further increases its inhbiting abilities. The complex then can go on to inhibit many enzymes of the clotting cascade responsible for creating a clot, specifically, Factor Xa and α-thrombin (*2, 3*).

This study focused on another α-thrombin inhibitor, theromin, which was isolated from the leech *Theromyzon tessulatum* by Salzet *et al.* (*4*). In their study, theromin was found to be a strict tight binding α-thrombin inhibitor with a K_i = 12 fM. This value is stronger than that obtained with hirudin (*5-7*)) and haemadin (100 fM) (*8*)) under similar conditions. Theromin monomer had little α-thrombin inhibition, leading them to suggest that dimerization is necessary to give the peptide an active structure configuration for complete binding to α-thrombin. The way this was discovered was to use a reducing agent on the theromin peptide to maintain it in a monomeric state and determine its K_i. The reported K_i was significantly higher for

the monomer than they measured for the dimer. Salzet also reported the monomer has some anti-α-thrombin activity. This idea led to the suggestion that each monomer binds to one of the exosites and blocks both active sites by wrapping around as a dimer. Theromin has no significant sequence similarity to other α-thrombin inhibitors. Theromin exists as a homodimer of 134 residues (important to note there were no post translational modifications to the peptide, this is in contrast to hirudin which has a sulfated tyrosine at residue 63 (*9, 10*)), each monomer containing 16 cysteine groups that form 8 disulfide bonds which would be important in creating its dimeric structure. It binds to α-thrombin denying access to both the fibrinogen site as well as the proteolytic site. Detailed understanding of the folding mechanism of theromin is likely to contribute vital information necessary for development of new anticoagulants. Due to its potential biomedical importance, there is need for further characterization of the recombinant theromin. A comparison should be drawn between the reduced and the oxidized forms then compared to hirudin. To carry out further studies on theromin, it is necessary to devise an easier and faster way of getting large amounts of the protein. A previous master's student, Joel Lwande (*11*), successfully designed and synthesized the theromin gene through the PCR amplification method and subsequently expressed the protein in *E. coli* and purified it. The α-thrombin binding affinity for the recombinant theromin, K_i, was determined.

4.2 Recombinant Expression of Theromin

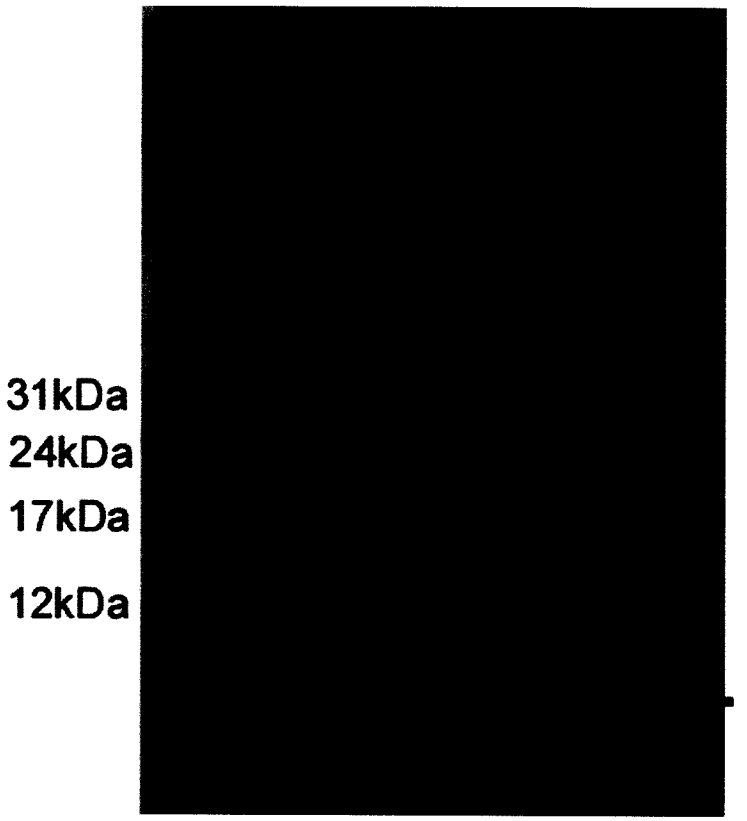

Figure 4.1: SDS-PAGE of theromin after 16 hours of cutting. Top arrow indicates the oxidized dimer of theromin (supposed active form), and bottom arrow shows the faint band of the monomer form.

The plasmid, pET42a, was transformed into Rosetta2(DE3) cells. The protein overexpressed by this plasmid was a 30kDa peptide of Glutathione S-Transferase tagged theromin (GST-theromin). The purification involved initially selecting for the tag using a column equipped with glutathione that can bind the tag, the protein was washed with several column volumes of buffer and eluted with a gradient of up to 10 mM glutathione. The elution from the GST-Tag column exhibited one peak that contained the fusion protein. The protein was then exchanged into Factor Xa buffer for cleavage; this was accomplished using a buffer exchange column. The exchanged protein was concentrated to approximately 10 mL and the concentration of the tagged protein determined and Factor Xa was added to 10 μg/mg protein (typical yield was about 20 mg of tagged protein in a liter prep). The cleavage was performed for 16 hr, monitored by SDS-PAGE. The protein was then loaded on the same column equipped with glutathione to remove the tag, leaving a pure theromin peptide that was 7.2 kDa in size observed by SDS-PAGE, there was also some oxidized dimer, at 14 kDa on the gel (**Figure 4.1**). This size of protein was similar to what Salzet noticed in the native form (*4*).

4.3 Theromin Inhibition Kinetics Toward α-Thrombin

The activity of theromin was monitored indirectly by measuring the rate of chromozyme S-2238 cleavage, both with and without theromin.

$$I_t = E_t i + K_t\left(\frac{i}{1-i}\right),\left(i = 1 - \frac{v_i}{v_0}\right) \qquad (4.1)$$

Equation 4.1 describes measuring the activity of α-thrombin at various inhibitor concentrations and then correlating each $[I]/(1-v_i/v_0)$ vs $1/(v_0/v_i)$, where v_i is the rate at each inhibitor concentration, v_0 is the v_{max} rate, and [I] is the inhibitor concentration. This correlation comes from a derivation by Henderson (*12*), which was further simplified by Bieth (*13*). The relationship comes from an assumption theromin is acting as a noncompetitive tight binding inhibitor (described by Salzet in ref. 5); this would mean that theromin doesn't compete for the active site, rather it binds to an allosteric site (in this case either or both of the exosites), which alters the state of the protein preventing substrate binding. The determination of the binding kinetics was based on hirudin, which binds to exosite 2 and causes an allosteric inhibition of the active site. Theromin is expected to do the same type of inhibition because Salzet suggested theromin wraps around α-thrombin. This wrapping event would cause allosteric changes throughout α-thrombin that could further enhance the binding of theromin. There is, however, no evidence yet for this.

The enzyme, in a noncompetitive inhibition model, can be described as existing in four distinct states: [E], [ES], [EI], and [ESI], in the case of several direct α-thrombin inhibitors that interact in a tight binding fashion the ESI complex is very low concentration or possibly even non-existent. Theromin fits the description as a very tight binding inhibitor, so a very small amount would be presumed in the ESI form. This allows for elimination of this factor from the kinetics equation and leaves the kinetics only dependent on the different reaction rates (v_0 and v_i, where the v_0 is

the rate in the absence of inhibitor and v_i is with inhibitor added) and the inhibitor concentration.

Plotting [I]/[1-(v_i/v_o)] vs [v_o/v_i] yields a linear correlation appears where $K_{i,app}$ can be calculated from the slope. Theromin was analyzed in this manner to determine the $K_{i,app}$. The peptide was added to the α-thrombin and allowed to equilibrate for 10

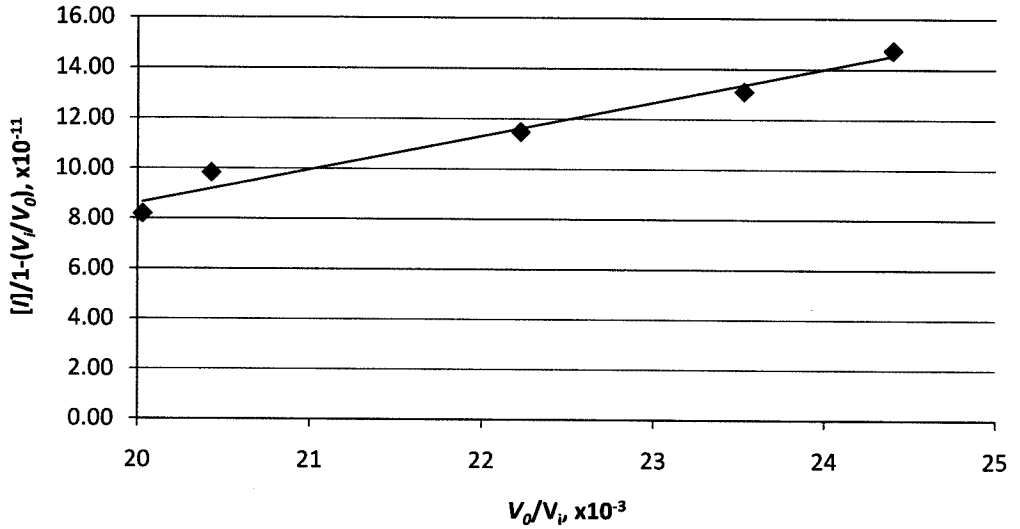

Figure 4.2: The slope of the line is the $K_{i,app}$, which is 13.5 fM, compared to the $K_{i,app}$ for the native peptide. The r^2 value of the line is 0.97.

minutes before substrate was added; this was sufficient time to allow the peptide to bind to α-thrombin and most likely eliminate the possibility of an ESI complex. **Figure 4.2** shows the resulting curve from the kinetics experiments. The slope of the plot is $K_{i,app}$, which was calculated to be 14.9±8 fM, which is in agreement with what has been published by Salzet (2001) of 12±5 fM. The K_i is an average of three assays that gave inhibition constants: 24.1 fM, 13.5 fM, and 7.2 fM. It seems based on comparison of inhibition, and mass spectrometry analysis by Salzet that there are no

modifications of the peptide in the leech, since the masses match up and both peptides exhibit the same inhibition capacity.

Theromin isn't the only direct α-thrombin inhibitor to date drugs such as Ximelagatran (*14, 15*). This drug is a small organic molecule that can be taken orally as a prodrug, which is converted in the liver and other tissues to the active form, melagatran. This conversion involves dealkylation and dehydroxylation. The proposed advantage to this drug is that it can be taken orally, and more importantly, it doesn't require constant monitoring of the blood coagulation time. This is a major advantage due to issues with patient compliance with taking their medicines. Another direct α-thrombin inhibitor, dabigatran, is considered to be superior to the drug warfarin in preventing stroke (*16*). This drug is also a prodrug that is converted to its active form by an esterase in the blood serum (*16*). It has the same advantages as ximelagatran does, with the exception that less of the dabigatran is bioavailable (20% for the Ximelagatran compared to 6.5% of the dabigatran). These drugs have inhibition constants of 4.5 nM for dabigatran (*17*), and 2 nM for Ximelagatran (*18*).

While these drugs look to be promising, they have significantly lower inhibition constants for α-thrombin than does hirudin (current drug Lepirudin®) (21 fM), and the newly discovered theromin (14.9 fM). The disadvantages of the new, stronger, direct α-thrombin inhibitors is they currently need to be interveinous. This would also be the likely route of entry for theromin, if it were to go to FDA approval. These types of strong direct α-thrombin inhibitors need to be monitored very closely, which is a disadvantage compared to ximelagatran and dabigatran. Not only do the

latter two drugs not need to be monitored, but they can be taken orally. These are two very important factors when considering a drug candidate. This poses the idea that these drugs need to be modified in some way to be taken orally and then possibly modified so they could be taken without constant monitoring.

Direct α-thrombin inhibitors seem to be the direction research has been going. They are much more efficient and more easily controlled than inhibitors to factors upstream of α-thrombin in the blood coagulation cascade. One example is Coumadin® (also referred to as Warfarin), the way it inhibits is the enzyme epoxide reductase which then interferes with the production of vitamin K (*19, 20*). This prevents blood clotting because vitamin K is important for post-translational modifications of proteins that create prothrombin (Factor II), the precursor to active α-thrombin (*19*). It also is required for production of coagulation Factors: VII, IX, and X (*19, 21*). This single inhibition has a very wide range of effects on the blood, requiring the need for constant monitoring and initial drug dose changes to get the proper dose based on body mass. This is a huge disadvantage for this drug, even though it is very effective. There are other issues, mentioned in **Chapter 1**, associated with another indirect inhibitor heparin. Briefly, this drug forms a complex with platelet Factor 4 and can activate antibodies to it through and autoimmune response. The tail of this antibody can activate platelets causing a secondary clot to form.

So direct α-thrombin inhibitors are very important to maintaining the blood in a fluid state, with few disadvantages as compared to historically used drugs.

Theromin is a strong direct α-thrombin inhibitor that can inhibit very efficiently. There is still a lot of characterization needed for theromin to get it close to being a drug candidate, as it is necessary to understand how it reacts with the other components in the blood. One observation was that it resembles metallothioneins and could possibly bind copper(I), so theromin might have multiple functions and cause many problems as a therapy for clot prevention.

4.4 Copper Binding Studies

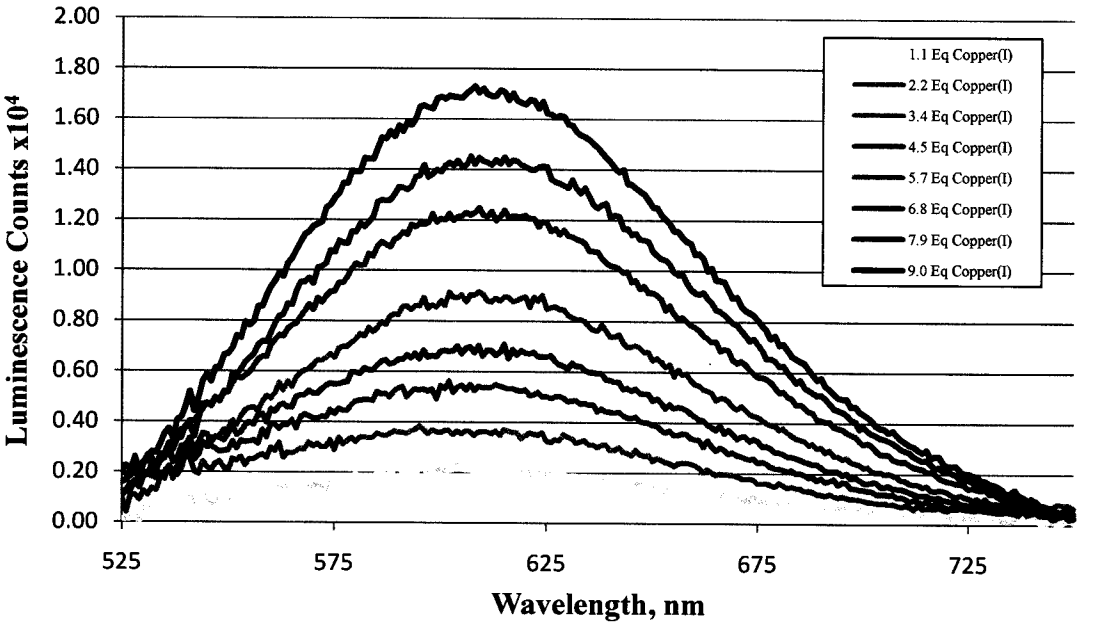

Figure 4.3: Titration of copper(I) into theromin. Theromin exhibits a metallothionein-like primary structure. Titration was up to 9 equivalents, based on ICP-AES measurements of copper(I) standards. The slit widths used were 5mm for both excitation and emission.

Theromin's main function seems to be its ability to bind α-thrombin and inhibit it with great efficiency. Structurally, however, it has a remarkable resemblance to metallothioneins (*22*). This was noted by its arrangement of the 16 cysteines within its structure and was tested by titrating copper(I) into it. It is not clear, however, if this is a function of the peptide, or if it is a method for protecting the peptide from proteases when being injected into the host.

Metallothioneins are low molecular weight peptides that are full of cysteines with the ability to bind different metals. In particular cadmium (*23, 24*), zinc (*25*), and copper (*26*). These metallothioneins are suggested to be involved in preventing heavy metal toxicity within cells (*27*). It wouldn't seem theromin is working with the ability to bind heavy metals, but that might be a role in the leech itself.

Figure 4.3 shows the fluorescence of the copper(I) thiolates at an excitation of 290 nm. The emission is around 615 nm, which is similar to what Fujisawa noted for aliphatic copper thiolates (he described a peak at 618 nm for an aliphatic complex containing 5 eq copper) (*28*). The titration was stopped after the emission plateaued, which turned out to be around 7 eq based on ICP-AES analysis done in Dr. Carla Koretsky's lab at Western Michigan University. This is a novel find for this peptide, copper(I) binding hasn't been shown for any of the other similar peptides, for example hirudin, but maybe be a good model system for metallothioneins. Even though it is shown here copper(I) binds, it is still not known what the clusters look like.

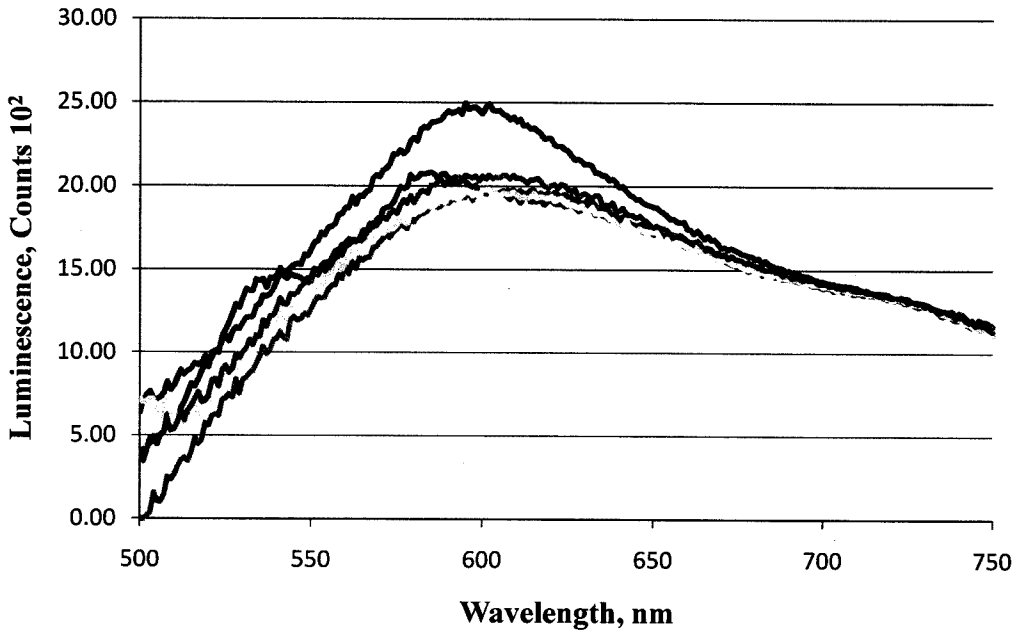

Figure 4.4: Azide titrations into copper(I) theromin to determine strength of copper(I) binding. Azide in excess of 50 equivalents isn't sufficient to pull copper(I) out of theromin. Excitation was at 290 nm. Brown: 0 eq azide, red: 16.7 eq azide, orange: 20 eq azide, yellow: 26.7 eq azide, and green: 50 eq azide.

Following the titrations of theromin with copper(I), it was important to determine what the binding affinity was. To do this sodium azide was titrated in up to 3 μmol (essentially 50 eq of azide to 1 eq copper) (**Figure 4.4**). The azide had very little effect on the copper(I) bound to theromin. One chelator that wasn't tried was cyanide, this is a very strong chelator for copper(I). For this reason cyanide is very deadly, as it can pull copper out of the respiratory proteins in the mitochondria.

4.5 Conclusion

Theromin shows a lot of promise for being a strong inhibitor to α-thrombin, it can bind and inhibit α-thrombin with an inhibition constant of 13.5 fM which is significantly stronger than the latest direct α-thrombin inhibitor hirudin (~21 fM). There is a need for stronger inhibitors to α-thrombin that can be easily regulated in therapies to prevent clotting. Currently the most widely used drug is heparin which in some patients can actually cause an autoimmune response to the heparin/α-thrombin complex that will activate platelets and cause clots. Recently, hirudin has been used as an alternative to heparin for this reason, it is a very effective drug, however, and it has to be tightly monitored because it can cause bleeding events.

Theromin's ability to bind copper(I) seems an unlikely characteristic *in vivo*. This is would be the case for two reasons, in the blood copper is available as copper(II), and not copper(I) and the affinity of this oxidation state of copper would be much lower due to hard soft acid base (HSAB) theory suggesting copper(II) would much rather bind to something like the nitrogen groups of histidine rather than the sulfides of cysteines. This attribute of theromin could have functionality in the leech itself though, but many more studies would need to be done to determine that aspect. A second reason copper(I) binding is unlikely *in vivo* is that even if there were to be copper(I) available for binding, the affinity would need to be low enough that there isn't competition between copper and α-thrombin. If the binding affinity of theromin for the metals in the blood were higher than the affinity for α-thrombin, then the leech

wouldn't be able to maintain the blood in a fluid state, independent of the host and would essentially die off.

4.6 Future Studies

There are many experiments that could be done to understand both what this peptide does in the host as well as what it does in the leech. The main experiment that could to be done as an independent verification of the peptide we were working with. A second verification would be to do N-terminal sequencing, giving us a stronger idea of the peptide we are measuring. This peptide does not behave well at all, but with the idea that it can bind copper, maybe a mass of the copper loaded peptide can be determined. Based on previous work the native protein didn't have any post translational modifications. It does beg the question to how the leech stores and maintains a stock of this peptide.

Other experiments would be biophysical in nature, using EXAFS and NMR. It would be interesting to determine what the copper(I) clusters look like using EXAFS, we could also titrate in cadmium(II) and do cadmium-113 NMR. The latter experiment would give more of a quantitative idea of the copper(I) thiolates that exist. It would also be interesting to determine which cysteines are involved in the binding of the copper(I) this could be done by NMR, selective labeling of the cysteines might give information about the assembly of the clusters in the Cu(I)theromin. It would also be interesting to determine if other metals can bind, such as zinc(II).

Further experiments involving the interaction with α-thrombin would be mutational analysis to determine if mutating certain residues makes a stronger hold on

α-thrombin resulting in a stronger inhibition constant. Again NMR could be done, $^{13}C,^{15}N$ labeling α-thrombin and titrating in theromin could give structural information as to how theromin binds. It was suggested that it binds initially to exosite I and wraps around similar to a Ziploc® seal around to exosite II. There is no evidence for this except that the peptide likes to be a dimer outside the leech, this may just be an inherent feature of the protein *in vitro* and not something that occurs *in vivo*. Understanding how theromin works could shed light on why hirudin can bind strongly and not need to wrap around to the other site to be a strong inhibitor. It was shown by Salzet that the dimer was, at least *in vitro*, how the peptide interacts with α-thrombin. It would be interesting to see if this is the case *in vivo*. One way to do this would be to develop NMR methods for looking at whole blood and selecting for α-thrombin in some way.

A few experiments that would be interesting on the leech would be to determine how the peptide is made and stored. This would give insight into understanding how to keep this peptide in working shape. In our studies the peptide did not hold up well on its own, it degraded within a day or two, so if we could understand how the leech makes and protects the peptide, we could do the same. Again, the copper(I) binding does this serve a purpose in the leech, like a multifunctional peptide? It would not be wrong to expect the leech to have metallothioneins, so what is the evolutionary idea behind making this peptide. The dimer of theromin doesn't utilize all the sulfides so it is possible they are needed to

mediate the wrapping of theromin around the α-thrombin. Mutation studies would give solid evidence to this idea.

Overall there is a lot of work that can be done on this peptide to understand its function in the host and its possible alterior role in the leech itself. These types of experiments could be done to determine new models and new functions of homologous proteins (for example theromin seems to be a homolog to metallothioneins).

4.7 References

1. Jorpes, J. E. (1964) The Early History of Heparin, *Ann N Y Acad Sci 115*, 392-398.

2. Bjork, I., and Lindahl, U. (1982) Mechanism of the anticoagulant action of heparin, *Mol Cell Biochem 48*, 161-182.

3. Chuang, Y. J., Swanson, R., Raja, S. M., and Olson, S. T. (2001) Heparin enhances the specificity of antithrombin for thrombin and Factor Xa independent of the reactive center loop sequence. Evidence for an exosite determinant of Factor Xa specificity in heparin-activated antithrombin, *J Biol Chem 276*, 14961-14971.

4. Salzet, M., Chopin, V., Baert, J., Matias, I., and Malecha, J. (2000) Theromin, a novel leech thrombin inhibitor, *J Biol Chem 275*, 30774-30780.

5. Rydel, T. J., Tulinsky, A., Bode, W., and Huber, R. (1991) Refined structure of the hirudin-thrombin complex, *J Mol Biol 221*, 583-601.

6. Chang, J. Y. (1991) Deciphering the structural elements of hirudin C-terminal peptide that bind to the fibrinogen recognition site of alpha-thrombin, *Biochemistry 30*, 6656-6661.

7. Grutter, M. G., Priestle, J. P., Rahuel, J., Grossenbacher, H., Bode, W., Hofsteenge, J., and Stone, S. R. (1990) Crystal structure of the thrombin-hirudin complex: a novel mode of serine protease inhibition, *Embo J 9*, 2361-2365.

8. Strube, K. H., Kroger, B., Bialojan, S., Otte, M., and Dodt, J. (1993) Isolation, sequence analysis, and cloning of haemadin. An anticoagulant peptide from the Indian leech, *J Biol Chem 268*, 8590-8595.

9. Folkers, P. J., Clore, G. M., Driscoll, P. C., Dodt, J., Kohler, S., and Gronenborn, A. M. (1989) Solution structure of recombinant hirudin and the Lys-47----Glu mutant: a nuclear magnetic resonance and hybrid distance geometry-dynamical simulated annealing study, *Biochemistry 28*, 2601-2617.

10. Haruyama, H., and Wuthrich, K. (1989) Conformation of recombinant desulfatohirudin in aqueous solution determined by nuclear magnetic resonance, *Biochemistry 28*, 4301-4312.

11. Lwande, J. (2004) SYNTHESIS AND CHARACTERIZATION OF A RECOMBINANT THROMBIN INHIBITOR, in *Chemistry Department*, Western Michigan University, Kalamazoo, MI, MS Thesis.

12. Henderson, P. J. (1972) A linear equation that describes the steady-state kinetics of enzymes and subcellular particles interacting with tightly bound inhibitors, *Biochem J 127*, 321-333.

13. Bieth, J. G. (1980) Pathophysiological interpretation of kinetic constants of protease inhibitors, *Bull Eur Physiopathol Respir 16 Suppl*, 183-197.

14. Schulman, S., Wahlander, K., Lundstrom, T., Clason, S. B., and Eriksson, H. (2003) Secondary prevention of venous thromboembolism with the oral direct thrombin inhibitor ximelagatran, *N Engl J Med 349*, 1713-1721.

15. Di Nisio, M., Middeldorp, S., and Buller, H. R. (2005) Direct thrombin inhibitors, *N Engl J Med 353*, 1028-1040.

16. Connolly, S. J., Ezekowitz, M. D., Yusuf, S., Eikelboom, J., Oldgren, J., Parekh, A., Pogue, J., Reilly, P. A., Themeles, E., Varrone, J., Wang, S., Alings, M., Xavier, D., Zhu, J., Diaz, R., Lewis, B. S., Darius, H., Diener, H. C., Joyner, C. D., and Wallentin, L. (2009) Dabigatran versus warfarin in patients with atrial fibrillation, *N Engl J Med 361*, 1139-1151.

17. Wienen, W., Stassen, J. M., Priepke, H., Ries, U. J., and Hauel, N. (2007) In-vitro profile and ex-vivo anticoagulant activity of the direct thrombin inhibitor dabigatran and its orally active prodrug, dabigatran etexilate, *Thromb Haemost 98*, 155-162.

18. Gustafsson, D., and Elg, M. (2003) The pharmacodynamics and pharmacokinetics of the oral direct thrombin inhibitor ximelagatran and its active metabolite melagatran: a mini-review, *Thromb Res 109 Suppl 1*, S9-15.

19. Whitlon, D. S., Sadowski, J. A., and Suttie, J. W. (1978) Mechanism of coumarin action: significance of vitamin K epoxide reductase inhibition, *Biochemistry 17*, 1371-1377.

20. Cranenburg, E. C., Schurgers, L. J., and Vermeer, C. (2007) Vitamin K: the coagulation vitamin that became omnipotent, *Thromb Haemost 98*, 120-125.

21. Kalafatis, M., Swords, N. A., Rand, M. D., and Mann, K. G. (1994) Membrane-dependent reactions in blood coagulation: role of the vitamin K-dependent enzyme complexes, *Biochim Biophys Acta 1227*, 113-129.

22. Huffman, D. L. Unpublished Observations.

23. Cousins, R. J. (1979) Metallothionein synthesis and degradation: relationship to cadmium metabolism, *Environ Health Perspect 28*, 131-136.

24. Klaassen, C. D., Liu, J., and Choudhuri, S. (1999) Metallothionein: an intracellular protein to protect against cadmium toxicity, *Annu Rev Pharmacol Toxicol 39*, 267-294.

25. Maret, W. (2000) The function of zinc metallothionein: a link between cellular zinc and redox state, *J Nutr 130*, 1455S-1458S.

26. Butt, T. R., Sternberg, E. J., Gorman, J. A., Clark, P., Hamer, D., Rosenberg, M., and Crooke, S. T. (1984) Copper metallothionein of yeast, structure of the gene, and regulation of expression, *Proc Natl Acad Sci U S A 81*, 3332-3336.

27. Petering, D. H., and Fowler, B. A. (1986) Roles of metallothionein and related proteins in metal metabolism and toxicity: problems and perspectives, *Environ Health Perspect 65*, 217-224.

28. Fujisawa, K., Imai, S., Kitajima, N., and Moro-oka, Y. (1998) Preparation, spectroscopic characterization, and molecular structure of copper(I) aliphatic thiolate complexes, *Inorg Chem 37*, 168-169.

CHAPTER 5

THE INTERACTION OF WILSON DISEASE PROTEIN METAL-BINDING DOMAIN 4 WITH HAH1

5.1 Introduction

There have been many studies, as noted in **Chapter 2**, looking at the Wilson disease protein and its interaction with its metallochaperone HAH1 in humans (*1, 2*). This interaction is a complicated interaction because of the individual characteristics of the N-terminal domains. To date the constructs investigated are WLN2 (*4*), WLN4 (*1, 5*), WLN3-4 (*1*), WLN4-6 (*6*), WLN5-6 (*7*), and WLN1-6 (*2*). Each of these various constructs gives vital information, as well as provide varying data, suggesting that the whole N-terminal domain works in concert and removing some of it strongly affects the behavior of the protein. One example of this is comparing the work done on the WLN1-6 with WLN5-6. When domains 5 and 6 are alone Cu(I)HAH1 doesn't seem to have any interaction with it, neither in the form of complex nor in copper(I) delivery (*7*). However, when WLN1-6 was investigated there was an interaction with WLN5-6, in the form of copper delivery, but no appreciable complex between WLN5-6 and Cu(I)HAH1 could be detected.

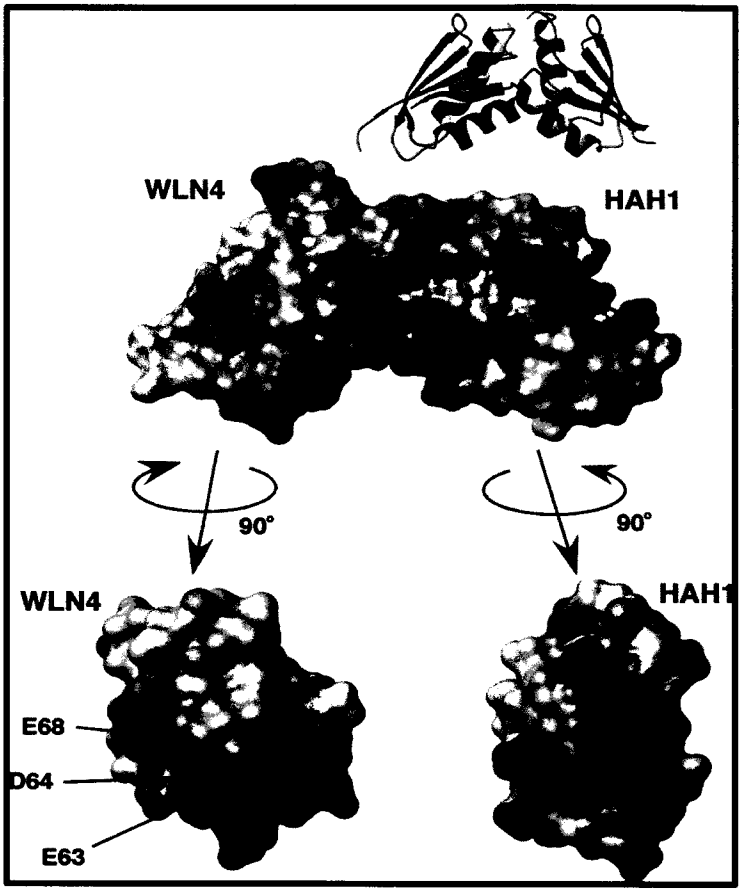

Figure 5.1: A model put together by Dr. David Huffman, Dr. Ivano Bertini, and Dr. Simone Ciofi depicting a possible electrostatic interaction between the positively charged HAH1 and the negatively charged WLN4.

There is still quite a bit to learn from these different interactions; one part of the puzzle that still needs to be investigated is the mechanism of the hand-off between the Cu(I)HAH1 and the different metal-binding domains of WLNP. Only three of the metal binding domains (WLN1, 2, and 4) can create an appreciable NMR-observable complex with Cu(I)HAH1. In the case of the WLN3, 5, and 6 there is no complex formation detected, and they are in slow exchange on the NMR timescale. There is

however, one domain that seems to be an excellent choice for determining this mechanism, WLN4. WLN4 (pI 3.9) is a highly negative domain, in contrast to HAH1 (pI 7.5) that is highly positive. On an NMR timescale this interaction, mediated by copper, is observed, possibly due to strengthened interaction via electrostatics. **Figure 5.1** shows a model developed by David Huffman, Simone Ciofi, and Ivano Bertini depicting the possible interaction between these two proteins. In light of this strong interaction, WLN4 and Cu(I)HAH1 have been chosen to determine the mechanism for copper delivery from the chaperone to the domains of WLNP. One study used computer modeling to show the interaction between these two proteins, and found that there are two different 3-coordinate species that may exist during the hand off (*8*). To determine if these types of intermediates could be formed, mutants were made where individual metal-binding cysteines of either WLN4 or HAH1 were mutated (*9-11*). These mutated proteins were then titrated with the wildtype partner and copper(I) to determine whether a complex could be found between them. This idea is very similar to the work by Banci *et. al.* with the ATX1/Ccc2a system in yeast (*3*). ATX1 is the yeast homolog to HAH1 and Ccc2a is the yeast ATPase homolog to WLNP. Their data showed that one cysteine from each of the binding partners could be mutated and still facilitate an NMR-observable complex. Data from this project found that both cysteines are necessary in the WLN4 domain to facilitate a complex formation, and only cysteine-12 of HAH1 was necessary.

5.2 Wilson Disease Protein Domain 4 Expression and Purification

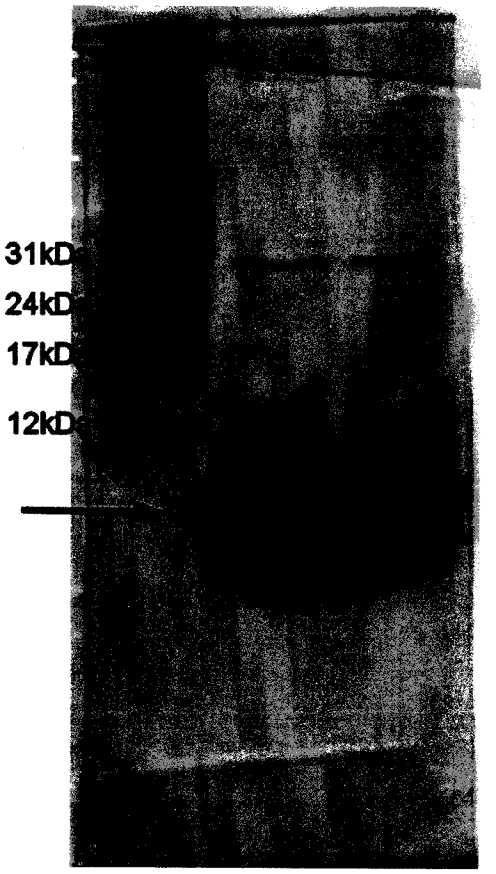

Figure 5.2: SDS PAGE showing a highly pure cleaved WLN4.

The WLN4 was expressed as a thioredoxin fusion protein with the vector pET32Xa/LIC. Expression and purification methods were described in **Section 3.2.3**. The induction was monitored by 15% SDS-PAGE. Once the induction was determined successful, the protein was purified using a HisPrep column to select TrxWLN4, followed by several buffer exchanges and concentration events to get it

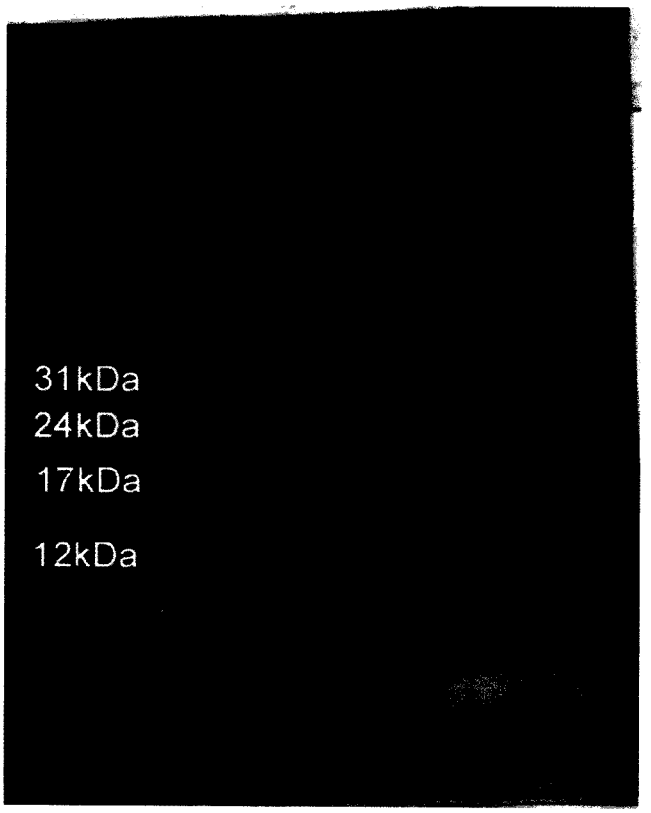

Figure 5.3: SDS PAGE showing pure HAH1 protein.

into Factor Xa cleavage buffer. The protein was cleaved for 18 hr at room temperature. After cleavage the protein was run through the HisPrep column again and subsequently concentrated using ultrafiltration and run through a gel filtration column to get purified WLN4 (**Figure 5.2**).

All purifications of the different isopically labeled or mutant WLN4 proteins were done the same way. The only differences lie in the expression procedures, noted in **Section 3.2.3- 3.2.5**.

5.3 HAH1 Expression and Purification

HAH1 was expressed using the vector pET11d-HAH1. The details of the expression and purification are detailed **Section 3.2.6**. The induction was again monitored using 15% SDS-PAGE. The purification for HAH1 was quite different from WLN4, mostly due to not having a thioredoxin tag and it being positive (pI around 7.5). The purification involved connecting a DEAE and CM column in tandem and using MES buffer, pH 6.0. The DEAE column was first, collecting most of the bacterial proteins, as they are negatively charged. The CM column then picked up the HAH1 that was eluted as a single peak on the chromatogram. The fractions containing the HAH1 were collected and concentrated to be run on the gel filtration column to be sure of their purity (**Figure 5.3**). Following the gel filtration the protein was highly pure and ready for experiments. Again, these gels represent the native HAH1 purification, but the purification of the isotopically labeled and mutated HAH1 exhibited exactly the same characteristics, so gels and purification methods were the same. The only difference being the methods for expressing the protein (**Section 3.2.6**).

5.4 NMR Titrations of WLN4 with HAH1 and Copper(I)

To investigate the possible intermediates involved in the mechanism of transferring copper to the WLN4, mutants were made of each of the proteins to be titrated together and analyzed using ^{1}H-^{15}N HSQC on a Bruker Avance NMR at either 700 MHz or 800 MHz at the Center for Magnetic Resonance, Florence, Italy. Each titration started out with 1 mM, labeled, mutant protein. The mutant protein was labeled to prevent detection of homodimerization that could give a false positive for interaction between the species. Two spectra were collected, a ^{1}H (proton), and a ^{1}H-^{15}N HSQC, the proton spectrum was collected to monitor the amide protons, making sure were still folded correctly (monitoring peak distributions), and to monitor the proline protons as a method for knowing when the titration reacted a 1:1 ratio for the protein. The temperature of these experiments was 300K. During the titration of the apo proteins, the ^{1}H-^{15}N HSQC was monitored for any shifts in the spectra due to interactions that weren't metal mediated. During the HSQC titrations, the native protein was titrated into the NMR solution containing the mutant. For all experiments there was no detectable interaction between the mutant and the native binding partner in the absence of metal. There was, however, one titration (C15A HAH1/wtWLN4) that did show some small shifts in the ^{1}H-^{15}N HSQC in the absence of metal, but when EDTA was titrated in the shifts moved back to the original positions. It was suggested that there was contamination of a divalent metal, most likely zinc(II), as this is a common metal and previous experiments had seen such contamination before, in the Bertini lab. The set up of the experiment was such that

metal mediated interaction could be monitored. **Table 5.1** shows list of the titrations done. Studies prior to this work have described the interaction of HAH1 with the various domains of WLNP. A recent study that mentioned a possible interaction between the domains in the absence of copper(I), however, there was up to 8% copper in the buffer solution, so the evidence was not substantiated (*7*).

Table 5.1: The NMR experiments used to monitor the titration using ^{1}H and ^{1}H-^{15}N HSQC.

Exp. Number:	Description:	Protein:	Titrant:
1 2	1 1D Proton Spectrum ^{1}H-^{15}N HSQC	apoC15A HAH1	-
3 4	1D Proton Spectrum ^{1}H-^{15}N HSQC	apoC15A HAH1	¼ eq apoWLN4
5 6	1D Proton Spectrum ^{1}H-^{15}N HSQC	apoC15A HAH1	½ eq apoWLN4
7 8	1D Proton Spectrum ^{1}H-^{15}N HSQC	apoC15A HAH1	¾ eq apoWLN4
9 10	1D Proton Spectrum ^{1}H-^{15}N HSQC	apoC15A HAH1	1 eq apoWLN4
11 12	1D Proton Spectrum ^{1}H-^{15}N HSQC	apoC15A HAH1/WLN4	¼ eq copper(I)
13 14	1D Proton Spectrum ^{1}H-^{15}N HSQC	apoC15A HAH1/WLN4	½ eq copper(I)
15 16	1D Proton Spectrum ^{1}H-^{15}N HSQC	apoC15A HAH1/WLN4	¾ eq copper(I)
17 18	1D Proton Spectrum ^{1}H-^{15}N HSQC	apoC15A HAH1/WLN4	1 eq copper(I)
19 20	1D Proton Spectrum ^{1}H-^{15}N HSQC	apoC15A HAH1/WLN4	1¼ eq copper(I)
21 22	1D Proton Spectrum ^{1}H-^{15}N HSQC	apoC15A HAH1/WLN4	1½ eq copper(I)

Following the proteins being titrated to a 1:1 ratio, copper(I) was titrated in under a nitrogen atmosphere chamber as a solution of tetrakis(acetonitrile)copper(I) hexafluorophosphate to a 1:1, protein:copper(I). The copper(I) was obtained from a 10 mM stock solution prepared in 100% deuterated acetonitrile.

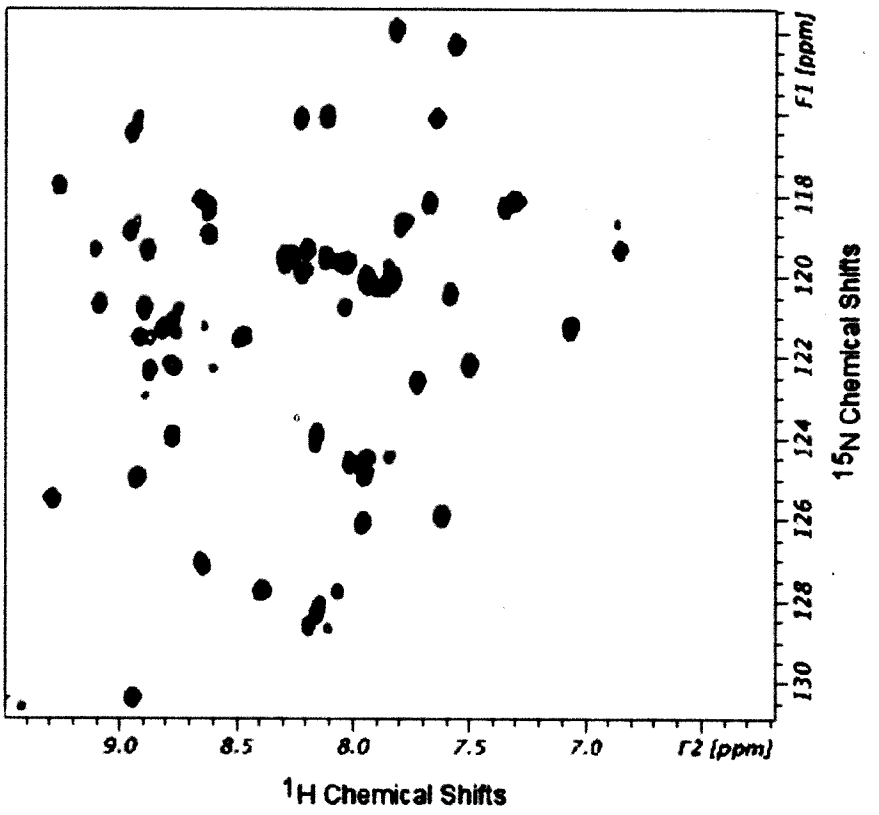

Figure 5.4: ^{1}H-^{15}N HSQC of apoWLN4 (red) overlaid with Cu(I)WLN4 (blue).

Figure 5.4 shows the spectrum overlay of apoWLN4 (blue) with Cu(I)WLN4 (red). There are many peaks that shift which are very close to the binding loop. It is important to note, not all peaks shift in the spectrum; if that were the case then it would be reasonable to expect that the folding of the protein was affected by the copper(I) binding. We see no effect on the structure due to copper(I) coordination, which is in agreement with the published data (*1, 5*).

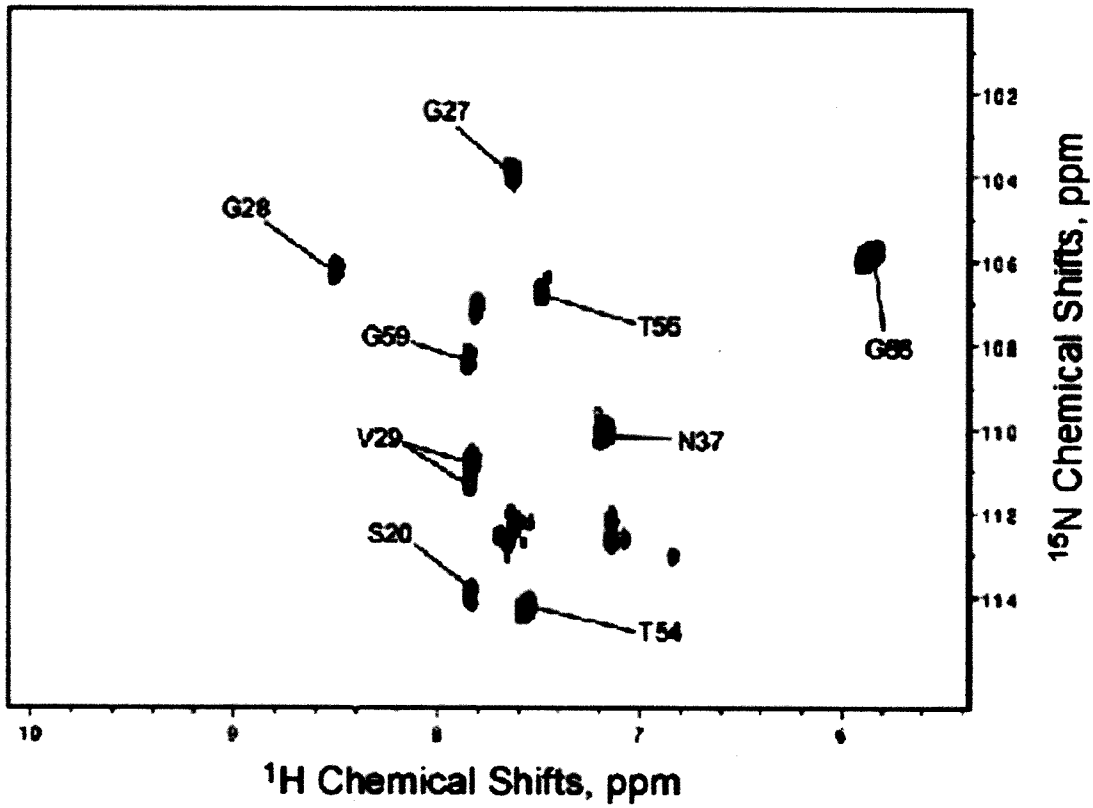

Figure 5.5: A ^{1}H-^{15}N HSQC overlay of ^{15}N C15A HAH1 before addition of CuWLN4 (red) and after (blue). The ratio of C15A HAH1:Cu(I):WLN4 was 1:1:1, however the titration was done past the 1:1:1 ratio and no further chemical shifts were observed.

Figure 5.5 shows a zoomed overlay of the WLN4/copper(I)/C15A HAH1 titration; depicting the most pertinent peaks that exhibit the highest chemical shift and even

some that disappear due to copper binding near them. Not all peaks in the spectrum are accounted for due to the unavailability of a double labeled sample. The peaks that are labeled are of the ^{15}N-C15AHAH1

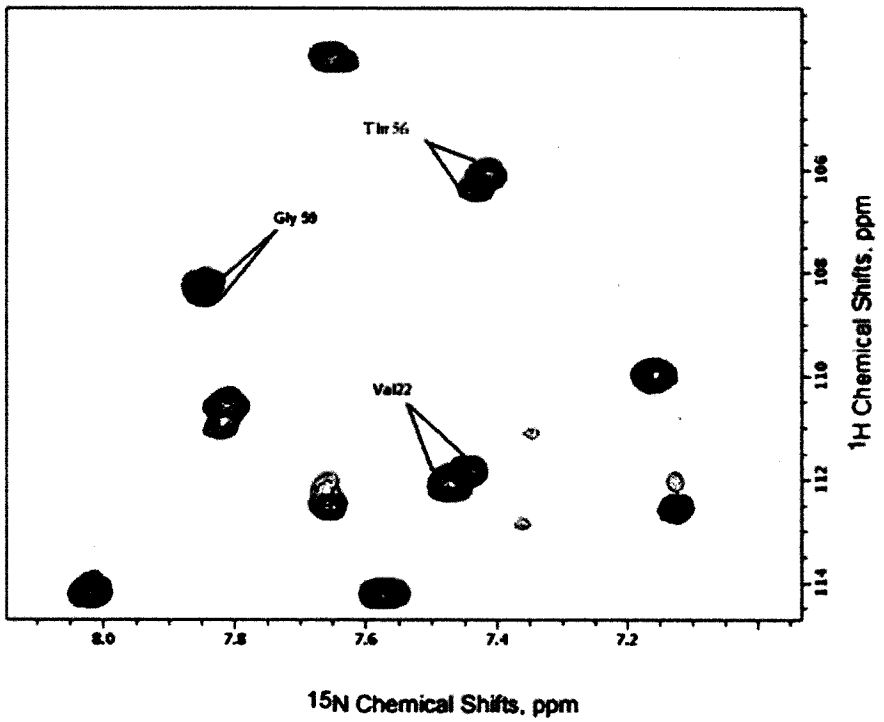

Figure 5.6: ^{1}H-^{15}N HSQC of 15N C12A HAH1 (green) titrated with Cu(I)WLN4 (blue). Ratio of C12A HAH1:Cu(I):WLN4 was 1:1:1, titration of copper past 1:1:1 was also done (not shown) and didn't show any further shifting of the peaks.

Figure 5.6 shows the C12A HAH1 titration overlay with selected peaks labeled. As can be seen from the spectrum, there are many peaks that shift, however this spectrum exemplifies the idea that shifts in the HSQC aren't necessarily indicative of an interaction. To determine whether there is interaction between two

proteins, it is imperative to determine the mobility of the proteins before and after the titration.

Mobility measures the tumbling time of a protein in solution. Proteins in a solution are dynamic and can rotate freely. This rotation is dependent on size and shape. The tumbling time is the time it takes a protein to rotate 1 radian. **Table 5.2** shows a typical set up for the mobility experiments. To determine the mobility there are two experiments that need to be done, one involving relaxation times along the Z-axis (called longitudinal relaxation or T_1) and the other of relaxation times in the XY-plane (called transverse relaxation or T_2). The relationship between these two times is $T_2<T_1$. The relaxation rates were measured using pulse sequences described by Farrow (1994), with refocusing times as described in **Table 5.2** (*12*). Water was suppressed using a "water flip-back" scheme (*13, 14*).

Table 5.3 shows the tumbling correlation times from the different experiments performed. Mobility was done on all combinations of wildtype protein and mutated partner. The table predicts that only the C15A HAH1 could facilitate complex formation with wtWLN4 in the presence of copper. The others didn't show a significant change in mobility from the apo monomer compared to what could be the complex. This is different from what was published for the yeast ATX1:CCC2a system. That data suggested that one of the cysteines could be mutated in each of the binding partners and still create a complex. Our data shows both cysteines need to be present in WLN4 to create a complex. This would be expected due to the fact that WLN4 seems to be one of the most stable domains, further suggesting it is a rigid

structure that can't accommodate, or can't efficiently accommodate loss of one of the cysteines.

Table 5.2: Typical delay times used to determine the relaxation rates.

Longitudinal Relaxation Experiments, T_1, ms:	Traverse Relaxation Experiments, T_2, ms:
2.5	16.96
35	33.92
75	50.88
125	84.80
200	118.72
370	186.56
500	220.48
675	271.36
1	152.64
1.5	305.28
	322.24

Table 5.3: Compilation of the tumbling times for the different titrations done.

Species:	Tumbling time, nanoseconds, τ_m	Interaction
Cu(I)HAH1 (*5*)	4.6 ± 0.4	-
apoWLN4/Cu(I)HAH1 (*5*)	7.2 ± 0.7	YES
apoC18A WLN4	4.3 ± 0.4	-
apoC18A WLN4/Cu(I)HAH1	4.4 ± 0.4	VERY LITTLE/NONE
apoC15A WLN4	4.8 ± 0.3	-
apoC15A WLN4/Cu(I)HAH1	ND	NONE
apoC12A HAH1	3.6 ± 0.2	-
apoC12A HAH1/Cu(I)WLN4	3.9 ± 0.4	VERY LITTLE/NONE
apoC15A HAH1	4.1 ± 0.4	-
apoC15A HAH1/Cu(I)WLN4	7.6 ± 0.6	YES
apoC18A ATX1 (*3*)	4.1 ± 0.7	-
apoC18A ATX1/Cu(I)Ccc2a (*3*)	5.7 ± 0.6	YES

5.5 NMR Technique to Investigate Protein Interactions

NMR has become a powerful technique to determine solution behaviors of proteins. NMR has been used to determine conformations in solution through ^{1}H-^{15}N HSQC measurements (*15*). Marcellus Ubbink's group has done a lot of work with NMR to look at the various interactions between protein partners (*15-18*). One specific study used paramagnetic NMR to investigate the interaction of cytochrome c

and cytochrome c peroxidase (*15*). This study was similar to this work in that they were mutating cysteines to determine the effects to the backbone and the interaction of the two proteins. Certain mutations caused perturbations in the protein backbone that resulted in disappearance of peaks in the HSQC. These disappearances indicated more flexibility in the backbone and in some cases perturbed the interaction between the two proteins. These types of interactions can be seen in other protein systems as well, for example the WLN4/HAH1 and Atx1/Ccc2a interactions. ^{1}H-^{15}N HSQC experiments have been used on both of these systems to investigate perturbations in the backbone due to either copper(I) binding or interaction with the binding partner.

5.6 Yeast Homolog System: Atx1/Ccc2a

The interaction of the yeast homolog to HAH1, Atx1 can deliver copper to the ATPase Ccc2. Ccc2 has two cytosolic metal binding domains that can accept copper. This work was done in comparison to titrations of Atx1 with the first metal-binding domain Ccc2a. Currently there are solution structures of both the copper(I) bound and apo forms of Atx1 (*19*) and Ccc2a (*20*). An interesting feature of the Atx1 protein is that when copper(I) is bound, the metal-binding cysteines take on a buried conformation and upon release of the copper the metal-binding cysteines become solvent accessible (*19, 21*). The Atx1 behavior is in contrast to the HAH1 because HAH1 has its copper(I) bound cysteines in a solvent accessible position (*22*).

Many similarities in the copper transport system between yeast and humans has led to a comparison of them. Previous work on the Atx1/Ccc2a system revealed there are no overall changes in the structure upon interaction with the binding partner,

this was a supported finding in the WLNP/HAH1 interaction as well (*1, 2, 5*). Following the native interactions, attention turned to the mechanism of how the copper(I) was delivered from the metallochaperone to the respective metal-binding domain on the ATPase. In the Atx1/Ccc2a system mutations were made to each of the metal binding cysteines in order to trap a possible intermediate (*3*). **Figure 5.7** shows the ^{1}H-^{15}N HSQC data obtained from the titration of various mutations to the Atx1/Ccc2a metal binding cysteines . Comparison of panel A and B of **Figure 5.7** (Ccc2a/Atx1 titration) to **Figures 5.6** and **5.5** (WLN4/HAH1 titration) respectively, they both represent a complex formation when the most buried cysteine is mutated, but can't facilitate interaction when the solvent accessible cysteine is mutated. Panels C and D of **Figure 5.7** indicate the difference between the yeast system and the human WLN4/HAH1 interaction. In the WLN4 mutants there was no interaction when either of the mutants were titrated with Cu(I)HAH1 (**Table 5.3**). However, in the yeast system the Ccc2a could facilitate an interaction when cysteine 16 was mutated (most buried metal-binding cysteine). This suggests WLN4 is a much more rigid domain that may not be dynamic enough to facilitate an interaction. This could be substantiated in the fact that the WLN4 domain is the most stable of all the domains (*23*).

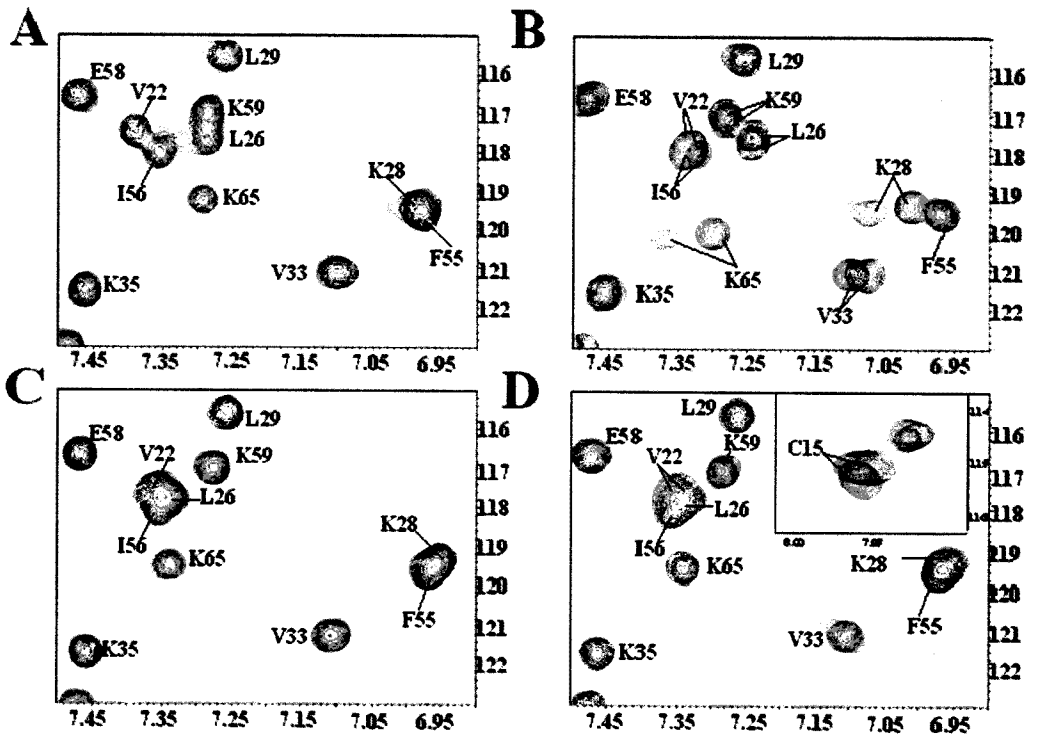

Figure 5.7: A. C15A Atx1 (green) titrated with wtCcc2a (red), B. C18A Atx1 (green) titrated with wtCcc2a (red), C. wt Atx1 (green) titrated with C13A Ccc2a (red), D. wt Atx1 (green) titrated with C15A Ccc2a (red). All titrations were done in the presence of 1 eq copper(I) with respect to the Atx1 protein (*3*).

5.7 UV-Vis Titrations of the WLN4:HAH1 Interaction in the Presence of Copper(I)

While NMR is the most informative way to determine complex formation there are other ways to detect it. The most convenient way is to do UV-Vis titrations. One protein is concentrated and exchanged into degassed buffer in a nitrogen atmospheres glove box. This protein is then measured initially on an Olis Cary 14 spectrophotometer to get an initial blank reading. This is necessary to remove any absorbance coming from the backbone of the protein and the intrinsic chromophores

within it, such as tryptophan, tyrosine, and disulfide bonds. The range of the measurement is from 600-190 nm in 1 nm increments. Starting out at 600 nm is a good way to determine if there is baseline shifting due to inaccurate additions or differences in the measurements, as the interaction should have no absorbance that close to the visible region. The interaction was monitored using two cuvettes, one for the blank and one for the measured sample. This too is important because there may be interactions of the titrants with the buffer or other material that could give baseline shifting or false positives.

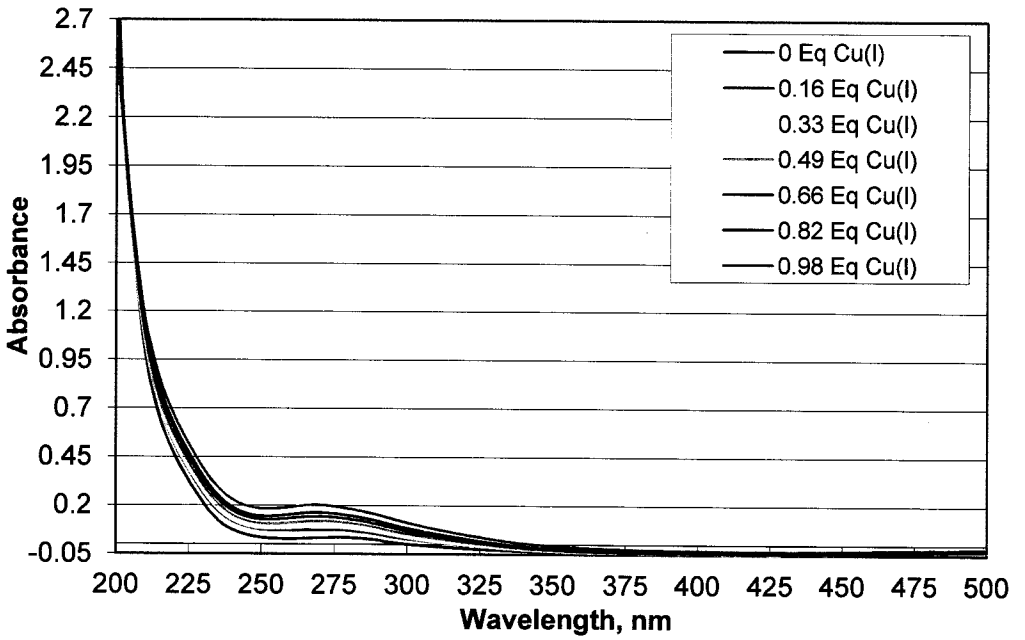

Figure 5.8: UV-Vis titration of copper(I) into apoWLN4 to nearly one equivalent.

Copper(I) was not the only metal used to do the titrations; they were also done with cadmium(II) and silver(I). This was in attempt to find a metal that could facilitate a strong interaction and could be detected using gel filtration studies.

Figure 5.8 shows the titration curve of copper(I) addition to WLN4; as expected there is a peak that starts to form at around 266 nm which would be due to

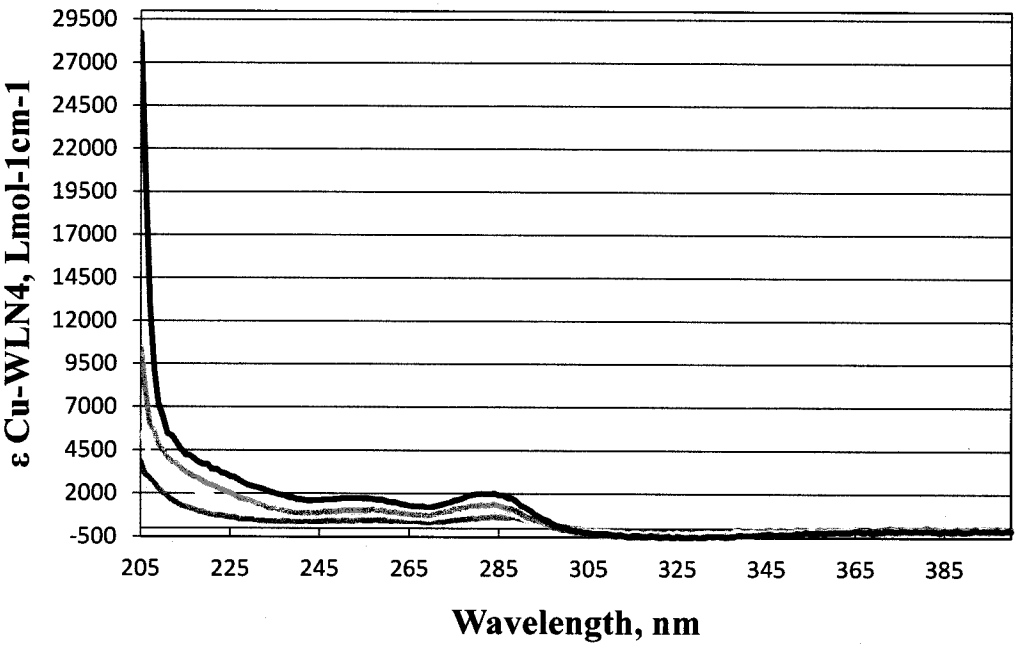

Figure 5.9: Titration of CuWLN4 with the mutant C15A HAH1 to one equivalent. Cu(I)WLN4 was titrated with increasing amounts of C15AHAH1. Green: 0.16 eq, yellow: 0.39 eq, orange: 0.71 eq, and red: 1.04 eq.

the formation of a 2-coordinate copper complex. Fujisawa made models trying to understand how the metal to ligand charge transfer (MLCT) bands change with varying metal coordination (*24*). His data suggested that a 2-coordinate copper(I) complex would exhibit a MLCT at around 254 nm which would then move out to

closer to 300 nm as the complex became 3-coordinate (*24*). This is similar to what is observed here, 5.9 shows a peak forming at 266 nm which can be attributed to a 2-coordinate copper(I) thiolate complex. It isn't quite the 254 nm described by Fujisawa, but his data was from models (*24*).

Once copper(I) was titrated into the WLN4, C15A HAH1 was titrated in. **Figure 5.9** shows the titration after addition of C15A HAH1. The new feature of this titration is the appearance of the peak at 280 nm which would suggest a higher coordinated state of the copper. At this point the coordination state of the metal can't be determined, but it seems it has shifted. Also the peak at around 266 nm has disappeared, indicating that the 2-coordinate state has been changed. The shift in MLCT band suggested a change in coordination state due to addition of the C15A HAH1. This data corroborates the NMR data, which also showed a complex formation between these two binding partners.

There were many experiments for the other binding mutant interactions, where the copper bound wildtype protein was titrated with the mutated binding partner (refer to **Table 5.3** for titrations done). For all titrations except the WLN4/Cu(I)/C15A HAH1 there was no MLCT bands indicative of complex formation. These findings also corroborate the NMR data, where no complex formation was detected for any of the other titrations.

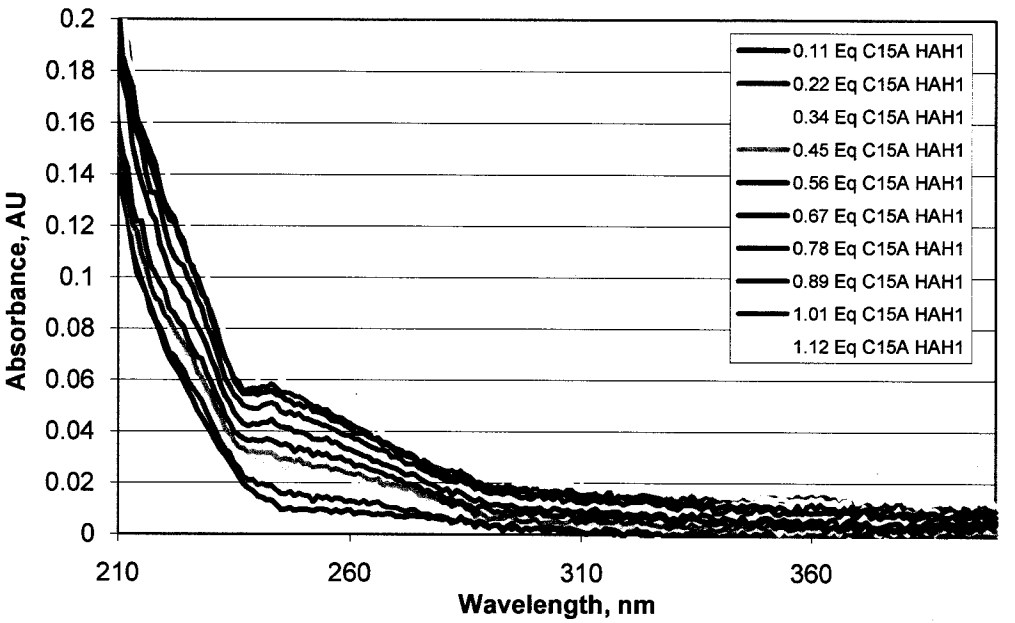

Figure 5.10: 66.5μM Cd(II)WLN4 was titrated with the mutant C15A HAH1. This was done to find a metal that would hold the complex together better than copper(I).

Gel filtration analysis was also used to detect the complex formed. This technique uses several well-behaving standards to determine the size of a protein that moves through the column. Each protein has a particular hydrodynamic radius that allows it to move through a gel filtration column and elute at a particular elution volume. The elution volume is dependent on several factors, the buffer and pH, the size of the protein, the size of the medium in the column, and the flow rate. The Cu(I)WLN4/C15A HAH1 complex doesn't hold together well as it is run through the Superdex75 gel filtration column (**Figures 5.11-5.14**).

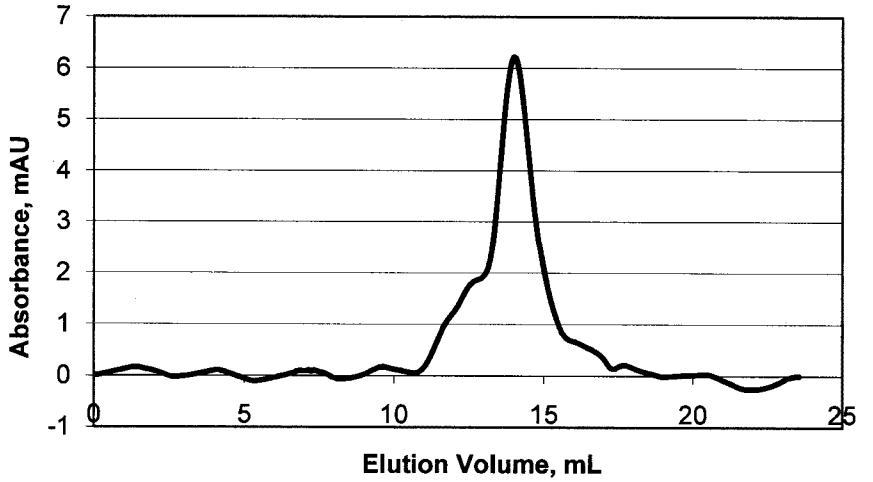

Figure 5.11: apoWLN4 elution profile from a high resolution gel filtration column. Elution volume was 14.0 mL.

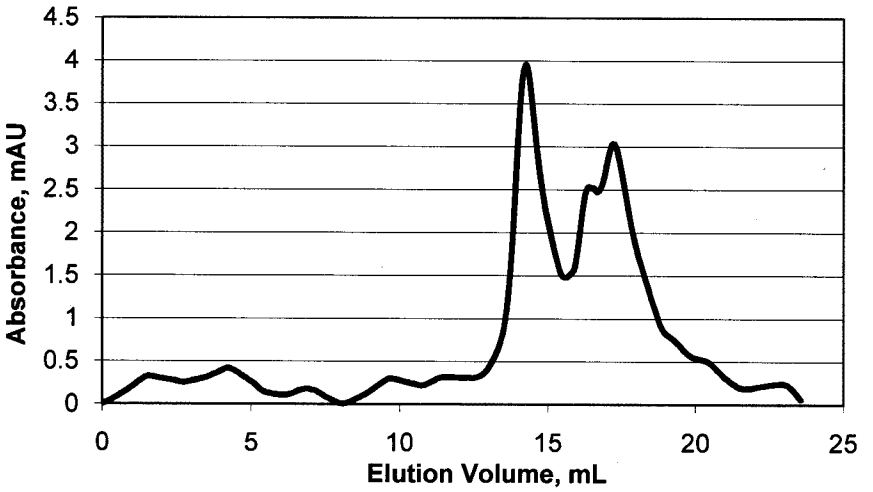

Figure 5.12: apoC15A HAH1 elution profile from a high resolution gel filtration column. Elution volumes were 14.2 mL, 16.4 mL, and 17.2 mL.

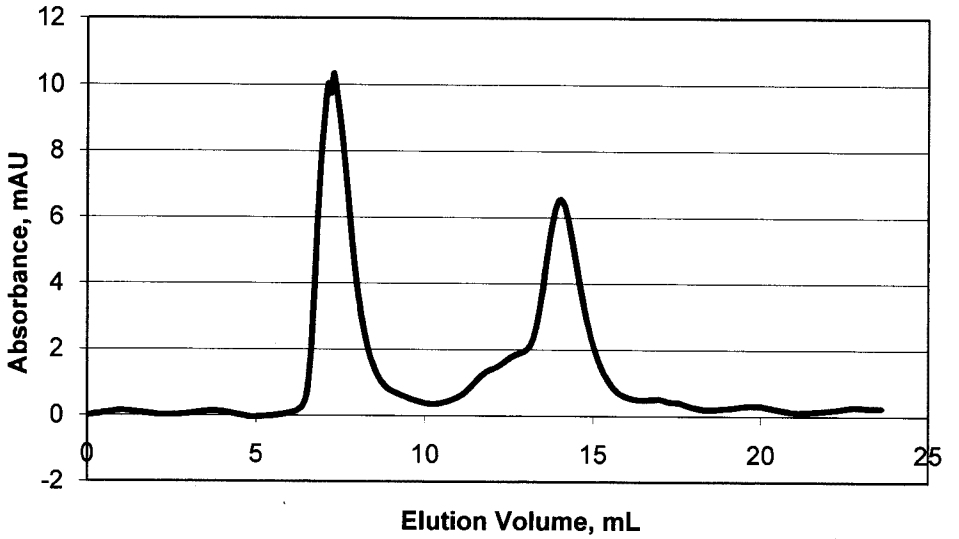

Figure 5.13: Cu(I)WLN4 elution profile from a high resolution gel filtration column. Elution volumes were 7.2 mL (inside the void volume) and 14.0 mL.

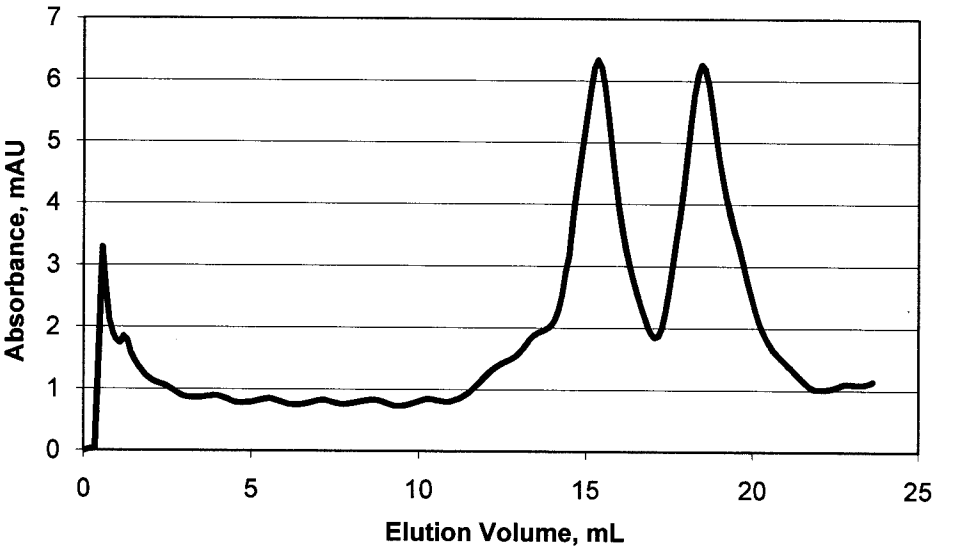

Figure 5.14: Cu(I)WLN4/C15A HAH1 elution profile from a high resolution gel filtration column. Elution volumes were 15.4 mL and 18.48 mL.

Comparing **Figures 5.11-5.14** indicates there is something happening in the interaction that isn't detected in the individual proteins. SDS-PAGE analysis was done but couldn't resolve WLN4 from C15A HAH1. The best way to do this would be to have antibodies to either of the binding partners and do Western blotting, or do a mass spectrometry analysis on each of the fractions to determine what species is present.

So other metals were titrated into the WLN4/C15A HAH1 interaction to find a metal that could hold the complex together well. Two particular metals were tried, the first was cadmium(II) which doesn't mimic copper(I) very well, but has a higher affinity for sulfides than copper(I). **Figure 5.10** shows the titration of the C15A HAH1 titrated into Cd(II)WLN4. There is a definite feature that appears around 245 nm that would account for a cadmium(II) thiolate complex. This complex seemed promising, but didn't fare well when run on the Superdex75 gel filtration column. It seemed the complex is still labile enough that the elution profile exhibits at least 3 peaks, most likely each monomer one with copper and one without, as well as the complex (data not shown). This data is, however interesting because future work could look at using ^{113}Cd(II) NMR to probe the coordination state of the complex. Another more recent technique would be to do ^{111m}Cd(II) perturbed angular correlation (PAC) (*25, 26*). Briefly, the metastable ^{111m}Cd(II) gives off two gamma radiation events to get back to the native isotope. As the nucleus spins there is an angle difference that can be measured between the first gamma radiation and the second. The electronic environment around the nucleus has a large impact on the tilt

of the nucleus and therefore the Larmour frequency, so the more tilt the slower the rotation and the smaller the angle between the gamma radiation events. The different angles can then be compared to model systems and a coordination of the cadmium determined. This is a very complicated technique for this, but would give very interesting information.

The most used technique for determining coordination is extended X-ray absorption fine structure (EXAFS). In this technique the sample is exposed to x-rays starting just before the absorption edge (the energy where the electrons of the metal absorbed the radiation). The absorption edge is indicative of the metal being probed, so this makes the technique selective. During the EXAFS measurements, the core electrons in the metal are excited by the x-rays and interact with the surrounding electrons (for example the electrons of a sulfide in the case of cysteines bound to a metal), if the electron is considered a wave in this case there is interference between it and the surrounding electrons that can be measured at the synchrotron. This interference pattern can then be interpreted using many different techniques and compared to known model systems to determine coordination state of the metal in the protein.

The interaction of Cu(I)WLN4/C15A HAH1 was analyzed by X-ray Absorption Near Edge Structure (XANES) and EXAFS (**Figures 5.15-5.17**) techniques in Professor Jim Penner-Hahn's laboratory at the University of Michigan by postdoctoral fellow Jay Stasser. In **Figure 5.16** the pre-edge features around 8980 eV are where the coordination can be distinguished (*27*).

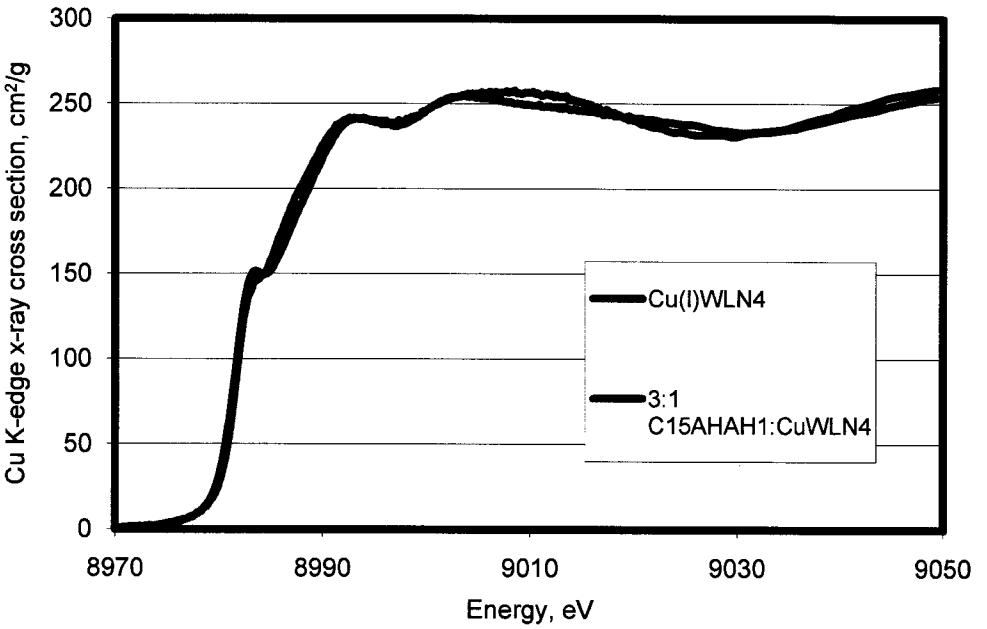

Figure 5.15: XANES data of the proposed interaction between 3 eq C15A HAH1 and 1 eq Cu(I)WLN4.

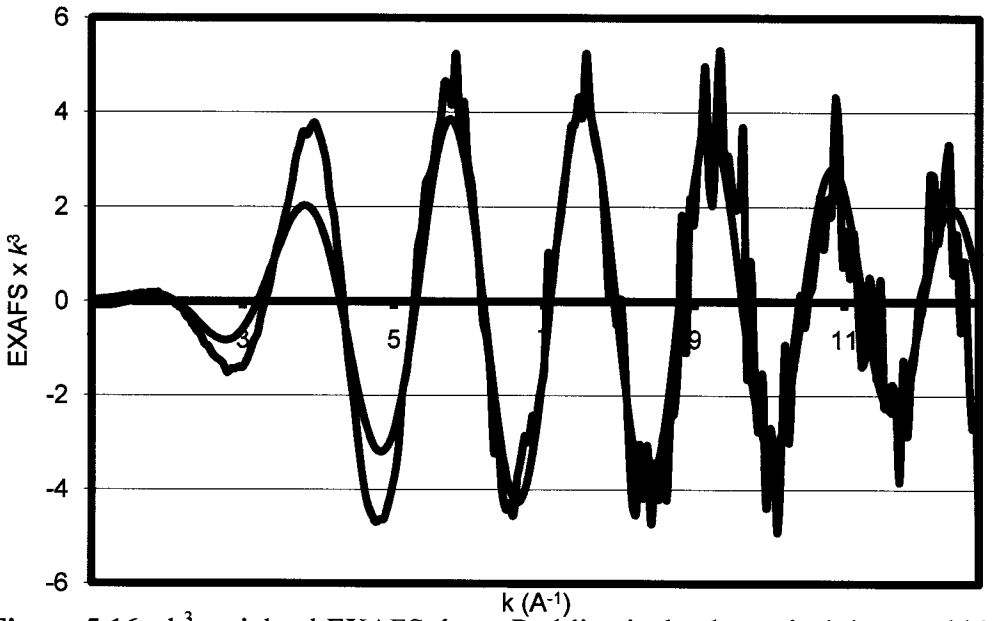

Figure 5.16: k^3-weighted EXAFS data. Red line is the theoretical data, and blue is the experimental, the fit is very poor.

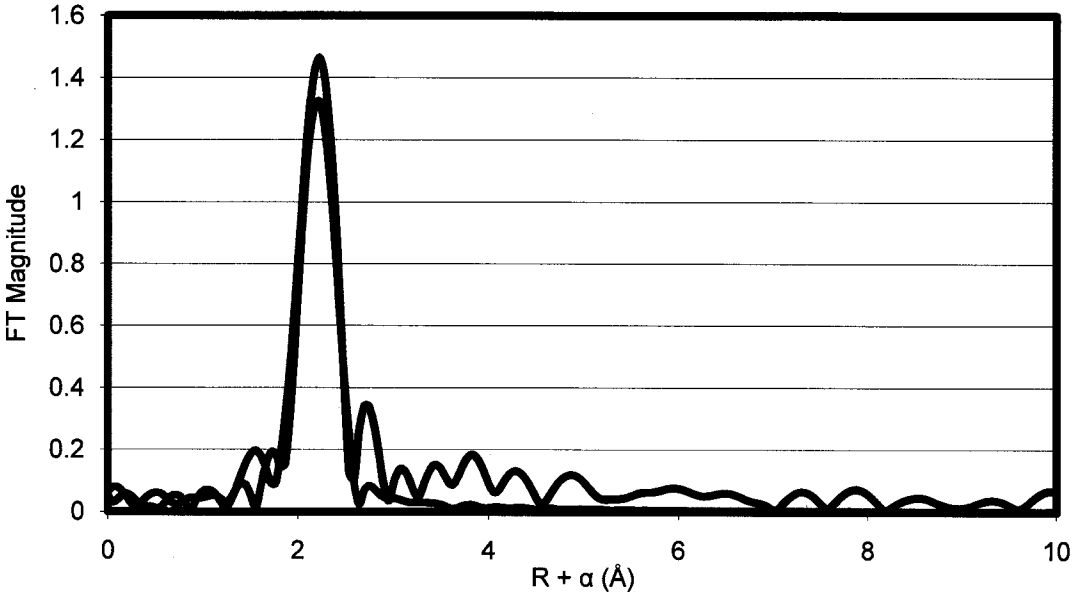

Figure 5.17: Fourier transforms of the Cu(I)WLN4 (blue) and 3:1 C15A HAH1:Cu(I)WLN4 interaction (red).

O'Halloran *et. al.* described the copper(I) coordination around Atx1 using EXAFS and XANES (*28*). Atx1 exhibits a 3-coordinate geometry noted by a weak shoulder around 8984 eV (*28*). In **Figure 5.16**, the WLN4 trace has a sharp shoulder around 8984 eV that is weaker WLN4/Cu(I) /C15A HAH1 interaction. The weakening of the shoulder may be indicative of a 3-coordinate state. **Figure 5.17** is the Fourier transform of the EXAFS data. It looks like the two traces are very close with some extra features present in the Cu(I)WLN4 trace (blue), that aren't present in the Cu(I)WLN4/HAH1 trace (red). Finally, **Figure 5.16** is the raw EXAFS data that is overlaid with a theoretical trace. The traces in **Figure 5.16** don't match up very well, making it more difficult to attribute the data to one type of coordination geometry. **Table 5.4** indicates a poor fit of the EXAFS data, that can be seen in the raw fitting of

the traces in **Figure 5.17.** This makes it difficult to describe the coordination environment around the copper(I) in these proteins. However, the XANES data does suggest there is some 3-coordinate character present based on previous work with Atx1 (*28*). NMR is a powerful technique, but it isn't efficient enough to determine the coordination state of metals in solution.

Table 5.4: EXAFS fit results. N is the coordination number, R is the bond length, σ^2 is the Debeye-Waller factor, E_0 is an energy offset to match the traces in **Figure 5.17**, and F is the mean-square-deviation between data and fit.

	N	R	σ^2	E_0	F
S	2	2.27	0.0027	-10.13	360
S	3	2.27	0.0047	-9.99	258
S	4	2.27	0.0065	-9.46	223

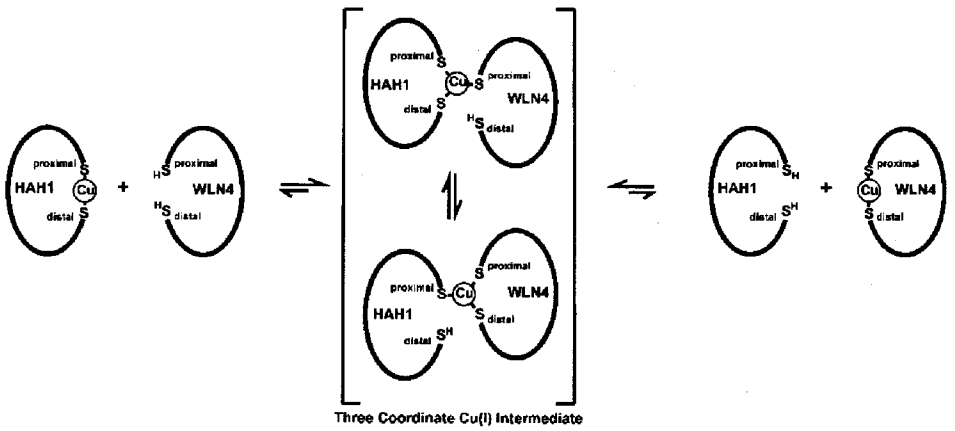

Figure 5.18: Possible mechanism for copper(I) handoff from HAH1 to WLN4 (*9*). NMR data supports the bottom intermediate.

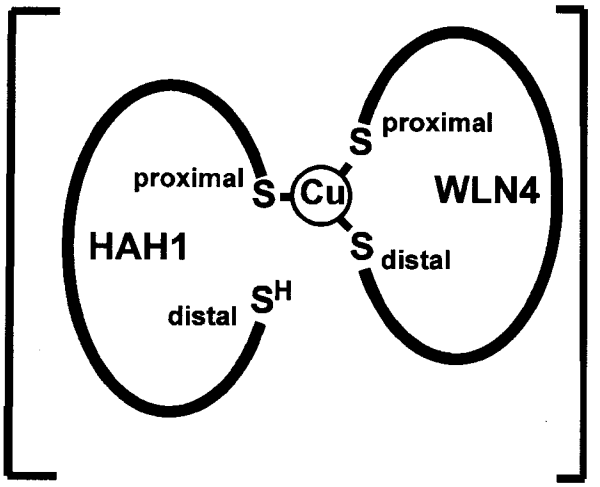

Favored Model

Figure 5.19: Favored intermediate model based on NMR experiments.

5.8 Conclusion

The data here suggests the copper delivery from HAH1 involves an intermediate where there is no binding to cysteine residue 15 of HAH1, but the other cysteines in the handoff are necessary for proper complex formation (**Figure 5.18**). Based on XANES data, it is possible there is a 3-coordinate intermediate formed, as the shoulder at around 8984 eV is smoothing, which is indicative of a 3-coordinate species, and the radii in the fit data (**Table 5.3**) are consistent with a 3-coordinate species. Previous work, with computer modeling, has shown there is a 3-coordinate intermediate formed with both the WLN4 and the HAH1 providing two of the ligands. This is contrary to our *in vitro* findings in this project. The NMR data suggested there was complex formation based on chemical shifts in the ^{1}H-^{15}N

HSQC, and mobility experiments that showed a definite increase in tumbling time for the complex compared to the apoWLN4 (**Table 5.3**). This mobility data turns out to be the most important data because as was depicted in **Figure 5.11** there were chemical shifts detected in that interaction (C12A HAH1 with Cu(I)WLN4), and they seemed to be in the proper areas for an interaction, but the mobility (**Table 5.3**), showed otherwise. It would have been inconceivable for the C12A HAH1 interaction to occur because the cysteine at residue 15 is more buried and would therefore be unlikely to interact well with the Cu(I)WLN4 on its own (**Figure 5.19**). **Figure 5.19** is the best fit model. The other mutant titrations, however, C15A and C18A WLN4 didn't show any chemical shifts in the HSQC at all, and the only one that was measured for mobility was the C18A WLN4/Cu(I)HAH1 interaction. As alluded to previously, this is quite novel compared to the yeast system (ATX1/Cu(I)/Ccc2a) (*3*). In that system at least one cysteine from each of the metal-binding partners could be mutated and a complex formed, whereas the HAH1/Cu(I)/WLN4 system needs both of the cysteines in the WLN4 and the cysteine at residue 12 in the HAH1. This might be what would be expected because in the yeast system Ccc2 has only two metal binding domains that may need to have flexibility in their function. The Wilson disease protein has six metal-binding domains that seem to have evolved to have specific duties. This is evident by the data that suggests domains 1,2, and 4 can form an NMR observable complex with HAH1, whereas domains 3, 5, and 6 cannot, rather they can accept copper from HAH1 without accumulation of complex (*2*). This may or may not be what is observed *in vivo* because there are many different experiments

that show different binding characteristics of the different domains. The WLN4 seems to be one of the most stable of the domains (*23*), which could be disrupted significantly when a cysteine was mutated to alanine. For these, and other reasons, the WLN4 could be expected to act differently than the Ccc2a system.

Overall, the WLN4/Cu(I)/HAH1 complex seems to involve at least one intermediate involving both cysteines of WLN4 and C12 of HAH1. There might be a second intermediate that is very labile and can't be detected on the NMR timescale involving one of the cysteines of WLN4. This interaction would be very hard to detect with the current techniques. One possible way to do this would be to get a crystal structure. This could force and maintain an interaction between the two binding partners that could then be structurally analyzed.

5.9 References

1. Banci, L., Bertini, I., Cantini, F., Rosenzweig, A. C., and Yatsunyk, L. A. (2008) Metal binding domains 3 and 4 of the Wilson disease protein: solution structure and interaction with the copper(I) chaperone HAH1, *Biochemistry 47*, 7423-7429.

2. Banci, L., Bertini, I., Cantini, F., Massagni, C., Migliardi, M., and Rosato, A. (2009) An NMR study of the interaction of the N-terminal cytoplasmic tail of the Wilson disease protein with copper(I)-HAH1, *J Biol Chem 284*, 9354-9360.

3. Banci, L., Bertini, I., Cantini, F., Felli, I. C., Gonnelli, L., Hadjiliadis, N., Pierattelli, R., Rosato, A., and Voulgaris, P. (2006) The Atx1-Ccc2 complex is a metal-mediated protein-protein interaction, *Nat Chem Biol 2*, 367-368.

4. Walker, J. M., Huster, D., Ralle, M., Morgan, C. T., Blackburn, N. J., and Lutsenko, S. (2004) The N-terminal metal-binding site 2 of the Wilson's Disease Protein plays a key role in the transfer of copper from Atox1, *J Biol Chem 279*, 15376-15384.

5. Achila, D., Banci, L., Bertini, I., Bunce, J., Ciofi-Baffoni, S., and Huffman, D. L. (2006) Structure of human Wilson protein domains 5 and 6 and their interplay with domain 4 and the copper chaperone HAH1 in copper uptake, *Proc Natl Acad Sci U S A 103*, 5729-5734.

6. Bunce, J., Achila, D., Hetrick, E., Lesley, L., and Huffman, D. L. (2006) Copper transfer studies between the N-terminal copper binding domains one and four of human Wilson protein, *Biochim Biophys Acta 1760*, 907-912.

7. Fatemi, N., Korzhnev, D. M., Velyvis, A., Sarkar, B., and Forman-Kay, J. D. NMR Characterization of Copper-Binding Domains 4-6 of ATP7B, *Biochemistry*.

8. Rodriguez-Granillo, A., Crespo, A., Estrin, D. A., and Wittung-Stafshede, P. Copper-transfer mechanism from the human chaperone Atox1 to a metal-binding domain of Wilson disease protein, *J Phys Chem B 114*, 3698-3706.

9. Sande, P. K. (2009) ISOLATION, EXPRESSION, AND PURIFICATION AND BIOCHEMICAL CHARACTERIZATION OF WILSON PROTEIN METAL BINDING DOMAINS 2 AND 1-2, in *Chemistry Department*, Western Michigan University, Kalamazoo, MI, MS Thesis.

10. Dickinson, S. E. (2007) BIOCHEMICAL CHARACTERIZATION OF DOMAIN FOUR OF THE WILSON PROTEIN, in *Chemistry Department*,

Kalamazoo College, Kalamazoo, MI, BA Thesis, Funded by Howard Hughes Medical Institute.

11. Muia, J. M. (2010) CHARACTERIZATION OF THE N-TERMINAL DOMAINS AND DISEASE-CAUSING MUTATIONS OF THE HUMAN WILSON PROTEIN, in *Chemistry Department*, Western Michigan University, Kalamazoo, MI, PhD Thesis.

12. Farrow, N. A., Muhandiram, R., Singer, A. U., Pascal, S. M., Kay, C. M., Gish, G., Shoelson, S. E., Pawson, T., Forman-Kay, J. D., and Kay, L. E. (1994) Backbone dynamics of a free and phosphopeptide-complexed Src homology 2 domain studied by 15N NMR relaxation, *Biochemistry 33*, 5984-6003.

13. Grzesiek, S., and Bax, A. (1993) The importance of not saturating H2O in protein NMR: Application to sensitivity enhancement and NOE measurements, *J Amer Chem Soc 115*, 12593-12594.

14. Bax, A., and Davis, D. G. (1985) MLEV-17 based two-dimensional homonuclear magnetization transfer spectroscopy, *J Magn Reson 65*, 355-360.

15. Volkov, A. N., Worrall, J. A., Holtzmann, E., and Ubbink, M. (2006) Solution structure and dynamics of the complex between cytochrome c and cytochrome c peroxidase determined by paramagnetic NMR, *Proc Natl Acad Sci U S A 103*, 18945-18950.

16. Crowley, P. B., and Ubbink, M. (2003) Close encounters of the transient kind: protein interactions in the photosynthetic redox chain investigated by NMR spectroscopy, *Acc Chem Res 36*, 723-730.

17. Ubbink, M., and Bendall, D. S. (1997) Complex of plastocyanin and cytochrome c characterized by NMR chemical shift analysis, *Biochemistry 36*, 6326-6335.

18. Worrall, J. A., Kolczak, U., Canters, G. W., and Ubbink, M. (2001) Interaction of yeast iso-1-cytochrome c with cytochrome c peroxidase investigated by [15N, 1H] heteronuclear NMR spectroscopy, *Biochemistry 40*, 7069-7076.

19. Arnesano, F., Banci, L., Bertini, I., Huffman, D. L., and O'Halloran, T. V. (2001) Solution structure of the Cu(I) and apo forms of the yeast metallochaperone, Atx1, *Biochemistry 40*, 1528-1539.

20. Banci, L., Bertini, I., Ciofi-Baffoni, S., Huffman, D. L., and O'Halloran, T. V. (2001) Solution structure of the yeast copper transporter domain Ccc2a in the apo and Cu(I)-loaded states, *J Biol Chem 276*, 8415-8426.

21. Arnesano, F., Banci, L., Bertini, I., Cantini, F., Ciofi-Baffoni, S., Huffman, D. L., and O'Halloran, T. V. (2001) Characterization of the binding interface between the copper chaperone Atx1 and the first cytosolic domain of Ccc2 ATPase, *J Biol Chem 276*, 41365-41376.

22. Anastassopoulou, I., Banci, L., Bertini, I., Cantini, F., Katsari, E., and Rosato, A. (2004) Solution structure of the apo and copper(I)-loaded human metallochaperone HAH1, *Biochemistry 43*, 13046-13053.

23. Okumu, W. (2010) The lipid acyl-chain dynamics in giant liposomes and characterization of domain 4 of the Wilson disease protein, in *Chemistry Department*, Western Michigan University, Kalamazoo, MI, PhD Thesis.

24. Fujisawa, K., Imai, S., Kitajima, N., and Moro-oka, Y. (1998) Preparation, Spectroscopic Characterization, and Molecular Structure of Copper(I) Aliphatic Thiolate Complexes, *inorg chem 37*, 168-169.

25. Matzapetakis, M., Farrer, B. T., Weng, T. C., Hemmingsen, L., Penner-Hahn, J. E., and Pecoraro, V. L. (2002) Comparison of the binding of cadmium(II), mercury(II), and arsenic(III) to the de novo designed peptides TRI L12C and TRI L16C, *J Am Chem Soc 124*, 8042-8054.

26. Hemmingsen, L., Sas, K. N., and Danielsen, E. (2004) Biological applications of perturbed angular correlations of gamma-ray spectroscopy, *Chem Rev 104*, 4027-4062.

27. Barnhart, T. M., Huang, H., and Penner-Hahn, J. E. (1995) Structural characterization of organocopper complexes by EXAFS and XANES: Evidence that cyanide does not coordinate to Cu in dimethyl cuprate solutions, *J. Org. Chem. 60*, 4310-4311.

28. Pufahl, R. A., Singer, C. P., Peariso, K. L., Lin, S. J., Schmidt, P. J., Fahrni, C. J., Culotta, V. C., Penner-Hahn, J. E., and O'Halloran, T. V. (1997) Metal ion chaperone function of the soluble Cu(I) receptor Atx1, *Science 278*, 853-856.

CHAPTER 6

BIOPHYSICAL CHARACTERIZATION OF MERCURY(II) HAH1 USING PERTURBED ANGULAR CORRELATION, MERCURY(II)-199 NMR, AND GEL FILTRATION STUDIES

6.1 Introduction

HAH1 is a copper chaperone that has the ability to bind other metals such as zinc(II), cadmium(II), and mercury(II) via its two metal binding cysteines. The affinity for these metals is mercury(II) > cadmium(II) > zinc(II) (*1*). For many years the method for determining mercury structures was to make models and collect mercury-199 NMR spectra. Mercury-199 has a spin of ½ making allowing it to exhibit sharp peaks indicative of various coordination geometries (*2*). O'Halloran *et. al.* (1995) published work using mercury-199 NMR to understand its binding to a regulatory protein MerR (*3*). MerR is a regulatory protein that binds mercury(II) with a very strong selectivity, even when presented with other metals or other competing ligands (*2-4*). Once mercury(II) binds, MerR induces expression of the mercury regulation proteins (*3-5*). Previous work with the MerR protein indicated it was a 3-coordinate geometry based on models containing the same bond lengths compared to EXAFS data (*6*). A lot of interest has involved understanding how heavy metals are regulated.

Another protein CueR is a highly selective copper(I) regulator in *E. coli* cells (*7, 8*). It is found in the MerR family of proteins and which includes MerR (*4*) and

ZntR (a zinc regulatory protein) (*9*). Copper is only necessary at the concentration of about 10 μM (*9, 10*) in *E. coli*, and the sensitivity of CueR is in the zeptomolar range (10^{-21} M) (*8*). The CueR activates CopA, an ATPase similar to Wilson disease protein or Menkes protein. Interestingly CueR has high selectivity toward gold, silver, and copper, but has no response to either zinc or mercury (*7, 11-13*). So it is important to understand the binding of the various metals to these proteins. This gives insight as to how these proteins are selecting out metals at such great efficiency, one distinctive feature resulting in selectivity of CueR for copper(I) and not higher valent species. This is a residue in the N-terminous of the dimerization helix that either interacts with the binding loop (CueR) or with the bound metal (ZntR) (*8*). In the case of the MerR homologs selective for metals in the +1 state, i.e. copper(I), this is a serine, and for MerR homologs selective for metals in the +2 state, i.e. mercury(II), it is a cysteine (*8*). Another fact is that metals in the +1 state prefer lower coordination states than do the +2, CueR facilitates this selectivity by sterically and electrostatically controlling the coordination environment, whereas the MerR homologs that prefer the +2 state use more solvent accessible ligands (*8*).

Understanding the structural features of the many proteins involved in regulation of heavy metals in the cells is important. This gives insight as to how the different attributes of the protein regulate the coordination environment, and in turn controlling which metals it selects.

This study was to look at how the mercury(II) interacts with the HAH1, as far as coordination and geometry. Previous work on an Hg(II)HAH1 homodimer

indicated a 3-coordinate species with a possible distorted fourth coordinating thiol (*14*). This fourth coordinate was at a distance that was too far for a covalent bond (*14*).

Recently, the Pecoraro group synthesized peptides that can bind metals and used various techniques to understand the metal coordination. One such peptide is the TRI peptide that is a synthetic alpha helical peptide that is capable of binding one mercury(II) atom per three helices. The geometry around the mercury is trigonal and resembles the binding found in MerR (*15*). The geometry around the trimer of alpha helices can be held together by various metals, including mercury(II) and cadmium(II) (*16*). To study these interactions a fairly new technique, perturbed angular correlation, was used to determine the ligand environments. This technique has been used on the TRI peptides and found that as the pH is increased, the metal favors a higher coordination state (*16, 17*).

The TRI studies (*16-20*) have led to the idea that other Hg(II) coordination environments can be determined where other techniques have fallen short (i.e. UV-Vis spectroscopy and NMR). Specifically, in Hg(II)HAH1 X-ray chrystallography studies weren't able to completely elucidate the coordination environment around the mercury. Also, the crystal structure may not reflect how the system behaves in solution. The goal of this project was to monitor mercury(II) coordination changes as a function of pH. This will provide information not only about coordination environments that are allowed, but also give information to the coordination of mercury at physiologically relevant pH values. This study used mercury(II)-199

NMR, mercury(II)-199m PAC, and gel filtration studies to determine the aggregation state of the proteins in the presence of mercury(II).

6.2 Mercury(II)-199 NMR

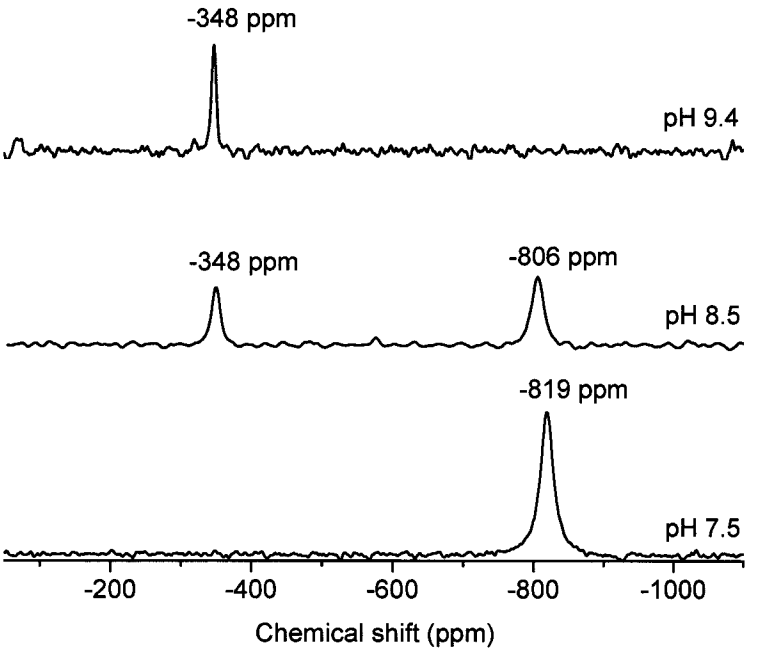

Figure 6.1: ^{199}Hg(II) NMR spectra at the various pH values, indicating a change in the coordination environment around the mercury(II).

Initial detection of Hg(II)HAH1 complexes in solution was done by ^{199}Hg NMR experiments. As the pH was increased there were definite changes in the chemical shifts (**Figure 6.1**). At physiological pH (~7.5) the ^{199}Hg(II) NMR revealed a single peak around -818 ppm which coincides with the chemical shift values obtained from 2-coordinate mercury(II) species (*21, 22*). O'Halloran's group showed

a single chemical shift at -821 ppm indicative of a 2-coordinate mercury(II) thiolate species (*22*). When the pH was increased to 8.5, a second complex appears with a chemical shift of -348 ppm. This chemical shift seems to fall within the range where 4-coordinate aliphatic mercury(II) thiolates are observed (-300 ppm to -500 ppm) (*5*). MerR has a 3-coordinate environment and has chemical shifts around -106 ppm (*22*). The range for a 3-coordinate mercury thiolate is -80 ppm to -160 ppm (*22*). **Figure 6.1** shows a 4-coordinate species emerging at pH 8.5 which becomes exclusive at the higher pH. This new peak isn't so easy to attribute to a particular geometry, and it doesn't account for any distorted 4-coordinate species identified in the Hg(II)HAH1 dimer. Very little data is available for distorted geometries, as they are very difficult to mimic as aliphatic models. There are other techniques developed to elucidate these types of geometries, such as perturbed angular correlation.

6.3 ^{199m}Hg(II) Perturbed Angular Correlation

^{199}Hg NMR is insufficient for the determination of the symmetry around the mercury(II) thiolates. Perturbed angular correlation (PAC), however, can provide this information, as long as the metal can exist as a metastable isotope. Briefly, PAC works by measuring the gamma radiation given off by a metal that has two distinctive energies of radiation (refer to **Section 3.2.10** for more information). The metal, in this case, mercury(II)-199m generated from liquid lead irradiated with 1GeV of energy for 1 hour, is put in the instrument that has many detectors at different angles. Some groups have shown that platinum metal will work for the production of ^{199m}Hg(II) as well (*23*). The spin of the nucleus (^{199m}Hg(II) has a spin of 13/2) is

affected by the electronic environment around it, so in essence the coordination will affect the tilt of the nucleus and therefore change the frequency. The frequency of spinning is called the Larmour frequency, which ultimately dictates the angles of gamma radiation detected. To get information about the coordination environment models were developed and measured to get signature spectra to use in comparison.

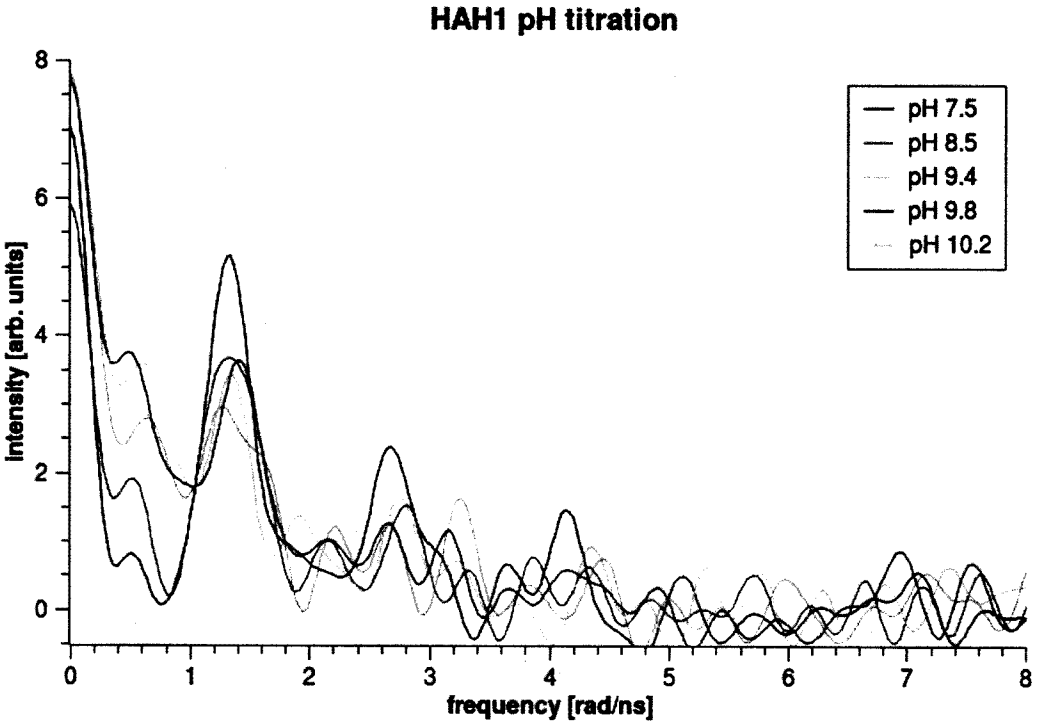

Figure 6.2: Raw data of the PAC experiments. The most important features to note is the decrease of the peak at around 1.4 rad/ns, and the increase at around 0.5 rad/ns. The increased feature was best fit for a distorted 4-coordinate mercury(II) thiolate species that increases as the pH is increased.

The PAC experiments were done using the same pH values used in the mercury(II) NMR experiments with the addition of a couple of values higher than pH 9.4. **Table 1**, along with **Figure 6.2**, shows the species detected at the different pH values. When the pH is below 8.5 the PAC experiments give one signal, with υ_Q about 1.43 GHz and low η (< 0.15). This signal compares well with literature data for a linear S-Hg-S structure. At higher pH values (>9.0) the major peak still occupies the same position but its amplitude drops by about one third. In the same spectrum a new peak appears at lower frequency, accounting for the loss of signal in the major peak. The pK_a of the observed transition is around 8.5. This new signal can be fitted in two different ways, either with low or high η. The best fit is achieved with the parameter set with low η, but it is only slightly better than the fit with high η (**Table 6.1**). This lower frequency and the relatively large η indicates most likely a highly distorted four-coordination geometry. These results are in relatively good agreement with ^{199}Hg NMR experiments which show the presence of only one resonance at pH 7.5 and two resonances at pH 8.5. A further increase in pH displays the presence of two signals. However, the amplitude of the high ω_Q NQI systematically drops, whereas, the amplitude of the low ω_Q NQI systematically increases (the high and low ω_Q refers to the frequencies in **Figure 6.2**.

Table 6.1: Parameters fitted to the PAC-data. The numbers in the parenthesis are the standard deviations of the fitted parameters. $\omega_Q$is the frequency, δ is the relative frequency spread, τ_C is the rotational correlation time, A is the amplitude of the signal, and χ_r^2 describes the fit of the Fourier transform.

pH	HAH1/ Hg(II)	ω_Q [rad/ns]	H	δ 100	$1/\tau_C$ [μs^{-1}]	A 100	χ_r^2
7.5	2:1	0.223(3)	0	4(2)	40(23)	14(1)	0.65
8.5	2:1	0.223(3)f 0.054(8)f	0.150(57) 0.738(110)	7(3) 350(163)	40(80)	13(6) 1(9)	0.91
9.4	2:1	0.223(3)f 0.054(8)f	0.095(181) 1.0(799)	11(9) 17(55)	81(138)	10(3) 4(3)	0.82
9.8	2:1	0.223(3)f 0.054(8)f	0.258(38) 0.447(320)	9(3) 22(36)	17(40)	11(2) 6(2)	0.85
10.2	2:1	0.223(3)f 0.054(8)	0.152(96) 1(0)	5(4) 22(22)	88(159)	8(3) 6(3)	0.70

* Two different possible fits are presented; the two upper lines represent one (with low frequency signal having low **η**) and the two lower lines represent the other (with low frequency signal having high **η**).

The partial NQI of thiolate bound species to Hg(II) was estimated from PAC data recorded for the known structure of $Hg(Cys)_2$, with υ_Q = 1.41 GHz and with a Hg-S bond lengths of 2.34 Å, giving υ_s = 0.705 GHz. This was used to predict the trigonal $[Hg(Cys)_3]^-$ giving υ_Q = 1.06 GHz in good agreement with the experimental value of 1.16 GHz. This indicates that the Bauer's axially symmetric independent ligands (BASIL) model might be a good model for ^{199m}Hg PAC (*24, 25*). Since the bond lengths for Hg(II) complexes of HAH1 are different, from 2.34 Å, the partial NQI for mercury(II) thiolate has been scaled (**Table 6.2**).

Table 6.2: Calculated partial NQI for Hg(II)HAH1.

Ligand	*Bondlength [Å]*	*partial NQI [GHz]*
Cys12A	2.3	0.753
Cys15A	2.5	0.586
Cys12B	2.5	0.586
Cys15B	2.8	0.417

The BASIL calculations based on X-ray structure of HAH1 predict the PAC parameters that compare well with the experimental constraints of trigonal complexes for a fit with low η as well as with experimental parameters for distorted tetrahedral complex where high η has been fitted (**Table 6.3**). Thus, the predicted PAC parameters actually agree fairly well with the experimental data, but either of the two options may be the correct structural interpretation of the PAC data.

Table 6.3: NQI's parameters calculated from the X-ray structure.

Structure	ν_Q *[GHz]*	η
Three-coordination	0.668	0.276
Four-coordination	0.602	0.529

Information from ^{199}Hg NMR and ^{199m}Hg PAC allowed us to elucidate the pH dependency of coordination properties of HAH1. At the physiological pH, Hg(II) forms, in solution, a preferred digonal HgS_2 form. While pH increases binding of

further thiolate ligand(s) is observed. Both techniques point to a 4-coordinate environment, and the PAC data suggests it is a distorted 4-coordinate environment. To further support the findings of the previous two techniques UV-Vis spectroscopy measurements were performed to determine the metal to ligand charge transfer bands for mercury(II) thiolate coordination at the different pH values (**Figure 6.3**). The presence of the ligand to metal charge transfer band at 278 nm (ε = 23100) indicates the formation of HgS_4 rather than HgS_3 complex, further corroborating the mercury(II) NMR data (*26*).

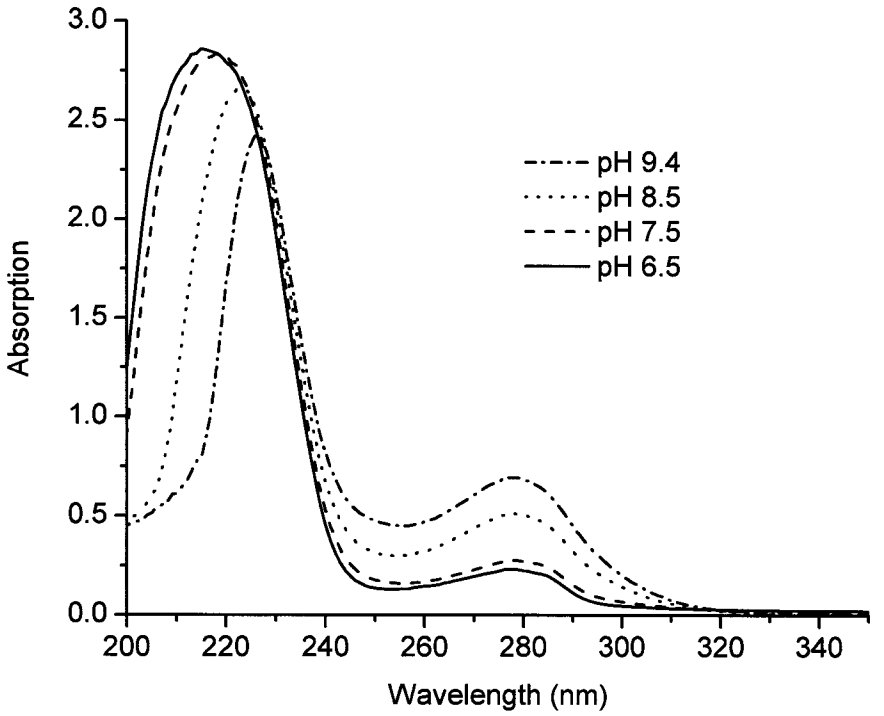

Figure 6.3: Electronic difference spectra of Hg(II) complexes of HAH1 with changes in pH.

6.4 Aggregation State Studies Based on pH Titrations Using Gel Filtration Analysis

One final experiment was performed to determine the aggregation state of the Hg(II)HAH1. This information would determine whether the different coordination species exist as monomers or dimers. To do this high resolution gel filtration studies were done to determine apparent masses. **Figure 6.4** shows the elution profiles at five different pH values. As the pH increases so does the mass, indicating aggregation or dimerization.

Table 6.4: Compilation of the elution volumes and apparent masses of Hg(II)HAH1 at the various pH values.

pH:	Elution Volume, mL:	Apparent Mass, kDa:
7.5	15.3	6.8
8.5	15.0	7.8
9.4	14.2	15.5
9.8	14.5	13.0
10.2	14.0	14.5

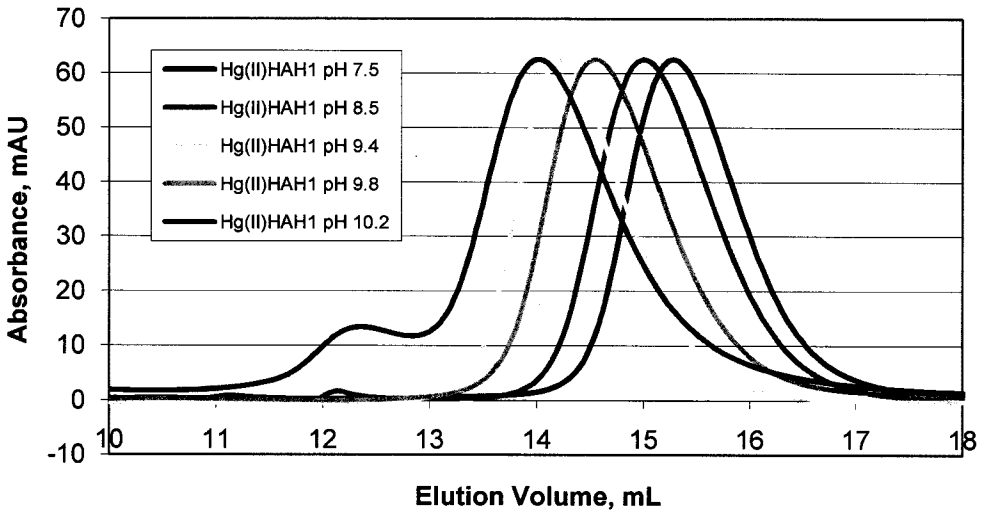

Figure 6.4: Hg(II)HAH1 high resolution gel filtration curves showing the elution profiles from a superdex 75 10/30HR column (pH range 7.5-10.2). It is evident that there are higher aggregation states at higher pH.

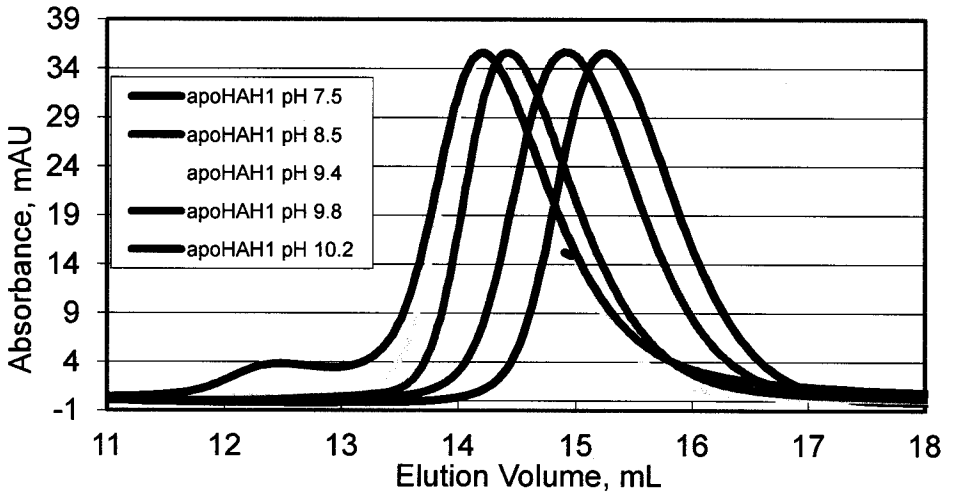

Figure 6.5: apoHAH1 high resolution gel filtration curves showing the elution profiles from a superdex 75 10/30HR column (pH range 7.5-10.2). It is evident that there are higher aggregation states at higher pH, most likely controlled by electrostatics due to the basic nature of the solution.

Table 6.4 shows the apparent masses of each of the metal-bound species. At pH 7.5 the mass clearly indicates a monomer, as does the mass at pH 8.5. In the NMR data there was strong evidence for two different species existing at the latter pH, however due to the conditions of the gel filtration study two peaks were not observed. As the pH was increased there was clear indication the HAH1 had homodimerized as the mass was approximately twice the monomeric mass. As the pH is increased the proteins become more negative. At the highest pH value it is starting to become basic enough to pull the proton off tyrosine groups (pK_a approximately 10), so electrostatics play a large role in controlling the environment around the mercury(II). This was evident in the apoHAH1 titrations done the same as the Hg(II)HAH1 gel filtration studies (**Figure 6.5**).

6.5 Conclusion

The crystal structure of the Hg(II)HAH1 dimer showed at least a 3-coordinate structure, but there seemed to be a distorted fourth coordinate. It wasn't clear whether this was fourth ligand because it wasn't close enough to be a covalent bond to the metal. It was not until this work that PAC was used to determine if the fourth ligand was close enough to be coordinated to the mercury(II). Analysis of the PAC data indicated the possibility of two different species based on model fitting, 3- or distorted 4-coordinate. The distorted 4-coordinate model fit better to the data and was considered to be the symmetry exhibited by the Hg(II)HAH1.

The NMR data and aggregation state data seem to only give clues as to changes based on pH differences. The NMR data corroborated with the mercury(II)-

199m PAC experiments where at low pH, there was only one species and it was definitely 2-coordinate based on previous work by the O'Halloran group on the ATX1 protein (*22*). They found the 2-coordinate Hg(II)ATX1 protein exhibited a peak at -821ppm which is very close to the chemical shift in this experiment, -819 ppm (*22*). As the pH was increased there was a second peak that emerged (-348 ppm). This chemical shift correlated to a range where 4-coordinate mercury(II) thiolates exist, but doesn't give any information as to the geometry of the complex. Finally, the highest pH showed a single peak at the new chemical shift.

Along with these biophysical measurements, it was important to look at the aggregation state of the Hg(II)HAH1. Once the coordination is known, it was necessary to understand if there was a dimer throughout the pH range studied, or if there was initially a monomer and then the pH increases made the environment such that dimers were favored. The latter is true in this case, at low pH the apparent mass was 6.8 kDa, but as the pH was increased the apparent mass increased. The apo proteins apparent mass was also determined using the gel filtration analysis. The masses of the apo compared to holo proteins didn't change dramatically, indicating that the pH increases are more conducive to forming dimers. This would be expected because the higher the pH the more negative the protein becomes and brings into play more electrostatic interactions.

These experiments showed the Hg(II)HAH1 can form a dimer at higher pH, but this isn't such a physiologically relevant experiment. In the crystal structure of the dimerized Hg(II)HAH1 is a lowest energy structure, however this may not be

indicative of the state of the complex in solution. Accordingly, near physiological pH the protein behaves as a monomer with a 2-coordinate Hg(II) thiolate environment. This work has shown Hg(II)HAH1 could support a distorted 4-coordinate dimer, but seems unlikely that it would in a physiological environment. Further, as the pH was increased, there was a higher likelihood for aggregation.

6.6 Significance of Study

These experiments probed the environment around the mercury(II) as it bound to HAH1. It is important to note however that physiologically, only a 2-coordinate monomer existed. The relevance of the titrations outside physiological pH was to corroborate relevance of a crystal structure of the Hg(II)HAH1 dimer. Even though the dimer may not exist physiologically, it does give information as to the effect of local changes to the protein, and provides a model for other 4-coordinate species. It was also a probe to further indicate the usefulness of PAC as a method for determining coordination geometries and symmetry.

6.7 References

1. Pearson, R. G. (1963) Hard and soft acids and bases, *J Amer Chem Soc 85*, 3533-3539.

2. Huffman, D. L., Utschig, L. M., and O'Halloran, T. V. (1997) Mercury-responsive gene regulation and mercury-199 as a probe of protein structure, *Met Ions Biol Syst 34*, 503-526.

3. Utschig, L. M., Bryson, J. W., and O'Halloran, T. V. (1995) Mercury-199 NMR of the metal receptor site in MerR and its protein-DNA complex, *Science 268*, 380-385.

4. Ralston, D. M., and O'Halloran, T. V. (1990) Ultrasensitivity and heavy-metal selectivity of the allosterically modulated MerR transcription complex, *Proc Natl Acad Sci U S A 87*, 3846-3850.

5. Watton, S. P., Wright, J. G., MacDonnell, F. M., Bryson, J. W., and O'Halloran, T. V. (1990) Trigonal mercuric complex of an aliphatic thiolate: A spectroscopic and structural model for the receptor site in the Hg(II) biosensor MerR, *J Amer Chem Soc 112*, 2824-2826.

6. O'Halloran, T. V., Frantz, B., Shin, M. K., Ralston, D. M., and Wright, J. G. (1989) The MerR heavy metal receptor mediates positive activation in a topologically novel transcription complex, *Cell 56*, 119-129.

7. Outten, F. W., Outten, C. E., Hale, J., and O'Halloran, T. V. (2000) Transcriptional activation of an Escherichia coli copper efflux regulon by the chromosomal MerR homologue, cueR, *J Biol Chem 275*, 31024-31029.

8. Changela, A., Chen, K., Xue, Y., Holschen, J., Outten, C. E., O'Halloran, T. V., and Mondragon, A. (2003) Molecular basis of metal-ion selectivity and zeptomolar sensitivity by CueR, *Science 301*, 1383-1387.

9. Outten, C. E., and O'Halloran, T. V. (2001) Femtomolar sensitivity of metalloregulatory proteins controlling zinc homeostasis, *Science 292*, 2488-2492.

10. Finney, L. A., and O'Halloran, T. V. (2003) Transition metal speciation in the cell: insights from the chemistry of metal ion receptors, *Science 300*, 931-936.

11. Petersen, C., and Moller, L. B. (2000) Control of copper homeostasis in Escherichia coli by a P-type ATPase, CopA, and a MerR-like transcriptional activator, CopR, *Gene 261*, 289-298.

12. Stoyanov, J. V., Hobman, J. L., and Brown, N. L. (2001) CueR (YbbI) of Escherichia coli is a MerR family regulator controlling expression of the copper exporter CopA, *Mol Microbiol 39*, 502-511.

13. Stoyanov, J. V., and Brown, N. L. (2003) The Escherichia coli copper-responsive copA promoter is activated by gold, *J Biol Chem 278*, 1407-1410.

14. Wernimont, A. K., Huffman, D. L., Lamb, A. L., O'Halloran, T. V., and Rosenzweig, A. C. (2000) Structural basis for copper transfer by the metallochaperone for the Menkes/Wilson disease proteins, *Nat Struct Biol 7*, 766-771.

15. Iranzo, O., Thulstrup, P. W., Ryu, S. B., Hemmingsen, L., and Pecoraro, V. L. (2007) The application of (199)Hg NMR and (199m)Hg perturbed angular correlation (PAC) spectroscopy to define the biological chemistry of Hg(II): a case study with designed two- and three-stranded coiled coils, *Chemistry 13*, 9178-9190.

16. Dieckmann, G. R., McRorie, D. K., Tierney, D. L., Utschig, L. M., C.P., S., O'Halloran, T. V., Penner-Hahn, J. E., DeGrado, W. F., and Pecoraro, V. L. (1997) De novo design of mercury-binding two- and three-helical bundles, *J Amer Chem Soc 119*, 6195-6196.

17. Pecoraro, V. L., Peacock, A. F. A., Iranzo, O., and Luczkowski, M. (2009) Understanding the biological chemistry of mercury using a de novo protein design strategy, *Bioinorg Chem, ACS Symposium Series*, 183-197.

18. Matzapetakis, M., Farrer, B. T., Weng T-C., Hemmingsen, L., Penner-Hahn, J. E., and Pecoraro, V. L. (2002) Comparison of the binding of cadmium(II), mercury(II), and arsenic(III) to the de novo designed peptides TRI L12C and TRI L16C, *J Amer Chem Soc 124*, 8042–8054.

19. Ghosh, D., and Pecoraro, V. L. (2005) Probing metal-protein interactions using a de novo design approach, *Curr Opin Chem Biol 9*, 97-103.

20. Ghosh, D., Lee, K. H., Demeler, B., and Pecoraro, V. L. (2005) Linear free-energy analysis of mercury(II) and cadmium(II) binding to three-stranded coiled coils, *Biochemistry 44*, 10732-10740.

21. Veglia, G., Porcelli, F., Sylvia, T., Prantner, A., and Opella, S. J. (2000) The structure of the metal-binding motif GMTCAAC is similar in an 18 residue linear peptide and the mercury binding protein MerP, *J Amer Chem Soc 122*, 2389-2390.

22. Pufahl, R. A., Singer, C. P., Peariso, K. L., Lin, S. J., Schmidt, P. J., Fahrni, C. J., Culotta, V. C., Penner-Hahn, J. E., and O'Halloran, T. V. (1997) Metal ion chaperone function of the soluble Cu(I) receptor Atx1, *Science 278*, 853-856.

23. Covey, R. L., and Davis, S. P. (1972) Hyperfine structure and isomeric shift of Hg 199m, *Phys Chem Rev C 5*, 1397-1402.

24. Butz, T. (1989) Analytic perterbation functions for static interaction in perturbed angular correlations of gamma rays, *Hyperfine Interact 52*, 189-228.

25. Hemmingsen, L., Sas, K. N., and Danielsen, E. (2004) Biological applications of perturbed angular correlations of gamma-ray spectroscopy, *Chem Rev 104*, 4027-4062.

26. Luczkowski, M., Stachura, M., Schirf, V., Demeler, B., Hemmingsen, L., and Pecoraro, V. L. (2008) Design of thiolate rich metal binding sites within a peptidic framework, *Inorg Chem 47*, 10875-10888.

VITA

The author was born October 19, 1979 in Plymouth, IN. He attended Triton Elementary in Bourbon, IN until sixth grade before moving on to Triton Jr./Sr. High School in Bourbon, IN. He graduated from Triton Jr./Sr. High School in June of 1998 and enrolled in the chemistry program at Indiana University South Bend (IUSB), South Bend, IN. While attending IUSB, he worked on the molybdopterin proteins: arsenite oxidase (PI Dr. Gretchen Anderson, IUSB) and xanthine oxidase (PI Dr. Russ Hille, Ohio State University). The molybdopterin protein work was presented at various local and national conferences, and one publication resulted from the arsenite oxidase project. He graduated from IUSB with his bachelors degree in May 2003.

Following his degree, he went to work for the Accra Pac Group as a research and development chemist. He formulated personal care products for many Fortune 500 companies. After working for the Accra Pac Group, he went on to pursue a PhD at Western Michigan University (WMU), Kalamazoo, MI.

At WMU, he joined the group of Dr. David Huffman working on a novel leech inhibitor, theromin and interactions of the Wilson disease protein metal-binding domains with the copper chaperone HAH1. The author presented many posters for this work at professional meetings both locally and internationally. He was also given a fellowship to work with Ivano Bertini's group at the Center for Magnetic

Resonance (CERM) in Florence, Italy, where he learned NMR techniques. Upon completion of his doctoral work in December 2010, he moved to Salt Lake City, UT where he accepted a postdoctoral position in the laboratory of Dr. Dennis Winge at the University of Utah. At the University of Utah he is studying electron transport chain protein assembly and discovery of a copper ligand housed in mitochondria.